

UNIVERSITY OF CALGARY

Studying Network Variants With Electroencephalography

by

Michael McCarthy

A THESIS

SUBMITTED TO THE FACULTY OF GRADUATE STUDIES
IN PARTIAL FULFILMENT OF THE REQUIREMENTS FOR THE
DEGREE OF MASTER OF SCIENCE

GRADUATE PROGRAM IN PSYCHOLOGY

CALGARY, ALBERTA

FEBRUARY, 2024

© Michael McCarthy 2024

Abstract

Functional MRI (fMRI) studies have shown that the human functional connectome exhibits reliable and substantial variability in organization across individuals, so-called network variants. However, it is unclear whether neuroimaging modalities that measure different aspects of brain function show similar evidence of such individual differences. Here we explored the feasibility of using electroencephalography (EEG) to study network variants using repeated measures eyes-closed and eyes-open resting state data from 14 participants taken across three sessions over the course of three months—estimating how much and in which ways band-limited phase coupling and amplitude coupling functional connectomes differed in similarity within and between individuals across contexts. For each coupling mode and frequency band, we hypothesized that if functional connectome organization was influenced by stable individual-dependent factors in our sample, then functional connectomes would be more similar within than between individuals across all contexts, on average, with smaller variations in similarity related to session or state. Overall, our results were inconclusive. Although we generally found consistently positive differences in functional connectome similarity across coupling modes, frequency bands, and contexts on average—depending on the comparison, these differences were either negligible or at most small, and were inconsistent across participants. We discuss several factors that may explain the differences between our results and the larger, more consistent effects reported in fMRI network variant studies, such as the spatial and temporal resolution of EEG and fMRI, and the methods used to estimate functional connectivity. We then offer suggestions for future EEG research that might address some shortcomings of our study.

Keywords: Electroencephalography, Functional Connectivity, Network Variants, Individual Differences

Preface

This thesis is original, unpublished, independent work by the author, M. McCarthy.

Acknowledgements

I thank my supervisor, Dr. Andrea Protzner, for her guidance, mentorship, and support throughout my degree and thesis; my committee members, Dr. Penny Pexman, Dr. Signe Bray, and Dr. Bradley Goodyear for their feedback on my thesis; Dr. Ford Burles for training me to work with EEG data; and Dr. Joshua Bourdage for his support towards completing my thesis. I also thank my father, Gord, my brother, Branden, and my grandparents, Joan and Walter, for their love and support—I could not have achieved all that I have without you.

This research was partially supported by funding received through the Natural Sciences and Engineering Research Council (NSERC) Canada Graduate Scholarship; University of Calgary Faculty of Graduate Studies Master's Research Scholarship and Graduate Studies Scholarship; and Alberta Graduate Excellence Scholarships (AGES) Master's Research Scholarship.

Table of Contents

Abstract	ii
Preface.....	iii
Acknowledgements.....	iv
Introduction.....	1
Intrinsic functional organization of the human brain.....	6
Measuring human brain oscillations	12
Revealing the intrinsic functional organization of the human brain.....	20
Individual differences and the functional organization of the human brain	28
Characterizing network variants	33
The present study	41
Methods.....	53
Data	53
Software, computational reproducibility, and code availability	55
EEG preprocessing.....	56
Analyses.....	58
Results.....	69
Functional connectivity analyses	70
Phase coupling functional connectome similarity analyses.....	75
Amplitude coupling functional connectome similarity analyses	95

Outcome variability of functional connectome similarity contrasts	99
Discussion	101
Consistency with related neurophysiological connectomics literature.....	105
Differences between phase and amplitude coupling.....	108
Factors that may contribute to differences between EEG and fMRI	110
Limitations	114
Conclusion	120
References	122
Appendix A	171
Individual-level contrast results	173
Phase coupling (Hilbert transform) results	177
Maximal model results.....	188
Amplitude coupling results (delta, theta, beta, gamma)	210
Appendix B	212

Introduction

Human brains, behaviour, and cognition exhibit important differences between and within individuals across the lifespan. A central goal of modern neuroscience is to identify the neural *causes of variation* (Sauce & Matzel, 2013) in human behaviour, cognition, and their dysfunction by characterizing how brain function differs between and within individuals under a variety of conditions using functional magnetic resonance imaging (fMRI), electroencephalography (EEG), and magnetoencephalography (MEG) (for fMRI, see Dubois & Adolphs, 2016; for EEG/MEG, see Sadaghiani & Wirsich, 2020). Each of these neuroimaging modalities measure different aspects of brain function across different spatial and temporal scales (and thus have their own strengths and limitations), however, a common point of interest between them is their application to the study of individual differences in whole brain functional network organization (Dubois & Adolphs, 2016; Sadaghiani & Wirsich, 2020).

Whole brain functional networks are graphs whose *nodes* are either spatially separate brain regions (for fMRI or source-reconstructed EEG/MEG) or sensors (for EEG/MEG) distributed across the entire cerebral cortex,¹ and whose *edges* quantify the observed statistical

¹ Although the nodes of fMRI functional networks can also include subcortical and cerebellar brain regions, we adopt a cortico-centric definition of whole brain functional networks here for inclusivity with EEG/MEG functional networks, which are generally limited to measuring cortical activity. This definition is not particularly limiting to the present discussion, as contemporary fMRI investigations largely ignore subcortical and cerebellar brain regions

dependency between two oscillatory neural signals originating from different nodes in the network. In common neuroscientific parlance, edges in the network represent *functional connectivity* or *coupling* between nodes, subgraphs in the network represent distinct *functional networks*, and the entire graph of the network represents a *functional connectome* (Barch et al., 2013; Van Essen et al., 2012; cf. Sporns, Tononi, & Kötter, 2005). Functional connectomes can be constructed by estimating phase coupling, amplitude coupling, or temporal correlations between all pairs of nodes after band-pass filtering the signals to frequency bands of interest (Bastos & Schoffelen, 2016), and are typically represented by an adjacency matrix of the weighted edges. For fMRI studies, functional connectivity is typically estimated using temporal correlations between signals in a single infraslow frequency band (e.g., 0.009-0.08 Hz), resulting in a single functional connectome; whereas for EEG/MEG studies, functional connectivity is typically estimated using phase coupling and/or amplitude coupling in multiple frequency bands over a wide frequency range (e.g., 1-50 Hz) due to neurophysiological signals containing a mixture of distinct neuronal oscillation frequencies, resulting in multiple concurrent functional connectomes (Sadaghiani & Wirsich, 2020).

Over the last two decades, convergent findings from group-averaged fMRI studies have identified that the human functional connectome is governed by an intrinsic functional architecture (M. D. Fox et al., 2005; Petersen & Sporns, 2015; Raichle, 2015) wherein functional networks exhibit spontaneous coupling between their nodes that can be captured in both the absence and presence of cognitive demands (Power et al., 2011; Uddin et al., 2019; Yeo et al.,

anyways (Uddin et al., 2023; Uddin, Yeo, & Spreng, 2019), and the fMRI network variant research to date has focused exclusively on cortical connectivity.

2011). A standardized taxonomy of these *intrinsic connectivity networks* (Seeley et al., 2007) has not yet been adopted (Uddin et al., 2023, 2019); however, the most prominent networks in the literature are commonly delineated and named according to their putative functions.² For example, the most common description delineates these networks into those associated with higher-level functions (default mode, central executive, and salience networks) and those associated with sensorimotor processing (auditory, visual, and sensorimotor networks). Some of these networks are most easily detected in the absence of cognitive demands (i.e., in a *resting state*); others are most easily detected in the presence of cognitive demands (i.e., in a *task state*); and some, such as the default mode network (Biswal, Yetkin, Haughton, & Hyde, 1995; Greicius, Krasnow, Reiss, & Menon, 2003; Raichle et al., 2001; Raichle & Snyder, 2007), can be easily detected in both resting and task states (Greicius & Menon, 2004; C. J. Honey et al., 2009). Additionally, the spatial organization of these networks has been found to be very stable, exhibiting only minor changes under varying cognitive demands (Cole, Bassett, Power, Braver, & Petersen, 2014; Gratton et al., 2018; Krienen, Yeo, & Buckner, 2014), and largely persisting in unconscious states such as sleep (Picchioni, Duyn, & Horovitz, 2013). More recent studies using group-averaged and source-reconstructed EEG/MEG or simultaneous fMRI-EEG have also corroborated these findings, implicating that (1) a similar organization of the human functional

² It is important to note that such naming conventions should not be taken to mean that these networks are solely involved in the putative function(s) associated with their assigned name or category (Uddin et al., 2019; Yeo et al., 2011), as multiple networks may be involved in the same function(s) (i.e., many-to-one mapping) and singular networks may be involved in multiple functions (i.e., one-to-many mapping; Pessoa, 2014).

connectome is present across the full range of oscillatory frequencies that are typically measured with EEG/MEG (Engel, Gerloff, Hilgetag, & Nolte, 2013; Mostame & Sadaghiani, 2021; Sadaghiani & Wirsich, 2020; Wirsich et al., 2021); and (2) hemodynamic and electrophysiological functional connectomes are likely different expressions of the same underlying brain activity (Daniel Arzate-Mena et al., 2022; Mantini, Perrucci, Gratta, Romani, & Corbetta, 2007; Sadaghiani & Wirsich, 2020).

However, following the discovery of a stable intrinsic organization of the group-averaged human functional connectome, a growing number of studies using fMRI (Bijsterbosch et al., 2018; Finn et al., 2015; Gordon, Laumann, Adeyemo, et al., 2017; Gordon, Laumann, Adeyemo, & Petersen, 2017; Gordon, Laumann, Gilmore, et al., 2017; Gratton et al., 2018; Kong et al., 2019; Kraus et al., 2021; Miranda-Dominguez et al., 2014; Mueller et al., 2013; Seitzman et al., 2019; D. M. Smith, Kraus, Dworetzky, Gordon, & Gratton, 2023)—and to a lesser extent—EEG (Nentwich et al., 2020) and MEG (Colclough et al., 2016) have identified reliable and substantial variability in functional connectome organization across *every* individual studied so far that is either underestimated or missed entirely by group-averaged models of the human functional connectome (Fedorenko, 2021; Fedorenko & Blank, 2020; Gordon, Laumann, Gilmore, et al., 2017; Gordon & Nelson, 2021; Mueller et al., 2013; Speelman & McGann, 2013; Zilles & Amunts, 2013). This has been demonstrated using a variety of approaches. For example, using community detection algorithms, Laumann et al. (2015) found evidence of an idiosyncratic spatial organization between individual and group-averaged functional connectomes such that certain functional networks present in the individual were not present in the group (and vice versa); comparing spatial correlations between individual and group-averaged functional connectomes, Seitzman et al. (2019) found similar evidence of an idiosyncratic spatial

organization across individuals, wherein certain spatially contiguous cortical regions were weakly correlated between individual and group-averaged functional connectomes (the location, size, and functional network assignments of these regions differed across individuals); and comparing functional connectome similarity between and within individuals, Gratton et al. (2018) found that functional connectomes were consistently more similar within than between individuals regardless of varying cognitive demands or time. Borrowing from Seitzman et al. (2019), here we use the term *network variants* as a catch-all shorthand to refer to individual differences in functional connectome organization relative to either a group-averaged functional connectome or other individuals' functional connectomes. These individual differences may present themselves in several forms, including interindividual variability in connectivity strength, the size and position of network nodes, or network topography (Gordon & Nelson, 2021; Uddin et al., 2023).

The purpose of this thesis is to explore the feasibility of studying network variants with EEG, addressing the growing need to incorporate findings derived from neurophysiological imaging modalities to enrich our understanding of individual differences in whole brain functional network organization beyond what can be learned from fMRI alone (Gratton et al., 2018; Sadaghiani & Wirsich, 2020; Uddin et al., 2023). Whereas the first studies of the group-averaged human functional connectome using fMRI date back to the mid-2000s (e.g., Beckmann, DeLuca, Devlin, & Smith, 2005), studies using EEG/MEG did not begin until the early 2010s (e.g., Brookes et al., 2011), and the investigation and characterization of whole brain functional networks continues to be heavily biased towards fMRI research methods (Uddin et al., 2023). Likewise, although the first studies of network variants using fMRI date back to the early 2010s (e.g., Mueller et al., 2013), we are only aware of one recently published study using EEG (Nentwich et al., 2020) and another using MEG (Colclough et al., 2016); thus, current knowledge

about network variants is almost exclusively based on infraslow frequency functional connectomes measured with fMRI, and it is an open question whether or not higher frequency functional connectomes measured with neuroimaging modalities such as EEG share similar evidence of stable individual differences (Gratton et al., 2018; Sadaghiani & Wirsich, 2020). Here we take one modest step towards addressing this question.

The remainder of the introduction is organized as follows: First, we review the intrinsic functional organization of the human brain, focusing on the features of computation and communication in neuronal networks that functional connectivity analysis seeks to (at least partly) quantify. Second, we review oscillatory neural signals measured by fMRI and EEG and their connection to underlying neuronal activity, as well as some of the challenges fMRI and EEG face in the pursuit of studying network variants. Third, we provide an overview of functional connectivity analysis, with a focus on methodology in order to build intuition around the interpretation of phase coupling and amplitude coupling. Fourth, we provide background on the motivations for network variant research, followed by a review of key findings. Finally, we introduce the study conducted for this thesis.

Intrinsic functional organization of the human brain

The adult human brain consists of approximately 86 billion neurons that are organized into a topologically complex network of spatially separate and functionally specialized neuronal populations connected by short and long range axonal projections upon which neurotransmission unfolds (Azevedo et al., 2009; Bullmore & Sporns, 2009; Cadwell, Bhaduri, Mostajo-Radji, Keefe, & Nowakowski, 2019; Cohen, 2014, 2017; Hagmann et al., 2008; Sporns et al., 2005; Yuste, 2015). Neuronal connectivity throughout this complex network is bidirectional and highly

branched, allowing for both the simultaneous broadcast of local computations to global areas and of global computations to local areas (Buzsáki & Watson, 2012); in turn, local and distant neuronal populations are able to dynamically couple to one another through transient synchronized rhythmic interactions between presynaptic senders and postsynaptic receivers, forming functional networks that are believed to support the vast repertoire of human behaviour, cognition, and normal brain function (Buzsáki, 2011; Buzsáki & Watson, 2012; Fries, 2015; Friston, 2002, 2011). Here, at the level of individuals, complex interactions between divergent initial conditions (i.e., genetic, environmental, and psychological differences) and experiences (i.e., episodes of behaviour and cognition in tandem with developmental histories) lay down the traces for highly individualistic developmental trajectories as the real-time processes of the brain unfold—sculpting individual patterns of network organization that progressively consolidate and self-reinforce their own emergent structures through synaptic proliferation, strengthening, and pruning over the course of the lifespan (Bateson, 2017; Brown, 2017; Cadwell et al., 2019; Gu & Kanai, 2014; Lewis, 2005; Stiles & Jernigan, 2010). Thus, the complexity of this network is also reflected in its dynamic features, such as its intrinsic activity, high energy costs, system of oscillatory rhythms, and moment-to-moment variability, as well as its inherent variability between and within individuals across the lifespan. (Buzsáki, 2011; Garrett et al., 2013; Lewis, 2005; Raichle, 2010, 2015).

Neuronal activity is primarily intrinsic—occurring in an ongoing manner not directly associated with external stimuli or cognitive demands—and can be characterized by its high energy costs, oscillatory patterning, and moment-to-moment variability (Buzsáki, 2011; Garrett et al., 2013; Raichle, 2010, 2015). Intrinsic activity accounts for the majority of the brain's energy costs (Raichle, 2010, 2015). In the absence of behavioural and cognitive demands, brain energy

consumption accounts for around 20% of all energy consumed by the body of the average adult human; however, this high rate of ongoing energy consumption is affected very little by behavioural and cognitive demands, with even the most arousing perceptual tasks and vigorous motor tasks causing at most a 5% difference in additional energy consumption compared to the resting state baseline (Raichle, 2010, 2015). The majority of this energy budget is devoted to neuronal signalling processes, such as postsynaptic glutamate receptors, action potentials, resting potentials, presynaptic neurotransmitter release, and neurotransmitter recycling (Howarth, Gleeson, & Attwell, 2012; Raichle, 2010, 2015; Raichle & Mintun, 2006), and therefore, to computation and communication in neuronal networks.

Oscillatory patterning, which reflects the timing of neuronal activity, is a basic property of normal brain function (Buzsáki, 2011; Buzsáki & Watson, 2012; Cohen, 2017; Fries, 2015). Neuronal networks have a natural tendency to engage in oscillatory activity because the intrinsic properties of both individual neurons and canonical circuit motifs favour rhythmic activity instead of continuous activity (Buzsáki, 2011; Buzsáki, Anastassiou, & Koch, 2012; Buzsáki & Draguhn, 2004; Singer, 2018; Turkheimer, Leech, Expert, Lord, & Vernon, 2015; Whittington, Traub, & Adams, 2018). In individual neurons, the refractory period following an action potential naturally imposes cyclic fluctuations of excitability wherein oscillatory patterning can appear as either fluctuations of the membrane potential or as rhythmic patterns of action potentials, which can then entrain postsynaptic neurons to oscillate in synchrony with the inducing pulses if the pulse frequency is close to their preferred membrane resonance frequency (Singer, 2018). At the level of local neuronal populations, canonical circuit motifs such as negative feedback loops can give rise to large-scale oscillations as excitatory neurons drive inhibitory neurons that subsequently inhibit the very same excitatory neurons, naturally leading to an oscillatory

patterning of responses between the presynaptic and postsynaptic networks (Buzsáki, 2011; Buzsáki & Wang, 2012; Fries, 2015; Singer, 2018).

Here the frequency, regularity, and probability of oscillatory coupling depends on the time constants of excitatory and inhibitory postsynaptic potentials, which provide windows of alternating reduced and enhanced excitability for action potentials to occur (Buzsáki, 2011; Buzsáki & Watson, 2012; Fries, 2015; Singer, 2018). If the time constants are similar between the presynaptic and postsynaptic networks, incoming excitatory postsynaptic potentials will arrive at the peak of enhanced excitability and have a high probability to summate effectively and generate action potentials; however, if the time constants are too dissimilar, excitatory postsynaptic potentials will arrive during inhibitory windows and have a lower probability to summate effectively and reach the firing threshold because of hyperpolarization (Buzsáki, 2011; Buzsáki & Watson, 2012; Fries, 2015; Singer, 2018). Thus, oscillations provide a putative mechanism through which the brain can dynamically coordinate the flow of information by effectively gating or biasing whether computations are amplified or ignored by different senders and receivers throughout the network (Bastos & Schoffelen, 2016; Buzsáki, 2011; Buzsáki & Draguhn, 2004; Buzsáki & Watson, 2012; Engel et al., 2013; Garrett et al., 2013; Schnitzler & Gross, 2005).

Neuronal networks in the cerebral cortex support several families of oscillations (oscillatory bands) that act relatively independently, are continuously present, and span from approximately 0.05 Hz to 500 Hz, covering more than four orders of magnitude on a temporal scale (Buzsáki, 2011; Buzsáki & Draguhn, 2004; Buzsáki & Watson, 2012). These oscillatory bands are defined as frequency bands with logarithmically increasing centre frequencies and relatively constant frequency width ratios between neighbouring bands (Figure 1; Penttonen &

Buzsáki, 2003). Each band is characterized by a distinct temporal processing window determined by its frequency, and several rhythms can temporally coexist, compete, or otherwise interact with each other locally or globally (Buzsáki, 2011; Buzsáki & Draguhn, 2004). The number of neurons that can participate in a given rhythm is constrained by the slow axon conduction velocity of neurons; thus, relative to higher frequency oscillations, lower frequency oscillations involve more neurons and are associated with larger membrane potential fluctuations because in longer temporal windows the action potentials of many more presynaptic neurons can be integrated (Buzsáki & Watson, 2012). Because of this structural constraint, when multiple oscillations are present simultaneously, the phase of slower oscillations modulates the amplitude of faster oscillations (Buzsáki & Watson, 2012).

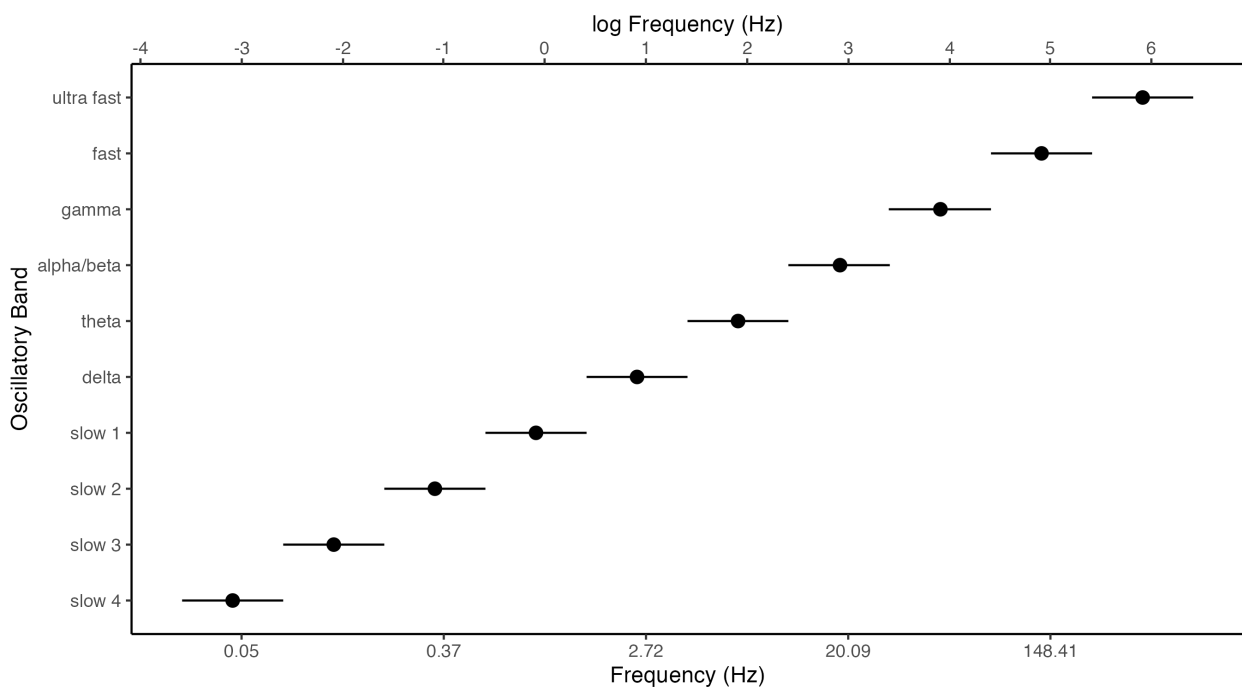


Figure 1. Oscillatory bands in the cerebral cortex follow a linear progression of frequencies on the natural logarithmic scale with relatively constant ratios between neighbouring bands (Penttonen & Buzsáki, 2003). The lower and upper limits of neighbouring bands overlap,

resulting in a frequency coverage of more than four orders of magnitude on a temporal scale. For each band, the approximate bandwidth and centre frequency is shown along with its commonly used name.

Along with their system of rhythms, neuronal networks in the cerebral cortex are characterized by their high moment-to-moment variability—wherein ever-changing conditions driven largely by intrinsic activity provoke unceasing transitions between qualitatively different states of coupling within and between neuronal populations throughout the network (Daniel Arzate-Mena et al., 2022; Faisal, Selen, & Wolpert, 2008; Garrett et al., 2013; Hutchison et al., 2013; Michel & Koenig, 2018; Stein, Gossen, & Jones, 2005). These state-to-state transitions are governed by itinerant dynamics (Kaneko & Tsuda, 2003), whereby the network explores multiple discrete states of coupling which may be continually revisited over time rather than settling into any particular state, providing a necessary level of moment-to-moment flexibility to respond to a greater range of imperfect, changing, and otherwise variable stimuli in a way that precludes overfitting whilst maintaining some level of stability and persistence (Breakspear, 2017; Deco & Corbetta, 2011; Garrett et al., 2013; Hutchison et al., 2013; Sporns, 2022). In other words, this balance of moment-to-moment variability with recurrence acts as a kind of dynamical scaffold around which the network can organize, capable of creating a large and variable repertoire of stable intrinsic network states when integrated over longer time periods (Daniel Arzate-Mena et al., 2022; Deco & Corbetta, 2011; Garrett et al., 2013; Hutchison et al., 2013; Sadaghiani & Wirsich, 2020; Sporns, 2022). Because of this behaviour, the coupling dynamics of neuronal networks can often be sufficiently modelled using methods that (1) do not take the temporal order of time points into account, and (2) assume that the time series is stationary (Daniel Arzate-Mena et al., 2022; Matković, Anticevic, Murray, & Repovš, 2023).

The purpose of functional connectivity analysis is to (at least partly) quantify these neurotransmission-mediated interactions, in order to better understand the nature of computation and communication in large-scale brain networks (Bastos & Schoffelen, 2016; Mostame & Sadaghiani, 2020). To this end, several neuroimaging and analysis methods have been developed to study group-averaged and individual whole brain functional networks. In the following sections we will focus on fMRI and EEG, and how the analysis of their oscillatory signals has contributed to our understanding of the human functional connectome.

Measuring human brain oscillations

Ongoing oscillations—reflecting synchronized rhythmic fluctuations in the excitability of local neuronal populations—are the most prominent feature of all neural signals and can be described by three pieces of information: frequency, amplitude, and phase (Cohen, 2014, 2017; Luck, 2014). Frequency is the number of oscillatory cycles per second and is measured in hertz (Hz); it describes the speed or timescale of an oscillation. Amplitude is the peak to trough distance of an oscillation and is typically measured in microvolts (mV) for EEG and percent change from baseline for fMRI, normalized from the arbitrary units (AU) of the raw BOLD signal by some baseline value (e.g., the signal mean; T. T. Liu, Nalci, & Falahpour, 2017); it generally has an inverse relationship with frequency such that higher frequency oscillations have lower amplitudes, and vice versa. Phase is the timing of an oscillation relative to where it is along its oscillatory cycle and is measured in radians or degrees; it is independent of amplitude, so the neural dynamics reflected in amplitude are distinct from those reflected in phase (Cohen, 2014). These properties of an oscillation are illustrated in Figure 2, which depicts two sinusoidal waves with the same amplitude (1 AU) and phase (0 degrees) but different frequencies (1 Hz and 2 Hz) evolving over the course of one second in both Cartesian and polar coordinates.

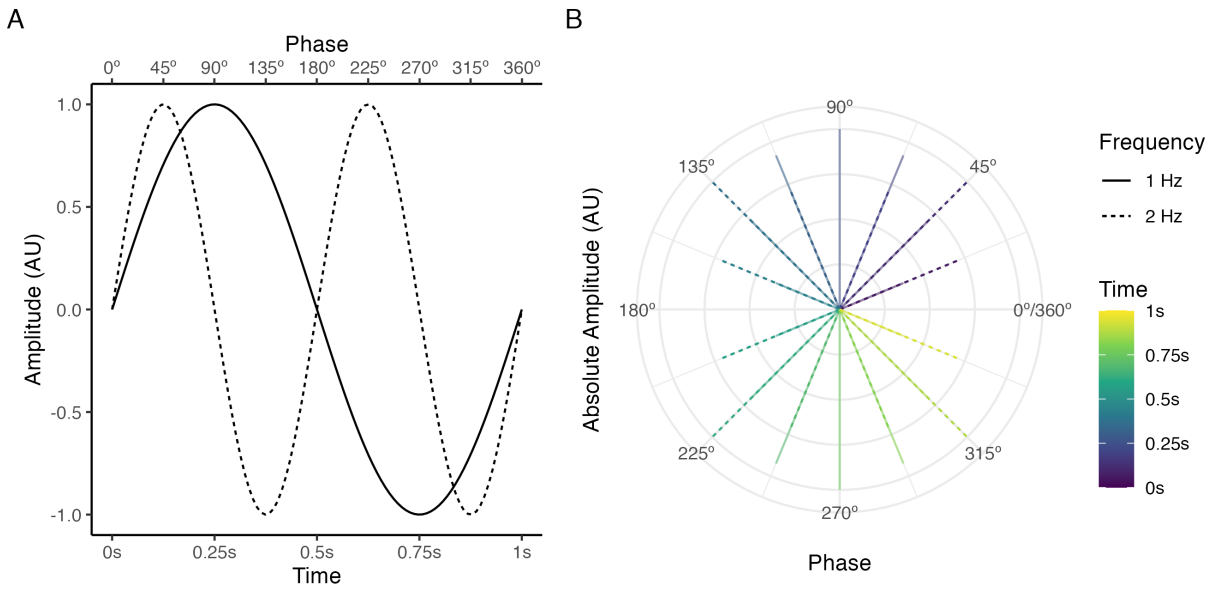


Figure 2. The three properties that define oscillations—frequency, amplitude, and phase—depicted in Cartesian (A) and polar (B) coordinates using 1 Hz and 2 Hz sinusoidal waves that share the same amplitude (1 AU) and phase (0 degrees). For the polar coordinates, 0.0625 second samples of each sinusoidal wave are depicted instead of continuous time for visual clarity; the length of each line corresponds to the absolute amplitude at a given time point, and the angle corresponds to the phase.

Neuronal interactions occur within one or many oscillatory frequency bands due to neuronal populations throughout the cerebral cortex being capable of generating multiple oscillation frequencies both concurrently and selectively, and responding selectively to inputs at multiple preferred frequencies due to the membrane resonances of individual neurons (Akam & Kullmann, 2010; Blankenburg, Wu, Lindner, & Schreiber, 2015; Hutcheon & Yarom, 2000; Kopell, Kramer, Malerba, & Whittington, 2010; Whittington et al., 2018). From a biophysics perspective, much is known about the origins of fMRI and EEG signals and their connection to

underlying neuronal activity (Buxton, 2013; Buzsáki, 2011; Cohen, 2017; Nunez & Srinivasan, 2006). Here we briefly review these origins, as well as some of the challenges fMRI and EEG face in the pursuit of studying network variants.

fMRI fMRI measures low frequency (< 0.1 Hz) oscillations in blood oxygenation level dependent (BOLD) signals caused primarily by decreases in local concentrations of paramagnetic deoxyhemoglobin in response to increases in local excitatory and inhibitory postsynaptic neuronal activity through the active process of neurovascular coupling (E. L. Hall, Robson, Morris, & Brookes, 2014; Hillman, 2014; Moon et al., 2021). When local neuronal activity increases, oxygen extraction from the blood increases, resulting in increased amounts of deoxyhemoglobin in the blood; however, within approximately 500 milliseconds and peaking around 3-5 seconds before slowly returning to baseline, neurovascular signals increase blood flow and volume to the responding region, bringing oxygenated blood in sufficient excess to overoxygenate the region and wash out deoxyhemoglobin (Hillman, 2014). Due to the magnetic properties of deoxyhemoglobin, this net decrease in local concentrations of deoxyhemoglobin causes changes in the magnetic field (i.e., T_2^* relaxation; Ogawa, Lee, Kay, & Tank, 1990) which are reflected as fluctuations in the magnetic resonance signal (Buxton, 2013). For typical whole brain fMRI studies, a single image of the brain (i.e., one volume) is obtained by sequentially acquiring images of all of the slices that cover the brain with a repetition time of about 3 seconds (i.e., the duration to obtain one volume); BOLD signals are recorded at voxels distributed throughout the brain volume, typically with a voxel size of about 3 mm³ (Bijsterbosch, 2017; Buxton, 2013). Thus, fMRI provides a spatially precise—but indirect, slow, and temporally delayed—proxy measure of underlying neuronal activity whose interpretation is intrinsically

linked to understanding the physiological and metabolic processes that modulate blood flow in the brain (Drew, 2022; C. N. Hall, Howarth, Kurth-Nelson, & Mishra, 2016; Hillman, 2014).

An important implication of this complication in interpreting fMRI data, particularly for studies of network variants, is that any individual differences in BOLD signal functional connectivity may reflect differences in neuronal activity, neurovascular coupling, or both (Bijsterbosch, 2017). Although it is commonly assumed that fMRI is detecting individual differences in neuronal activity, it cannot be ruled out that any individual differences observed with fMRI are the result of non-neuronal factors known to influence BOLD signal functional connectivity (e.g., the maximum oxygen carrying capacity of the blood, which is known to vary considerably and systematically between individuals; Hillman, 2014; Ward et al., 2020; Yang, Craddock, & Milham, 2014).

In addition, fMRI is a generally non-portable resource-demanding method, which places a basic restriction on who can collect fMRI data—and consequently—who can participate and benefit from fMRI research. For instance, all of the network variant studies cited in this thesis were conducted by researchers from high-income countries like the United States. Given that the broad purpose of these studies is to investigate variability in functional connectome organization across individuals—with the ultimate goal of identifying the neural causes of variation in human behaviour, cognition, and their dysfunction—our understanding of these individual differences may be distorted or otherwise undermined by the use of samples that differ in many concrete ways from the broader human population living in low-income and middle-income countries, such as their genetic, environmental, social, economic, political, and demographic diversity (Battel et al., 2021; Campbell & Tishkoff, 2008; Falk et al., 2013; Henrich, Heine, &

Norenzayan, 2010; Muthukrishna et al., 2020); and prevalence of neurological disease (Parra et al., 2018) and neurodevelopmental disorders (Bitta, Kariuki, Abubakar, & Newton, 2017).

EEG EEG measures oscillations in extracellular currents caused primarily by summed excitatory and inhibitory dendritic postsynaptic potentials from thousands of cortical pyramidal cells in parallel alignment, whose dipoles are oriented perpendicularly to the cortical surface (Cohen, 2014). Large-scale synchronous events of this nature create electrical fields powerful enough to conduct instantaneously through the brain, meninges, skull, and scalp, to scalp electrodes that measure fluctuations in these fields in real time (Cohen, 2014, 2017; Luck, 2014). Other sources of oscillations such as individual neurons, smaller populations of neurons, large populations of neurons with opposing dipoles oriented tangentially to the cortical surface, or deep brain sources either produce no electrical fields or weak electrical fields that cannot be measured at the scalp (Cohen, 2014). Furthermore, although oscillations occur across a wide frequency range (Buzsáki, 2011), very slow oscillations (< 0.1 Hz) can be difficult to measure due to limitations of most EEG systems, as can faster oscillations (> 80 Hz) due to their low amplitude making them hard to distinguish from noise (Cohen, 2014). For typical EEG studies, electrophysiological oscillations are recorded simultaneously at electrodes distributed evenly across the scalp (usually 64, 128, or 256 electrodes) with sampling rates of ≥ 500 Hz, then further processed into single or multiple frequency bands that are thought to capture distinct oscillations within this range (Buzsáki, 2011). Thus, EEG provides a direct (albeit incomplete) measure of neuronal activity with a high temporal resolution, whose interpretation bypasses the complications of linking BOLD signals to the dynamics of underlying neuronal activity. However, because EEG signals are measured using electrodes on the scalp rather than voxels in the brain, the spatial interpretation of EEG is intrinsically linked to understanding how the

volume conduction properties of the human head mediates the relationship between EEG signals measured at the scalp and their underlying neuronal sources (Lai, Demuru, Hillebrand, & Fraschini, 2018; Nunez & Srinivasan, 2006; Schoffelen & Gross, 2009).

Volume conduction simply refers to the effects of measuring electrical fields at a distance from their source. The primary effect of volume conduction in EEG is field spread—wherein the electrical fields generated by a source can spread not only to the nearest electrode, but also to other electrodes (up to tens of centimetres away) (Cohen, 2014; Nunez & Srinivasan, 2006; Schaworonkow & Nikulin, 2022; Schoffelen & Gross, 2009). This creates two challenges for studying whole brain functional networks with EEG. First, because the locations of electrodes are not trivially related to the locations of their sources, the topography of scalp-level EEG cannot be interpreted in terms of the underlying neuroanatomy (Lai et al., 2018; Mahjoory et al., 2017). For example, occipital alpha sources (8-13 Hz) can account for a very large part of the activity measured by frontal electrodes in simulated and empirical data, with the extent of this effect varying based on the dipole orientation of the source, the amplitude of the oscillations, cortical anatomy, and the choice of the reference electrode (Chella, Pizzella, Zappasodi, & Marzetti, 2016; Cohen, 2014; Haufe, Nikulin, Müller, & Nolte, 2013; Schaworonkow & Nikulin, 2022). Consequently, functional connectivity between, for example, a frontal and occipital electrode may not reflect functional connectivity a frontal and occipital source. However, by these same physical laws, differences in functional connectivity imply that different distributions of neuronal sources are active in the brain over space and time; thus, although volume conduction precludes a neurophysiological interpretation of the topography of scalp-level EEG, differences in functional connectome organization within and between individuals provide an opaque indication of differences in global network activity (Michel & Koenig, 2018; Schoffelen & Gross, 2009).

Second, because the same source can be measured by multiple electrodes simultaneously, there is a potential for estimates of functional connectivity between two electrodes to be confounded by those two electrodes measuring the same source (Cohen, 2014; Lai et al., 2018). Given that the ultimate purpose of functional connectivity analysis is to identify and quantify interactions between spatially separate neuronal populations, the challenges caused by volume conduction are non-trivial and it is now widely acknowledged that volume conduction should be accounted for in EEG functional connectivity analyses (Bastos & Schoffelen, 2016; Haufe et al., 2013; Lai et al., 2018; Nolte et al., 2004; Schoffelen & Gross, 2009).

To date, two main approaches have been employed throughout the literature to address the challenges caused by volume conduction. The first approach is to use inverse source reconstruction methods, which attempt to unmix the activity measured across all electrodes to estimate the location of the underlying sources (Michel & Brunet, 2019). Source localization is an ill-posed problem (i.e., it has an infinite number of solutions) that works by first modelling the volume conduction properties of the human head to determine the potential at each scalp electrode that would be generated by hypothetical dipoles in the brain (the forward model); then—taking into consideration the forward model and electrode noise—using an inverse source reconstruction algorithm (the source model) to estimate the dipole parameters that best explain the observed scalp potential measurements, based on constraints and assumptions imposed by the source model about the underlying sources (Grech et al., 2008; Michel & Brunet, 2019). The spatial fidelity and accuracy of source localization and subsequent functional connectivity estimates is affected by several factors, including the accuracy of the forward model (e.g., Akalin Acar & Makeig, 2013; C. Liu et al., 2023; Nielsen, Puonti, Xue, Thielscher, & Madsen, 2023; Taberna, Samogin, Marino, & Mantini, 2021), the chosen source model (e.g., Hatlestad-Hall et

al., 2023; Haufe et al., 2013; Q. Liu, Ganzetti, Wenderoth, & Mantini, 2018; Mahjoory et al., 2017), instrumental or biological noise (e.g., Ryynanen, Hyttinen, Laarne, & Malmivuo, 2004; Ryynanen, Hyttinen, & Malmivuo, 2006; Whittingstall, Stroink, Gates, Connolly, & Finley, 2003), and electrode density (e.g., Hatlestad-Hall et al., 2023; Michel & Brunet, 2019; Seeck et al., 2017); because of these factors, the validity of source space functional connectivity estimates may be in question in the absence of other sources of convergent evidence (e.g., fMRI, animal models, etc.). Inverse source reconstruction methods primarily address the first challenge for studying whole brain functional networks with EEG—by estimating the location of the underlying sources, signals are localized to dipoles in the brain, making it possible to interpret EEG in terms of the underlying neuroanatomy. However, artifacts of volume conduction persist in all source estimates (where they are often referred to as source or signal leakage), thus source-reconstructed EEG can still contain spurious estimates of functional connectivity (Bastos & Schoffelen, 2016; Haufe et al., 2013; Schoffelen & Gross, 2009).

The second approach to addressing the challenges caused by volume conduction is to use functional connectivity metrics that are unlikely to be explained by common sources and are thus robust to volume conduction (Nolte et al., 2004; Stam, Nolte, & Daffertshofer, 2007). A variety of robust functional connectivity metrics have been developed to accomplish this (Bastos & Schoffelen, 2016; Hipp, Hawellek, Corbetta, Siegel, & Engel, 2012), all of which operate under the same basic principle: Because volume conduction from a common source to multiple electrodes is instantaneous, electrodes measuring a common source will have their signals phase locked with a time lag of zero; conversely, phase locking with a nonzero time lag cannot be caused by volume conduction from a common source, so signals with a consistent nonzero phase difference are likely to have been generated by separate sources (Nolte et al., 2004; Stam et al.,

2007). Functional connectivity between such signals can, therefore, be interpreted in terms of true interactions between the underlying neuronal sources (Nolte et al., 2004; Stam et al., 2007). However, it is important to note that true zero lag interactions also occur in neuronal networks (Gollo, Mirasso, Sporns, & Breakspear, 2014), and it is likely that this approach misses parts of the brain's interactions, leading to the underestimation of connectivity strength between nodes (Cohen, 2015; Nolte et al., 2004; Stam et al., 2007). Thus, weak or absent functional connectivity with these metrics could either mean there truly is no interaction, or that the interaction between two sources is not consistently delayed such that one of the sources regularly leads or lags the other one (Nolte et al., 2004; Stam et al., 2007).

Finally, because EEG measures oscillations across a broad range of frequencies, and because neuronal populations are capable of generating and responding to multiple oscillation frequencies, it is generally necessary to further process EEG signals into single or multiple frequency bands using band-pass filtering in order to investigate oscillations occurring at different timescales (Sadaghiani & Wirsich, 2020). EEG is typically limited to investigating canonical frequency bands (i.e., Delta, 1-4 Hz; Theta, 4-8 Hz; Alpha, 8-13 Hz; Beta, 13-30 Hz; Gamma, 30-80 Hz). Furthermore, because of EEG's susceptibility to 60 Hz electrical line noise, the upper bound of the Gamma band is often reduced to a frequency below 60 Hz where artifacts from line noise are less prominent.

Revealing the intrinsic functional organization of the human brain

As the previous section established, EEG and fMRI signals reflect synchronized rhythmic fluctuations in the excitability of local neuronal populations, the timing of which is encoded by the phase of the signal and the magnitude of which by the amplitude. These fluctuations vary in

frequency, amplitude, and phase over time, reflecting the dynamics of neuronal activity caused by ongoing interactions within and between anatomically connected neuronal populations distributed throughout the cortex. As the dynamics of ongoing activity unfold upon this structural network, spatially distributed neuronal populations dynamically and recurrently couple to one another, forming creating a large and variable repertoire of stable intrinsic network states when integrated over longer time periods (Daniel Arzate-Mena et al., 2022; Deco & Corbetta, 2011; Garrett et al., 2013; Christopher J. Honey, Kötter, Breakspear, & Sporns, 2007; Hutchison et al., 2013; Sadaghiani & Wirsich, 2020; Sporns, 2022).

Functional connectivity analysis provides a useful framework for describing the coupling that occurs in neuronal networks and is based on the following assumption: If two nodes in a functional connectome have a (strong, consistent) statistical dependency between their signals over time, they are both likely to be involved in the same brain function(s), and thus functionally connected (Bijsterbosch, 2017; Engel et al., 2013). Because both EEG and fMRI signals are most strongly related to synchronized postsynaptic activity and not to neuronal firing rates, it is important to keep in mind that the coupling described by functional connectivity analysis is based on the inputs to local neuronal populations rather than their outputs (Bijsterbosch, 2017). Moreover, we limit our discussion here to same-frequency undirected functional connectivity analysis, which is currently the primary means of estimating functional connectivity used throughout the literature as well as this thesis. For discussions of cross-frequency coupling and directed functional connectivity analysis, we direct the reader to reviews by Canolty & Knight (2010) and Bastos & Schoffelen (2016), respectively.

A common acquisition method for functional connectivity analysis in the context of individual differences research is the resting state paradigm, which involves a passive state

wherein participants are simply required to sit or lie still with their eyes either closed or open and fixated on a cross (while blinking normally) for the duration of the recording, without being instructed to think of anything in particular (Gratton et al., 2020; S. M. Smith et al., 2013). The primary motivation behind this paradigm is that it is a robust method for measuring the intrinsic activity that accounts for the majority of the brain's energy demands (Raichle, 2010, 2015) that is: easy to acquire and standardize across sites and populations, including those that may not be able to perform more demanding cognitive or behavioural tasks during acquisition (Bijsterbosch, 2017; M. D. Fox & Greicius, 2010); and less vulnerable to confounds related to more demanding cognitive or behavioural tasks such as performance, motivation, strategy, practice, or repetition effects, making it suitable for longitudinal designs where stability over time is a point of interest (Finn et al., 2017; M. D. Fox & Greicius, 2010). Although the behavioural and cognitive demands of eyes closed and eyes open resting state are similar, each brain state is qualitatively distinct—with associated changes (on average) in the global power and topography of all oscillatory bands from eyes closed to eyes open resting state, the most prominent of these being a widespread reduction in alpha band oscillations (Barry, Clarke, Johnstone, & Brown, 2009; Barry, Clarke, Johnstone, Magee, & Rushby, 2007; Barry & De Blasio, 2017).

To date, two distinct modes of same-frequency intrinsic coupling have been identified throughout the EEG literature: *phase coupling* and *amplitude coupling* (Engel et al., 2013; Sadaghiani & Wirsich, 2020). Phase coupling involves the timing of rhythmic neuronal activity and is defined as the coupling between the phases of two signals, estimated by the consistency of their phase angle differences (i.e., phase lags) over time (Mostame & Sadaghiani, 2020; Stam et al., 2007). Many distinct metrics have been developed to quantify phase coupling between two signals, each of which differ in their assumptions, motivations, availability in statistical software,

and popular usage; however, what they have in common is their basic aim to capture and quantify different properties of the consistency of the distribution of phase angle differences over time (Bastos & Schoffelen, 2016).³ To clarify this concept, we simulated two scenarios depicting how the consistency of phase angle differences behaves for phase-coupled signals (Figure 3A) and independent signals (Figure 3B). For Figure 3A, we generated two 5 Hz sinusoidal waves with an initial phase of 145 degrees (Signal 1) and 25 degrees (Signal 2) and uncorrelated Gaussian white noise added to each signal, then calculated the instantaneous phase angle difference between the signals at each time point. For Figure 3B, the instantaneous phase angle difference was instead calculated between Signal 1 and a third signal of Gaussian white noise (Signal 3). A narrow peak in the instantaneous phase angle difference distribution can be observed with the phase-coupled signals (Figure 3A), in contrast to the relatively even distribution of instantaneous phase angle differences with the independent signals (Figure 3B).

³ Mathematical details and discussion of several widely used phase coupling metrics can be found in a review by Bastos & Schoffelen (2016).

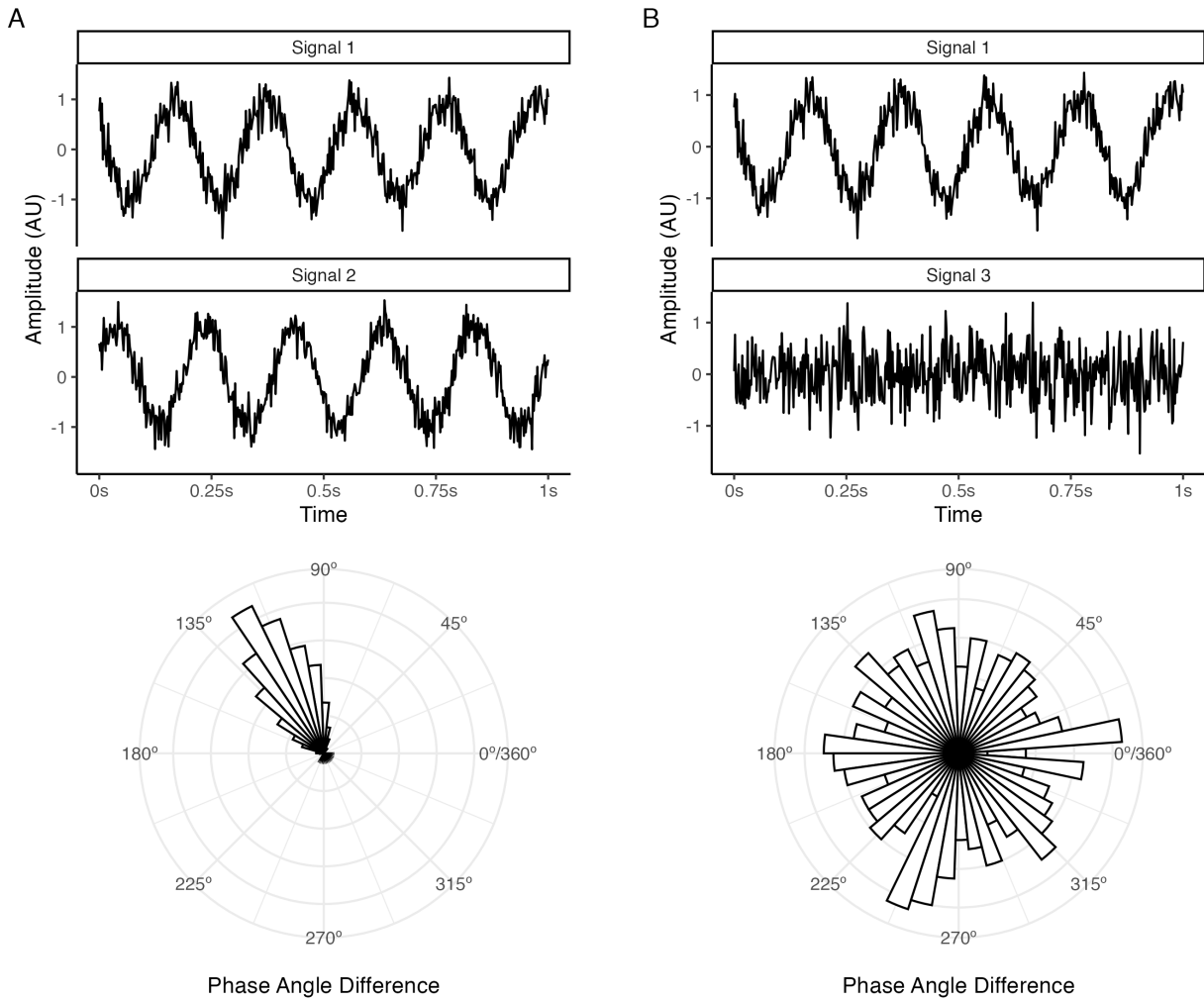


Figure 3. Illustration of instantaneous phase angle differences between two phase-coupled signals (A) and independent signals (B). The top plots in each panel depict the time course of two 5 Hz signals with a 145-degree phase (Signal 1) and 25-degree phase (Signal 2), and Gaussian white noise (Signal 3). The polar histogram plots depict the distribution of instantaneous phase angle differences between phase-coupled Signals 1 and 2 (A) and independent Signals 1 and 3 (B); a narrow peak in the instantaneous phase angle difference distribution can be observed with the phase-coupled signals, in contrast to the relatively even distribution of instantaneous phase angle differences with the independent signals.

Stable, state-invariant local and long range phase coupling has been observed across all oscillatory bands at both zero and nonzero phase lags using a variety of phase coupling metrics (Engel et al., 2013). The role of phase coupling in neuronal communication is fairly well-understood; as we described earlier, effective neuronal communication requires rhythmic synchronization within presynaptic and postsynaptic networks and coherence between them so that inputs consistently arrive during oscillatory phases of enhanced postsynaptic excitability, maximizing the probability they summate effectively and generate action potentials (Buzsáki, 2011; Buzsáki & Watson, 2012; Fries, 2015; Singer, 2018). Finally, we note that although it is also possible to assess phase coupling between fMRI BOLD signals (Honari, Choe, & Lindquist, 2021), these methods have not been used in the fMRI literature for network variant research; thus, phase coupling is generally regarded as a coupling mode unique to electrophysiological methods such as EEG and MEG (Engel et al., 2013).

Amplitude coupling involves the number of neurons active in a given rhythm and is defined as the coupling between the amplitude envelopes of two signals, estimated by the correlation of their amplitude envelopes over time (Bruns, Eckhorn, Jokeit, & Ebner, 2000; Hipp et al., 2012; Mostame & Sadaghiani, 2020). This is similar in principle to fMRI BOLD functional connectivity analysis—wherein coupling between two BOLD signals is assessed by the correlation of their amplitudes over time—as both methods can be used to capture slow fluctuations in neural activity (Engel et al., 2013). To clarify this concept, we simulated 1000 realizations of two amplitude modulated signals consisting of either a 30 Hz or 50 Hz sinusoidal wave modulated by a 3 Hz sinusoidal wave, with Gaussian white noise added to both the carrier and modulating waves; for each realization, we then estimated the absolute correlation coefficient between either the real signals or their amplitude envelopes. Figure 4A illustrates the basic

mechanism behind amplitude modulation, wherein the phase dynamics of a low frequency signal modulates the amplitude of a higher frequency signal, and of how this is captured in the amplitude envelope of the amplitude modulated signal. Figure 4B displays the simulation results. A strong correlation can be observed between the low frequency amplitude envelopes of the two signals, in contrast to the correlations between the high frequency real signals which are clustered around zero.

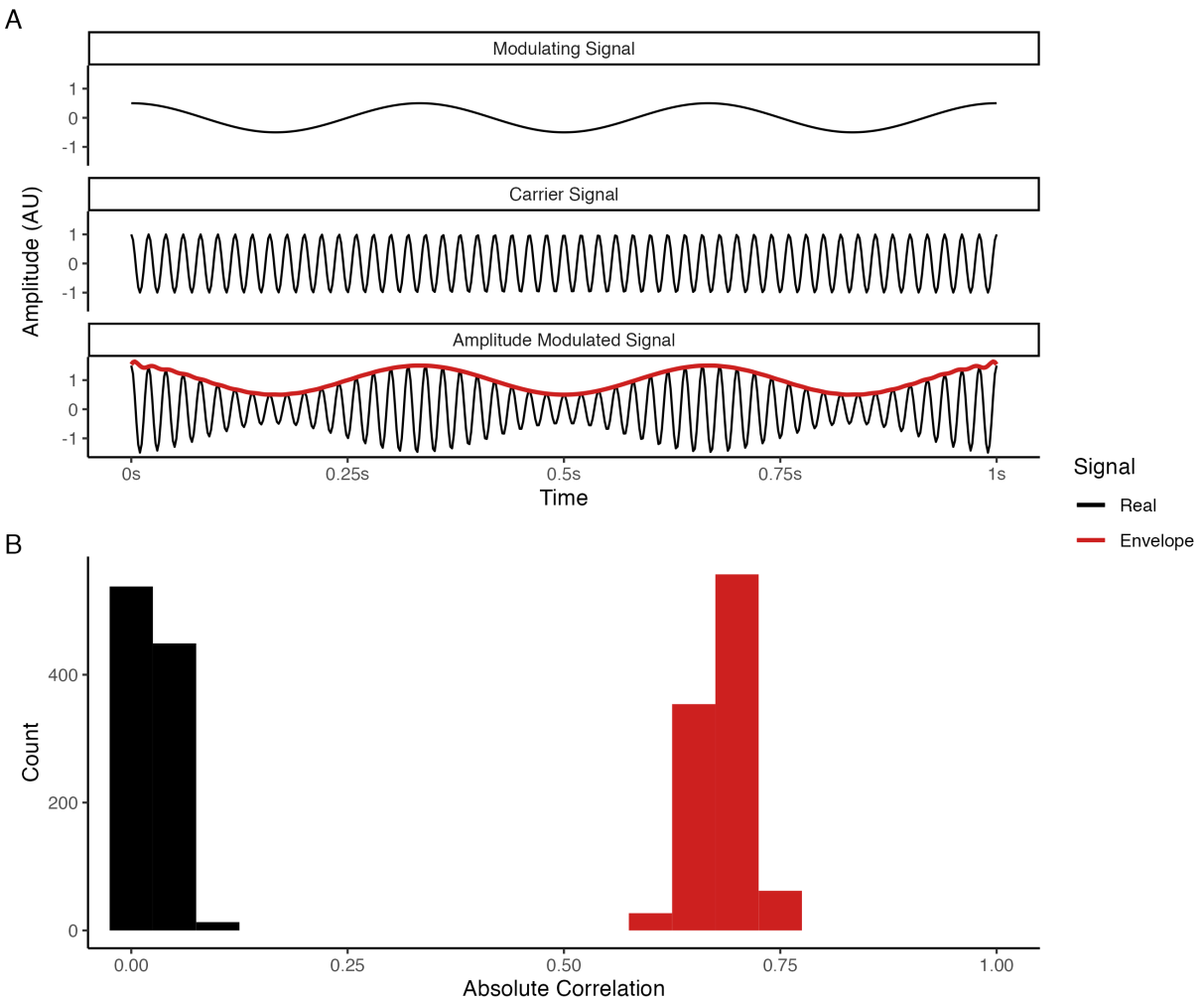


Figure 4. Illustration of amplitude modulation (A) and the difference between the amplitude correlation and amplitude envelope correlation of high frequency signals. Panel A depicts how

the amplitude envelope of an amplitude modulated signal captures the phase dynamics of a low frequency modulating signal. Panel B displays the simulation results; a strong correlation can be observed between the amplitude envelopes of the two signals, in contrast to the correlations between the real signals which are clustered around zero.

Stable, state-invariant local and long range amplitude coupling has predominantly been observed at frequencies below 0.1 Hz (in terms of the amplitude envelope frequency) for both zero and nonzero phase lagged signals in all oscillatory bands (Buzsáki & Watson, 2012; Engel et al., 2013; Hipp et al., 2012; Z. Liu, Fukunaga, De Zwart, & Duyn, 2010). The role of amplitude coupling in neuronal communication is poorly understood; however, investigations comparing the spatiotemporal dynamics of phase coupling and amplitude coupling have found that the two coupling modes can occur independently of one another, with each mode containing common, but also complementary and divergent spatiotemporal dynamics under various conditions (Bruns et al., 2000; Hindriks & Tewarie, 2023; Mostame & Sadaghiani, 2020; Siems & Siegel, 2020). Thus, amplitude coupling is generally assumed to fulfill a dissociable function from phase coupling in neuronal communication (Engel et al., 2013; He et al., 2019). Although more investigation is needed, a putative role of amplitude coupling based on several proposals is that high amplitude bursts in one population may be sufficient to make another population jump from low to high amplitude oscillatory activity—even when their phase and preferred frequencies are independent—providing a less restrictive, parallel mechanism for coordinating which neuronal populations participate in a functional network (Brookes et al., 2011; Bruns et al., 2000; Engel et al., 2013; Hindriks & Tewarie, 2023; Mostame & Sadaghiani, 2020).

Individual differences and the functional organization of the human brain

Due to the highly individualistic trajectories of human brain development, the structural organization of neuronal networks varies greatly between individuals across the lifespan (Bateson, 2017; Brown, 2017; Gu & Kanai, 2014; Lewis, 2005). Unsurprisingly, the spatiotemporal dynamics of neuronal activity unfolding upon this network also varies greatly between individuals, which has been known since various neuroimaging modalities—including EEG (e.g., Adrian & Mathews, 1934; Berger, 1929; Henry, 1941) and fMRI (e.g., Roland & Zilles, 1998)—were first used to measure human brain activity. Despite this knowledge, network neuroscience research has mainly relied on group-averaged statistical approaches based on abstract models of the average human brain, wherein functional connectivity analysis is either performed on the concatenated recordings of all participants, or where functional connectivity estimates are averaged across participants (e.g., Power et al., 2011; Yeo et al., 2011). Under these approaches, individual differences are typically treated as a nuisance factor to be eliminated (e.g., Brett, Johnsrude, & Owen, 2002), and it is not uncommon for researchers using these approaches to commit an ecological fallacy (e.g., Caramazza, 1986; Henson, 2005), wrongly assuming that conclusions drawn from abstract models of the average human brain are universal and generalizable to (almost) every human brain (Van Horn, Grafton, & Miller, 2008; Viola, 2020). In turn, deviations from this abstract model are typically treated as either abnormal “outliers” or “noise” to be ruled out for the sake of generalizability (Van Horn et al., 2008; Viola, 2020).

Previous work using these group-averaged statistical approaches has established that the human functional connectome is governed by an intrinsic functional architecture, wherein functional networks exhibit spontaneous coupling between their nodes that can be captured in both the absence and presence of cognitive demands (M. D. Fox et al., 2005; Petersen & Sporns,

2015; Power et al., 2011; Raichle, 2015; Uddin et al., 2019; Yeo et al., 2011). Although consensus around the taxonomy of these networks is considerably variable (Uddin et al., 2023), many studies have replicated the presence of these networks across different samples (e.g., Power et al., 2011; Yeo et al., 2011) and with different neuroimaging modalities (Engel et al., 2013; Mostame & Sadaghiani, 2021; Sadaghiani & Wirsich, 2020), establishing that their organization is relatively stable when data are concatenated or averaged across groups of participants (Kraus et al., 2023). This work suggests that the human functional connectome is governed by some common organizational aspects across individuals, which can be measured using either fMRI or EEG/MEG.

Despite these commonalities, a growing body of evidence has found reliable and substantial interindividual variability in connectivity strength, the size and position of network nodes, and network topography across individuals (Gordon & Nelson, 2021; Uddin et al., 2023, 2019). Emphasizing the significance of these forms of interindividual variability to our understanding of whole brain functional network organization, Uddin et al. (2023) write:

Given this variation, how can we determine that a network is the same entity across different individuals or groups? If we find an individual missing specific components of Network A or with a spatial topography similar but slightly displaced relative to Network A, would it be accurate to call this Network A? In what ways, and to what extent, can a network vary but still represent the same underlying entity? To what extent should we expect certain networks to only be expressed in some individuals but not others? (p. 878)

Whether or not these individual differences constitute unique network entities or deviations from the same entities remains an open question; however, the implications of each of

these forms of interindividual variability for interpreting measures of functional connectivity are clear: Without studying the functional connectomes of individuals to identify real, concrete examples of how much and in which ways people do and do not vary, our understanding of whole brain functional network organization and its relationship to behaviour, cognition, and their dysfunction will remain rather abstract and nebulous (Gordon & Nelson, 2021; Naselaris, Allen, & Kay, 2021; Uddin et al., 2023, 2019; Van Horn et al., 2008).

It is only over the past decade that individual differences have become a topic of focus in network neuroscience research, as the field has begun to confront the challenges associated with developing and refining a taxonomy of whole brain functional networks—recognizing that developing a standardized taxonomy of whole brain functional networks requires an understanding of individual differences in functional connectome organization, and a clear assessment of the degree to which these differences affect our ability to identify common principles of organization across individuals (Dworetzky et al., 2021; Gordon & Nelson, 2021; Uddin et al., 2023, 2019). These developments mark a substantial paradigm shift (Kuhn & Hacking, 2012) in the basic efforts of network neuroscience research—away from the near-exclusive use of group-averaged statistical approaches based on abstract models of the average human brain (which by definition cannot represent the types of connectional, spatial, and topological variation found in individual brains), and towards individual-level approaches that seek to answer *how much* and *in which ways* whole brain functional networks differ between and within individuals—and it is anticipated that the results of these efforts will lead to more robust, precise, and replicable accounts of the neural causes of variation in human behaviour, cognition,

and their dysfunction (Elliott et al., 2020; Fedorenko, 2021; Finn et al., 2017; Gordon & Nelson, 2021; Gratton, Nelson, & Gordon, 2022; Uddin et al., 2023, 2019).⁴

Much of the growing interest in individual-level approaches has been driven by large research consortia projects such as the Human Connectome Project (Elam et al., 2021; Van Essen et al., 2012), which have made it feasible to study connectivity in whole brain functional networks across large numbers of people using high-quality open data; intensive (single-person) longitudinal studies such as the MyConnectome project (Poldrack et al., 2015), which have served as proofs of concept for studying within-individual change in connectivity over the course of days or months; technological and methodological advances that have made the characterization of brain function at an individual level possible with fMRI and EEG/MEG (for fMRI, see Dubois & Adolphs, 2016; for EEG/MEG, see Sadaghiani & Wirsich, 2020); a growing number of studies demonstrating that interindividual variability in connectivity strength, the size and position of network nodes, and network topography is the norm, *not* the exception, for the

⁴ For historically interested readers, this renewed interest in individual differences for network neuroscience research is much akin to Cronbach's (1957) treatise on the historic separation of scientific psychology into two distinct disciplines—the so-called *experimental* and *correlational* disciplines, which broadly speaking studied variance only among either treatments or individuals, respectively—and the need for these disciplines to combine their efforts if the field ever hopes to solve its most important problems. Similar reflections are now being seen in the field of network neuroscience, as researchers increasingly recognize the importance of studying the variation that already exists between and within individuals to further our understanding of the human brain (e.g., Elliott et al., 2020; Gratton et al., 2022; Uddin et al., 2023, 2019).

functional organization of the human brain (e.g., Bijsterbosch et al., 2018; Finn et al., 2015; Gordon, Laumann, Adeyemo, et al., 2017; Gordon et al., 2017; Gordon, Laumann, Gilmore, et al., 2017; Gratton et al., 2018; Kong et al., 2019; Miranda-Dominguez et al., 2014; Mueller et al., 2013; Seitzman et al., 2019; D. M. Smith et al., 2023); and most recently, working groups within the network neuroscience community such as the Organization for Human Brain Mapping's Workgroup for Harmonized Taxonomy of Networks, who have identified interindividual variability as a key issue in building a standardized taxonomy of whole brain functional networks (Uddin et al., 2023).

Coinciding and resulting from these efforts, there has been an increased awareness over the past decade that although group-averaged statistical approaches based on abstract models of the average human brain can provide us with clues about common organizational aspects of the human functional connectome, they can also underestimate or entirely miss real features that can be reliably measured in individuals (Fedorenko, 2021; Fedorenko & Blank, 2020; Mueller et al., 2013; Speelman & McGann, 2013; Zilles & Amunts, 2013). Likewise, these efforts have also found that although reliable brain-behaviour relationships can be identified using group-averaged statistical approaches such as cross-sectional designs, doing so requires large samples and the effect sizes underlying these relationships are typically small (Marek et al., 2020); whereas more robust brain-behaviour relationships can be identified in small, focused samples using individual-level approaches such as intensive (single-person) longitudinal designs with highly sampled neuroimaging data recorded over multiple sessions (Gordon & Nelson, 2021; Gratton et al., 2022; Naselaris et al., 2021; Newbold et al., 2020). Finally, it has become apparent that tasks originally developed to elicit robust group-averaged effects when contrasting specific experimental conditions (e.g., from cognitive neuroscience) have poor test-retest reliability when used to study

individual differences (Elliott et al., 2020)—highlighting the importance of selecting tasks which have been demonstrated to be reliable and valid for studying individual differences in functional connectivity, such as resting state or naturalistic paradigms (Finn & Bandettini, 2020; Finn et al., 2020; Finn et al., 2017), and more broadly, of developing and identifying tasks that can be used to bring out meaningful idiosyncrasies across individuals (Elliott et al., 2020; Finn et al., 2017; Greene, Gao, Scheinost, & Constable, 2018; Kraus et al., 2021). Thus, studying network variants involves a shift in both the types of questions asked and the methods used to examine them relative to the group-averaged statistical approaches that have accounted for the vast majority of network neuroscience research to date—a shift that places focus on the individual as the primary unit of analysis (Fedorenko, 2021; Gordon & Nelson, 2021; Gratton et al., 2022; Kraus et al., 2023; Naselaris et al., 2021).

Characterizing network variants

Although neurophysiological imaging modalities such as EEG have been identified as an important component to enrich our understanding of individual differences in whole brain functional network organization (Gratton et al., 2018; Sadaghiani & Wirsich, 2020; Uddin et al., 2023), current characterizations of network variants are almost exclusively based on fMRI research methods. Below we discuss the key findings of this work, including: (1) methods that reliably capture individual whole brain functional networks; (2) what studies of individual whole brain functional networks reveal about common and idiosyncratic forms of organization; and (3) the relationship between individual whole brain functional networks and behaviour.

As we noted in the previous section, group-averaged statistical approaches to studying the human functional connectome have traditionally proceeded by either performing functional

connectivity analysis on the concatenated recordings of all participants, or by averaging functional connectivity estimates across participants (e.g., Power et al., 2011; Yeo et al., 2011). Moreover, in response to published recommendations, these approaches typically collect only a small amount of data per participant in terms of recording duration (e.g., 5-10 minutes), as this amount of data is generally sufficient to obtain reliable results when averaging across participants (Shehzad et al., 2009; Van Dijk et al., 2010); however, doing so precludes the possibility of reliably characterizing whole brain functional network organization at an individual level due to the relatively low temporal signal-to-noise ratio of fMRI data (Anderson, Ferguson, Lopez-Larson, & Yurgelun-Todd, 2011; Gordon, Laumann, Gilmore, et al., 2017; Laumann et al., 2015; Xu et al., 2016).

In contrast, capturing individual whole brain functional networks requires functional connectivity analysis and other measures of interest (e.g., graph theoretical measures) to be performed at an individual level prior to making any comparisons between individuals in order to preserve interindividual variability (Elliott et al., 2019; Gordon, Laumann, Gilmore, et al., 2017; Laumann et al., 2015). The exact quantity of data needed for reliable individual-level estimation has been found to vary depending on the measure of interest and across different sampling methods (Anderson et al., 2011; Elliott et al., 2019; Gordon, Laumann, Gilmore, et al., 2017; Hacker et al., 2013; Laumann et al., 2015; Noble et al., 2017). For example, Gordon, Laumann, Gilmore, et al. (2017) found that, on average, a minimum of 30 minutes of eyes open resting state data (retained after motion correction) was required to achieve reliable functional connectivity estimates across participants ($r > .85$); whereas reliable network assignment using community detection algorithms required a minimum of 90 minutes (Dice coefficient $> .75$), and other graph theoretic measures (participation coefficient, global efficiency, and modularity) required a

minimum of anywhere from 10 to 80 minutes. With less than 10 minutes of resting state data all measures yielded low reliability estimates, as well as systematic bias for graph theoretical measures. Additionally, Elliott et al. (2019), Laumann et al. (2015), and Noble et al. (2017) each found that similar or greater reliability could be obtained by acquiring shorter recordings over more sessions compared to longer recordings over fewer sessions (e.g., 15 minutes from two sessions compared to 30 minutes from one session) when combining recordings into a single data set.

Together, these results emphasize the importance of collecting sufficient data per participant to counteract the sampling variability of the fMRI BOLD signal and obtain reliable estimates at an individual level (Anderson et al., 2011; Elliott et al., 2019; Gordon, Laumann, Gilmore, et al., 2017; Hacker et al., 2013; Laumann et al., 2015; Noble et al., 2017). Additionally, care is needed when collecting and preprocessing these data, as non-neural artifacts such as motion (Power, Barnes, Snyder, Schlaggar, & Petersen, 2012; Power, Lynch, Adeyemo, & Petersen, 2020; Power et al., 2014; Satterthwaite et al., 2012; Van Dijk, Sabuncu, & Buckner, 2012), respiration (Birn, Smith, Jones, & Bandettini, 2008; Chang & Glover, 2009), and signal loss due to acquisition parameters, head shape or head position (Noble et al., 2017) can also induce unintentional interindividual variability in functional connectivity (Uddin et al., 2023).

When such confounds are adequately addressed, it becomes evident that at least three different forms of reliable and substantial interindividual variability are present in individual whole brain functional networks: connectivity strength, the size and position of network nodes, and network topography (Gordon & Nelson, 2021; Uddin et al., 2023, 2019). Connectivity strength—the magnitude of BOLD signal coupling between nodes—is the most commonly studied form of interindividual variability (Gordon & Nelson, 2021; Uddin et al., 2023).

Interindividual variability in connectivity strength has been found to be largely stable over time and across different tasks, suggesting that the majority of whole brain functional network organization arises from stable factors involved in individualistic developmental trajectories (e.g., genetic, environmental, and psychological differences; developmental histories; etc.), rather than more transient factors (e.g., ongoing cognition, day-to-day fluctuations, etc.) (Finn et al., 2017; Gratton et al., 2018; Kraus et al., 2021).⁵ The relative magnitude of these differences has been found to be large enough that functional connectome similarities are consistently greater within than between individuals (Gordon, Laumann, Gilmore, et al., 2017; Gratton et al., 2018) to such an extent that (1) functional connectomes from the same individual can be accurately matched when comparing a given individual's connectome against all other connectomes in a sample across scan conditions (Finn et al., 2017, 2015), and over months, years, and the lifespan (Horien, Shen, Scheinost, & Constable, 2019; Jalbrzikowski et al., 2020; St-Onge et al., 2023); and (2) the functional network affiliation of a given network node can vary across individuals, even when that node is spatially consistent across individuals (Gordon, Laumann, Gilmore, et al., 2017; Gordon & Nelson, 2021).

⁵ To be clear, this is not to say that brain state or time have no influence on interindividual variability in connectivity strength. Indeed, the relative magnitude of functional connectome similarities within and between individuals has been found to vary moderately by behavioural or cognitive state and mildly by time such that individualization is measurably greater during certain brain states than others, and slightly greater for recordings taken during the same session (Finn et al., 2017; Gratton et al., 2018; Seitzman et al., 2019). However, this influence is considerably smaller relative to the influence contributed by individuals themselves (Gratton et al., 2018).

Spatial variability in the size and position of network nodes represents a second form of interindividual variability (Gordon & Nelson, 2021; Uddin et al., 2023). It is well-established that cortical areas vary in their size, shape, and location across individuals, even after precise surface-based anatomical alignment (Frost & Goebel, 2012; Van Essen, Glasser, Dierker, Harwell, & Coalson, 2012); thus, it follows that this spatial variability would also be present in the organization of functional networks across individuals (Gordon & Nelson, 2021). Indeed, such spatial variability has been repeatedly found throughout the cortex (Gordon et al., 2017; Harrison et al., 2015; Kong et al., 2019; Li et al., 2019; Wang et al., 2015), taking the form of areal expansions, contractions, or displacements of network nodes that lead to variation in (1) the exact positions of functional network borders across individuals; and (2) the functional network affiliation of a given network node across individuals (Gordon & Nelson, 2021; Uddin et al., 2023). The relative magnitude of this variability has been found to be large enough that many details of functional network organization are lost when using group-averaged approaches (e.g., the fractionation of larger networks into parallel distributed subnetworks), such that these features can only be identified at an individual level (Braga & Buckner, 2017; Braga, Van Dijk, Polimeni, Eldaief, & Buckner, 2019; DiNicola, Braga, & Buckner, 2020; Gordon et al., 2017; Gordon, Laumann, Gilmore, et al., 2017; Gordon et al., 2020; Gordon & Nelson, 2021). Additionally, at an individual level, areal expansions and contractions appear to be interdependent within and between functional networks, such that (1) nodes of the same functional network tend to expand or contract together; and (2) the relative expansion of a given functional network tends to reduce the amount of cortex available to other adjacent, connected functional networks (Gordon et al., 2017).

Neither connectional nor spatial variability appear to be evenly distributed throughout the cortex—instead there appears to be a characteristic distribution of interindividual variability across individuals, such that certain functional networks and network nodes show greater individualization than others (Gratton et al., 2018; Seitzman et al., 2019). For example, recent work suggests that functional networks associated with higher-level functions show greater individualization than functional networks associated with sensorimotor processing (Gratton et al., 2018; Mueller et al., 2013; Seitzman et al., 2019); that nodes near the borders of functional networks previously described using group-averaged approaches tend to have more variable network affiliations across individuals than nodes that are not near borders (Gordon et al., 2017); and that individuals can be separated into trait-like subgroups based on similar distributions of interindividual variability in connectivity strength or the size and position of network nodes (Gordon et al., 2017; Gratton et al., 2018; Seitzman et al., 2019). Together, these findings suggest that the interindividual variability described thus far stems from (systematic) individual deviations from a basic organizing structure that is common across individuals (Gordon et al., 2017; Gratton et al., 2018; Seitzman et al., 2019).

Indeed, an important assumption when studying each of the previous forms of interindividual variability is that every individual functional connectome has the same network topography—that is, they each have the same set of matched network nodes (Gordon & Nelson, 2021). These nodes may vary in their connectivity strength, size, position, or even their functional network affiliations, however, ultimately they are assumed to represent the same cortical components across individuals, making direct comparisons between individuals possible (Gordon & Nelson, 2021). This assumption is broadly supported in the literature. Although reliable and substantial interindividual variability is present in whole brain functional networks,

these networks also appear to share common organizing principles across individuals, such that individuals largely seem to have the same set of functional networks composed of the same sets of network nodes (Gordon et al., 2017). For example, recent work has found that the boundaries between the default mode network and other functional networks can be readily identified within individuals (Braga & Buckner, 2017; Braga et al., 2019; DiNicola et al., 2020; Gordon et al., 2017; Gordon, Laumann, Gilmore, et al., 2017; Gordon et al., 2020; Uddin et al., 2023), in line with the idea that a common basic organizing structure exists across individuals (Gordon et al., 2017; Gratton et al., 2018; Seitzman et al., 2019).

However, on a local level, interindividual variability in network topography can cause single cortical areas representing network nodes—which appear unitary in group-averaged data and most individuals—to split into multiple discontinuous regions, creating apparent extra network nodes in every individual that are not typically present in other individuals (Glasser et al., 2016; Gordon & Nelson, 2021; Laumann et al., 2015; Seitzman et al., 2019; Uddin et al., 2023). In some cases, these apparent extra network nodes have been found to exhibit the same properties as the unitary area (Glasser et al., 2016); however, in others these nodes have been found to exhibit strong, idiosyncratic connectivity with a functional network different from the one they are situated within (Gordon & Nelson, 2021; Laumann et al., 2015; Seitzman et al., 2019; Uddin et al., 2023). As Gordon & Nelson (2021) explain, the interpretation of this third form of interindividual variability is currently unclear, as it represents network nodes that are so connectionally and spatially divergent from group-averaged data and most other individuals that they may not be classifiable using existing approaches: Topographical variability may simply represent extreme examples of the spatial or connectional variability described above, or it may

indeed represent cortical components that do not exist in the networks of most other individuals. Such possibilities remain to be investigated in future work.

An important question for studies of network variants is whether or not interindividual variability in connectivity strength, the size and position of network nodes, or network topography relates to individual differences in behaviour, cognition, and their dysfunction (Finn et al., 2017; Seitzman et al., 2019). One possibility is that this interindividual variability is functionally significant, with at least some aspects of this variability interacting within individuals to produce differences in behaviour and cognition (Gordon et al., 2017; Seitzman et al., 2019). Conversely, an alternative possibility is that this interindividual variability is functionally degenerate (Friston & Price, 2003; Price & Friston, 2002; Tononi, Sporns, & Edelman, 1999)—that is, this variability may represent diverse but equivalently effective modes of functional organization, such that equivalent behavioural and cognitive outcomes may be instantiated by different patterns of organization (Gordon et al., 2017; Seitzman et al., 2019).

Although such possibilities have yet to be directly addressed, several studies have demonstrated that predictive models trained on features derived from connectivity strength, network size, and network topography can be used to predict individual differences in behaviour and cognition in novel participants. For example, features derived from connectivity strength have been demonstrated to predict individual differences in age (Pervaiz, Vidaurre, Woolrich, & Smith, 2020), sex (Pervaiz et al., 2020), fluid intelligence scores (Finn et al., 2015; Greene et al., 2018; Pervaiz et al., 2020), composite scores of cognition and emotion (Finn & Bandettini, 2020), neuroticism scores (Pervaiz et al., 2020), sustained attention ability (Monica D. Rosenberg et al., 2016), and changes in attentional state over minutes, days, weeks, and months (Monica D. Rosenberg et al., 2020). Features derived from network size and network topography have been

demonstrated to predict individual differences in scores on several cognition, personality, and emotion measures (Kong et al., 2019). Together these results suggest that all three of these forms of interindividual variability may indeed be functionally significant for a wide range of behavioural and cognitive measures. However, in order to move us closer to an understanding of how much and in which ways these forms of variability may interact within individuals to produce differences in behaviour and cognition, further research is needed to characterize these relationships with greater precision, accuracy, and detail (Finn & Rosenberg, 2021; Mantwill, Gell, Krohn, & Finke, 2022; Seitzman et al., 2019; Wu, Li, Eickhoff, Scheinost, & Genon, 2023).

The present study

The purpose of the present study is to explore the feasibility of studying network variants with EEG across several canonical frequency bands using measures of both phase coupling and amplitude coupling. To address this question, we used EEG data from fourteen participants previously collected by our lab as part of a larger study, containing a total of 30 minutes eyes open resting state data (over 6 recordings) and 30 minutes eyes closed resting state data (over 6 recordings) from each participant collected during three sessions over the course of approximately three months. Each session consisted of four 5-minute recordings (2 eyes open, 2 eyes closed), with the time between sessions ranging from approximately one to two weeks from the first to second session, and approximately three months from the second to third session. With this design we were able to explore how functional connectomes differed within and between individuals, sessions, and states, and thus, whether or not higher frequency functional connectomes measured with EEG share similar evidence of stable individual differences to what has been described in the fMRI literature (e.g., Gordon, Laumann, Gilmore, et al., 2017; Gratton

et al., 2018). Specifically, we were interested in how much and in which ways patterns of sensor-space connectivity strength varied within and between individuals across these different contexts.

To facilitate these comparisons, we estimated the strength of sensor-space connectivity using the phase lag index (PLI; Stam et al., 2007) and the orthogonalized amplitude envelope correlation (AEC; Hipp et al., 2012), which measure phase coupling and amplitude coupling, respectively. We then used matrix correlations to quantify the similarity between pairs of functional connectomes, reducing the dimensionality of these data to a single interpretable number suitable for subsequent analyses, which served as an index of (inter)individual differences in underlying global network activity. These correlations take values between 0 (no linear relationship) and 1 (perfect linear relationship), defining a scale of similarity between two functional connectomes that can be interpreted in a straightforward manner in much the same way as the familiar squared Pearson correlation coefficient (Josse & Holmes, 2016; Mayer, Lorent, & Horgan, 2011).

This dataset was particularly well-suited to address this question, given that we had sufficient data per participant, session, and state to examine how functional connectome similarity differed within and between individuals across contexts via the interaction of (1) session-dependent variability over the course of weeks and months, and (2) state-dependent variability over the course of minutes during different resting states. Figure 5 depicts six hypothetical outcomes we could find based on different assumptions about the underlying global network activity. The left column shows outcomes that would occur in cases where functional connectomes *do not* differ between individuals. In particular, we might expect to see (1) a *group effect* with high similarity among all measurements regardless of individual, session, or state, which might occur if the underlying activity we measured is largely intrinsic and common across

individuals (cf. Raichle, 2010); (2) a *group-session effect* with high similarity among all measurements regardless of individual or state, but not session, which might occur if the underlying activity we measured is largely intrinsic, common across individuals, and varies over time in the same way across individuals; or (3) a *group-state effect* with high similarity among all measurements regardless of individual or session, but not state, which might occur if the underlying activity we measured is largely reactive in a way that is common across individuals (cf. Raichle, 2010). The right column shows outcomes that would occur in cases where functional connectomes *do* differ between individuals. In particular, we might expect to see (4) an *individual effect* with high similarity among all measurements regardless of session or state, but not individual, which might occur if the underlying activity we measured is largely intrinsic and unique within individuals; (5) an *individual-session effect* with high similarity among all measurements regardless of state, but not individual or session, which might occur if the underlying activity we measured is largely intrinsic, unique within individuals, and varies over time within individuals; or (6) an *individual-state effect* with high similarity among all measurements regardless of session, but not individual or state, which might occur if the underlying activity we measured is largely reactive in a way that is unique within individuals.

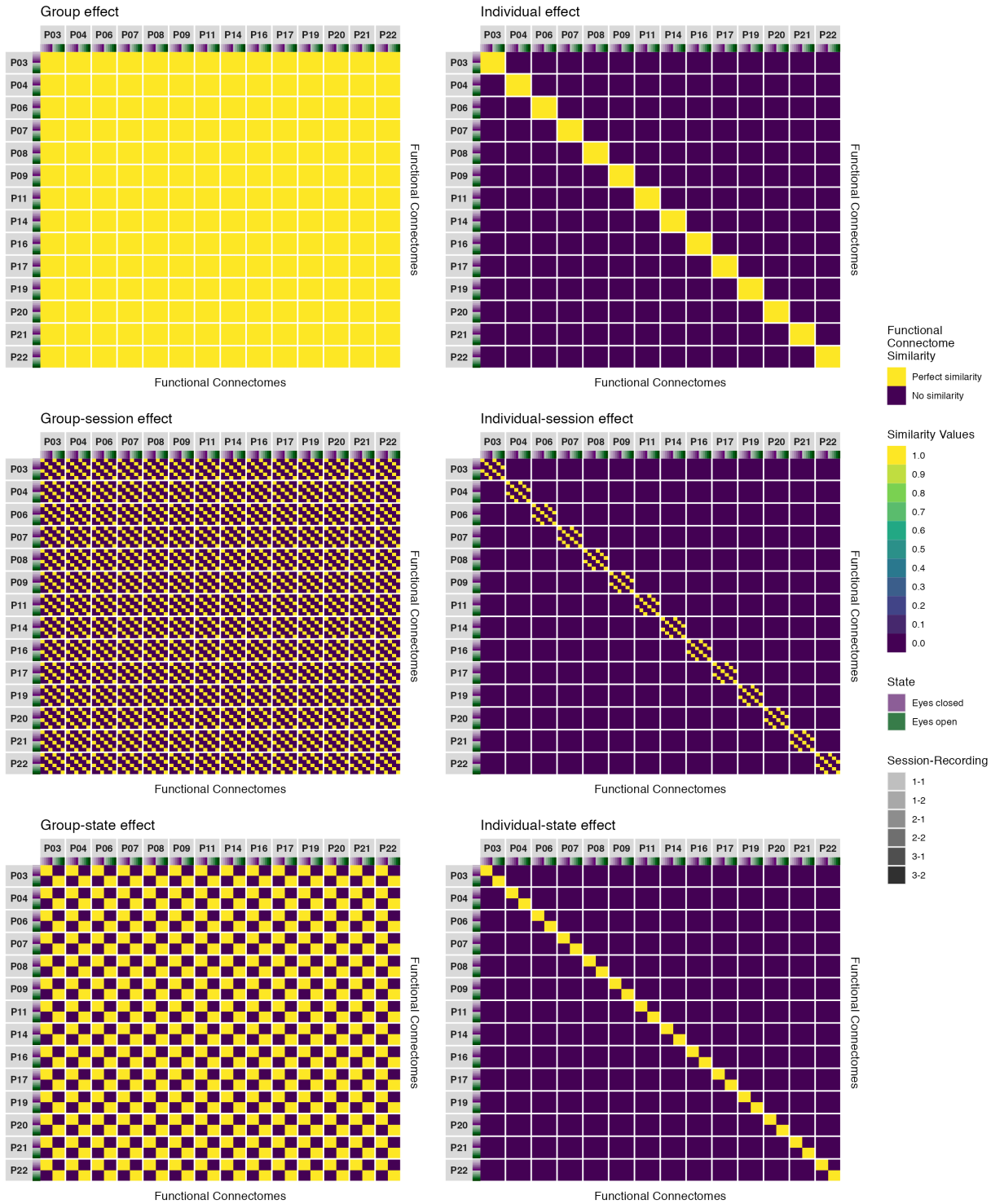


Figure 5. Similarity matrices depicting six hypothetical outcomes of functional connectome similarity that could occur if brain activity is common across individuals (group, group-session,

or group-state effects) or unique within individuals (individual, individual-session, or individual-state effects).

To quantify these effects, we used pairwise contrasts to estimate the direction and magnitude of differences in functional connectome similarity within and between individuals across sessions and states. Figure 6 illustrates these contrasts as they relate to the six hypothetical outcomes depicted in Figure 5 above. These contrasts were the estimands (i.e., the target quantities; Lundberg, Johnson, & Stewart, 2021) of this study, with differences estimated for (1) the overall difference in similarity within and between participants, which we term the *main effect*; (2) the difference in similarity within and between participants for each level of one predictor (e.g., within session similarity) while averaging over levels of the other predictor (e.g., within and between state similarity); (3) the difference in similarity within and between participants for the unique combinations within and between session and state. As Figure 6 makes clear, when there are equal amounts of functional connectome similarity within and between participants (i.e., when the underlying activity is common across individuals) there is zero difference in functional connectome similarity within versus between participants regardless of the underlying group, session, or state effects; however, when functional connectomes are more similar within than between participants (i.e., when the underlying activity is unique within individuals) there is a positive, non-zero difference which varies according to the type of individual effect (individual, individual-session, or individual-state effects). Thus, under this approach, a necessary condition for network variants to be detected is a positive, non-zero difference in functional connectome similarity.

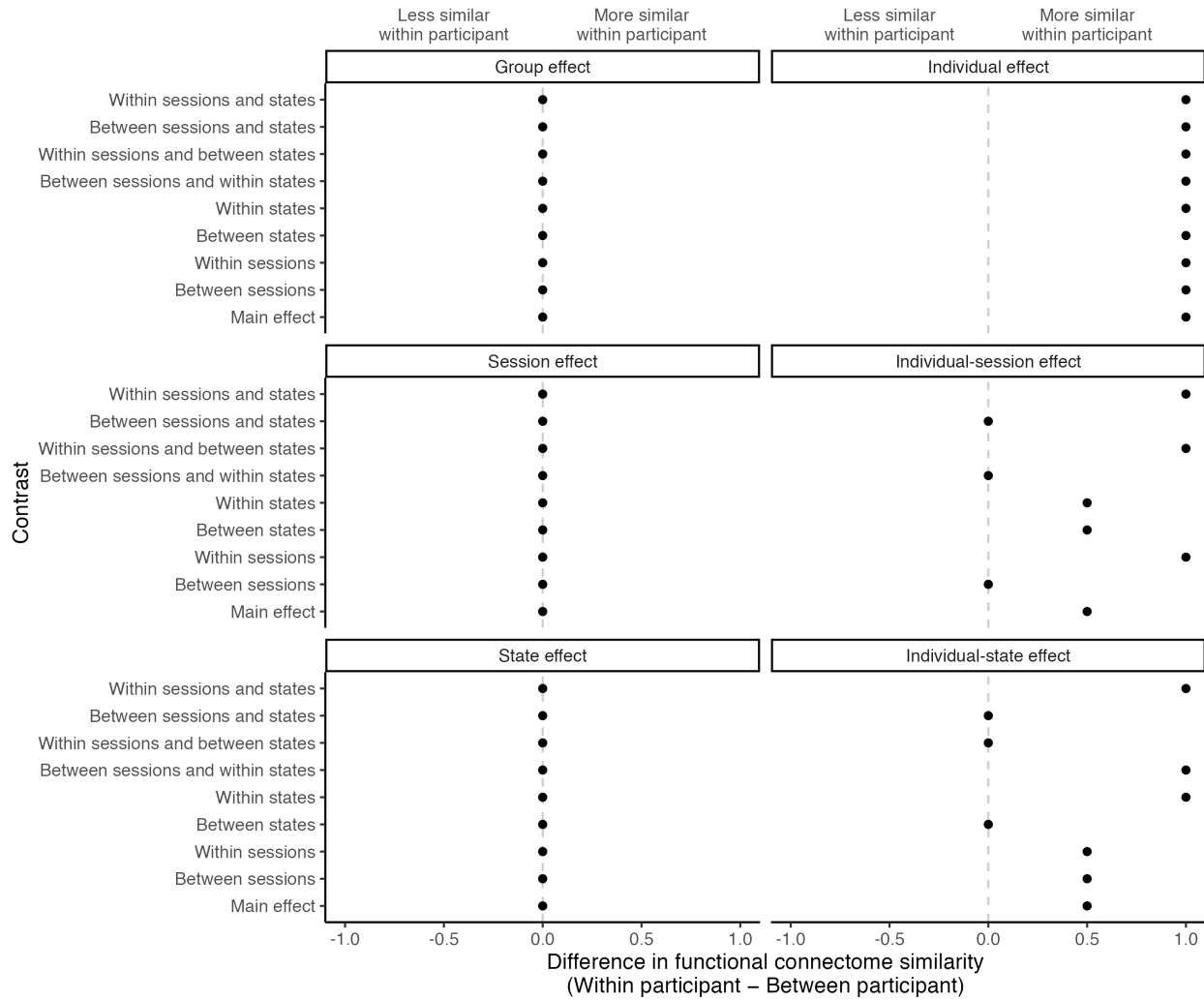


Figure 6. Contrasts illustrating differences in functional connectome similarity across the six hypothetical outcomes depicted in Figure 5. When brain activity is common across individuals (group, group-session, or group-state effects) there is zero difference in functional connectome similarity within versus between individuals; however, when brain activity is unique within individuals (individual, individual-session, or individual-state effects) there is a positive, non-zero difference which varies according to the type of individual effect.

Here we focus on the estimation of the direction, strength, and uncertainty of these effects in our sample—explicitly refraining from a null-hypothesis significance testing approach in

favour of an estimation approach (Berner & Amrhein, 2021). We favour an estimation approach for the following reasons: First, as we illustrated in Figures 5 and 6, the motivation behind the present study was the exploration of broad empirical questions about how much and in which ways functional connectome similarity differed within and between individuals across sessions and states, which requires an approach describing and discussing the range of effect sizes that are most compatible with our data (given our background model), rather than the testing of narrow hypotheses that could either be “rejected” or “accepted” (Amrhein & Greenland, 2022; Amrhein, Greenland, & McShane, 2019; Amrhein, Trafimow, & Greenland, 2019; Berner & Amrhein, 2021). Second, as numerous statisticians and scientists have warned for decades, the abuse of ritualistic dichotomous inference in lieu of statistical thinking across scientific disciplines has created a crisis of validity for scientific conclusions, including their replicability (Gigerenzer, 2018; Wasserstein & Lazar, 2016; Wasserstein, Schirm, & Lazar, 2019). Rather than contribute to this crisis, we recognize that the primary scientific contribution of the present study is the estimation of the direction, strength, and uncertainty of individual differences in functional connectome similarity in our sample; whereas meta-analytic studies and other cumulative approaches that combine information from multiple studies—each with their own set of conditions, assumptions, patterns of variation, and sources of systematic error—will typically be required to come to more generalized scientific conclusions about electrophysiological network variants (Amrhein et al., 2019; Berner & Amrhein, 2021; Nichols, Kendall, & Boomer, 2019; Nichols, Oli, Kendall, & Boomer, 2021).

It is likely that the real data will be representative of more than one of the hypothetical outcomes illustrated in Figures 5 and 6. Figure 7 illustrates what this might look like should the individual, individual-session, and individual-state effects be equally represented in the

underlying global network activity, based on the simple averaging of each effects' contrasts. We emphasize that this illustration represents an unrealistic scenario where each individual's functional connectomes are perfectly similar with themselves and perfectly dissimilar with others; therefore, the magnitude of these effect sizes is greatly exaggerated. In reality, we would expect to find smaller effect sizes whose magnitudes decrease as the dynamics of underlying global network activity becomes more similar across individuals. Moreover, it is rather unlikely that the individual, individual-session, and individual-state effects would be equally weighted; thus, we would also expect to find an additional degree of variation in this hypothetical pattern of results based on the relative contribution of these effects to the stability of functional connectome similarity within individuals across sessions and states (Gratton et al., 2018). We illustrate the relative influence of these effects in the second, third, and fourth plots of Figure 7. In the second plot we see that as the individual effect makes a greater relative contribution, the magnitude of effect sizes across all contrasts becomes greater; whereas, in the third and fourth plots we see that as either the individual-session or individual-state effects make a greater relative contribution, an additional degree of effect size variation appears with both more and less pronounced differences in functional connectome similarity occurring across sessions and states.

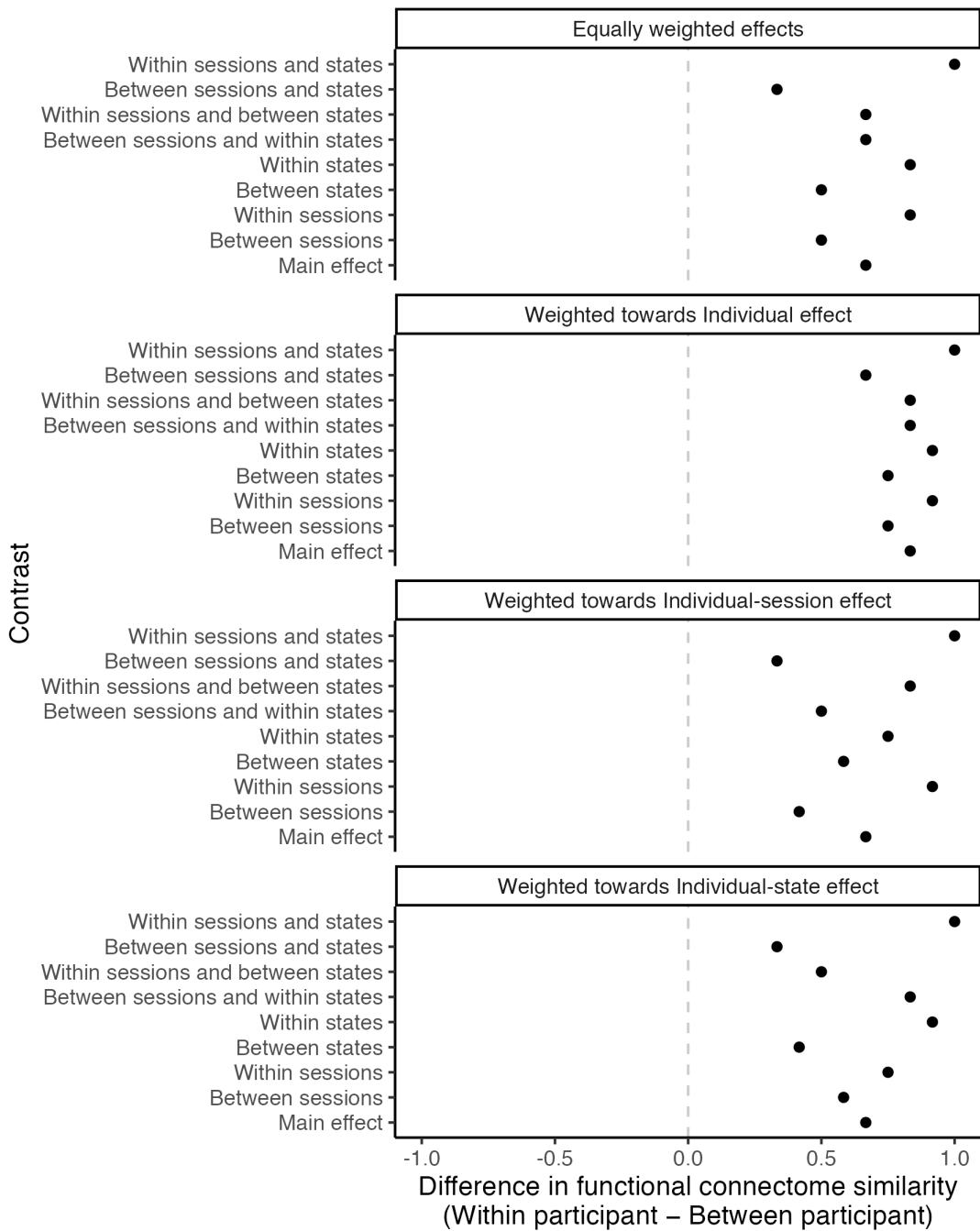


Figure 7. Illustrations of still-exaggerated but more realistic hypothetical outcomes of individual differences in functional connectome similarity, based on the simple and weighted averaging of the individual, individual-session, and individual-state effect contrasts. The weights

corresponding respectively to each effect are $\frac{1}{3}, \frac{1}{3}, \frac{1}{3}$ (first plot); $\frac{4}{6}, \frac{1}{6}, \frac{1}{6}$ (second plot); $\frac{2}{6}, \frac{3}{6}, \frac{1}{6}$ (third plot); and $\frac{2}{6}, \frac{1}{6}, \frac{3}{6}$ (fourth plot).

Based on the findings of previous fMRI network variant research (e.g., Gratton et al., 2018; Seitzman et al., 2019), we expected to find patterns of results consistent with the fourth plot in Figure 7 across all frequency bands for both phase coupling and amplitude coupling functional connectomes—consistent with functional connectomes that were more similar within than between individuals across all contrasts, with greater variations in similarity related to state than session. However, we emphasize that any of the result patterns depicted in Figure 7 would provide supportive evidence of stable individual differences in EEG functional connectomes, albeit with somewhat different interpretations as we described above for the individual, individual-session, and individual-state effects. Thus, our primary scientific hypothesis was that if the phase coupling and/or amplitude coupling dynamics of underlying global network activity in a given frequency band was influenced by stable individual-dependent factors *in our sample*, then functional connectomes would be more similar within than between individuals across all contrasts, on average, with smaller variations in similarity related to session or state.

We had no expectations regarding the possible range of effect sizes we could find, but again note that relatively higher values correspond to greater within-individual functional connectome stability and between-individual differentiation across contexts, whereas relatively lower values correspond to lesser within-individual functional connectome stability and between-individual differentiation. Thus, we reiterate the importance of considering the range of effect sizes most compatible with our data (given our background model) when drawing conclusions about our primary scientific hypothesis, rather than merely drawing conclusions based on the

direction of these effects and whether or not they included zero (Amrhein et al., 2019).

Additionally, to contextualize our results against the relevant fMRI literature, we considered the results of Gratton et al. (2018) as a cautious point of reference, keeping in mind that finding equivalent effect sizes would be surprising, given the differences in measurement, design, and analysis between our studies, on top of random variation in the data between our samples. In their study, Gratton et al. (2018) investigated how functional connectome similarity—measured using the Pearson correlation coefficient between the vectorized lower triangles of each functional connectome pair—differed within and between individuals across ten separate fMRI sessions and five different states (eyes-open resting state, and visual coherence, semantic, memory, and motor tasks). They found that functional connectomes were more similar within participants than between participants across contexts, on average, at both the group-level and individual-level by approximately 0.2 points ($\text{Mean}_{\text{within}} = 0.556$, $\text{Mean}_{\text{between}} = 0.357$) on the response scale when functional connectivity was estimated at the recording level, and by approximately 0.3 points ($\text{Mean}_{\text{within}} = 0.795$, $\text{Mean}_{\text{between}} = 0.512$) on the response scale when functional connectivity was estimated using the split-half method (see, respectively, Figures S2 and 3 in Gratton et al. (2018)).⁶ A similarity matrix for the eyes-open resting state functional connectomes

⁶ These values correspond to the *main effect* contrasts in our study and were obtained by back-transforming the Fisher-transformed Pearson correlation coefficients for the group and individual effects reported in Gratton et al. (2018), then taking their difference. For the split-half method, functional connectivity was estimated for each individual and task on the basis of two 5-session groups (by concatenating the recordings from a given task in each group together to increase the

from this sample was also reported by this group of researchers in a separate study, which showed individual differences in functional connectome similarity of a similar magnitude across sessions to those discussed above (see Figure 2H in Gordon, Laumann, Gilmore, et al. (2017)).

Finally, given our focus on individual differences, we considered it naturally important to investigate outcome variability of these effects across participants; particularly because network variants have been characterized as a common phenomenon present in all individuals, rather than an idiosyncrasy of just a few individuals (Seitzman et al., 2019). This served as a compliment to the group-level analysis of individual differences described above, allowing us to evaluate whether the group-level outcomes we observed would hold at the level of individuals (i.e., the level of observation where these differences originated from) in terms of the direction of these effects. Indeed, a central aim of investigating outcome variability was to dispel any misconceptions about the implications of our findings that could be caused by focusing only on the group-level outcomes—which can lead even highly trained experts to overestimate the importance and generalizability of findings due to uncertainty about average effects often being quite precise even in the presence of substantial outcome variability (Zhang et al., 2022).

reliability of functional connectivity estimates), rather than at the recording level (for further details, see Gratton et al., 2018).

Methods

Data

In this study, we used EEG data previously collected by our lab as part of a larger study. The larger study involved the collection of EEG recordings during resting state (eyes open and eyes closed) and during a lexical decision task (Meyer & Schvaneveldt, 1971) across three repeated measures sessions. The data collected during the lexical decision task is described in detail by Cnudde et al. (2021) and is available at <https://osf.io/da478/>. Here we only use the EEG recordings collected during resting state, which has not been previously described or made publicly available. All participants provided written informed consent before taking part in the study and were provided with monetary compensation for their participation. Ethics approval was received from the Conjoint Faculties Research Ethics Board of the University of Calgary.

Participants Twenty-one healthy adults (10 males, 11 females) whose ages ranged from 20 to 28 years ($M = 23.90$, $SD = 2.86$) and whose years of education ranged from 13 to 24 years ($M = 17.48$, $SD = 2.75$) participated in the original study. All participants were right-handed, spoke English as a first language, and had normal or corrected-to-normal vision. Exclusion criteria included a history of neurological disease or disorder, mental illness, head trauma, alcoholism or drug abuse, or use of psychotropic medications in the last two years preceding data collection, as determined through a screening questionnaire. We excluded EEG data for analysis from four participants because they did not participate in the final session, and three participants because they had one or more recordings with excessive noise. The final sample used for analysis consisted of fourteen participants (7 males, 7 females) whose ages

ranged from 20 to 28 years ($M = 23.86$, $SD = 3.13$) and whose years of education ranged from 13 to 23 years ($M = 17.21$, $SD = 2.72$).

Electrophysiological Data Acquisition

Electrophysiological data acquisition was completed in a dimly lit, radio frequency shielded, and sound attenuated chamber. During each session, an EasyCap with 64 gel-based active electrodes positioned following the 10-10 system (Chatrian, Lettich, & Nelson, 1985, 1988) was used to continuously record electrophysiological activity at the scalp (Brain Products GmbH, Gilching, Germany). Channel Cz was used as the reference electrode. A Brain Vision Solutions actiCHamp amplifier was used to amplify microvolt signals from the electrodes and transform them into digital format for storage and analysis (Brain Products GmbH, Gilching, Germany). All data were sampled at 500 Hz, and band limited with a built-in 0.05-100 Hz band-pass filter. All electrode impedances were below 17 kW at the start of recording. EEG recording lasted for a total of 80 minutes. We first recorded five minutes of eyes open and five minutes of eyes closed resting state data, with the order of these conditions counter-balanced across participants. This was followed by approximately 60 minutes of task state data recorded during performance of a lexical decision task (for a detailed description, see Cnudde et al., 2021). Finally, eyes open and eyes closed resting state data were recorded for five minutes each, again counter-balanced across participants.

Across all three sessions, we collected a total of 30 minutes eyes open resting state data (over 6 recordings) and 30 minutes eyes closed resting state data (over 6 recordings) from each participant. The time between the first and second session ranged from 8 to 13 days ($M = 9.57$, $SD = 1.55$), and between the second and third session ranged from 91 to 101 days ($M = 94.29$, $SD = 3.17$).

Software, computational reproducibility, and code availability

All computational steps were done using the open-source programming language R (version 4.1.2, <https://www.R-project.org/>; R Core Team, 2021). We maintained a reproducible workflow for the entire pipeline—from data cleaning to reporting—using the targets package (Landau, 2022), and managed R and Python dependencies using the renv package (Ushey, 2022). All EEG preprocessing and functional connectivity analysis was done using the open-source Python package MNE-Python (version 2.2.0, <https://doi.org/10.5281/zenodo.4338426>; Gramfort et al., 2013), which was called from R using the reticulate package (Ushey, Allaire, & Tang, 2022). We estimated the RV coefficient using the FactoMineR package (Husson, Josse, Le, & Mazet, 2020), and fit the mixed beta regression and contrasts using the glmmTMB (Magnusson et al., 2021) and emmeans (Lenth, 2022) packages, respectively. The DHARMA (Hartig, 2022) and performance (Lüdecke et al., 2023) packages were used for model diagnostics. All data visualization was done with a combination of the ggplot2 (Wickham et al., 2022), ggdist (Kay, 2022), ggh4x (van den Brand, 2021), ggnewscale (Campitelli, 2022), and patchwork (Pedersen, 2020) packages; and all tables were made with a combination of the flextable (Gohel & Skintzos, 2023), ftExtra (Yasumoto, 2023), and gtsummary (Sjoberg et al., 2023) packages. Other computations were done using the tidyverse (Wickham, 2021) suite of packages. Finally, this manuscript itself was written in R Markdown (Allaire et al., 2022) using officedown (Gohel & Ross, 2023) with the papaja package’s APA template (Aust & Barth, 2022), and all reported numbers, figures, and tables were printed using inline code to ensure their accuracy.

The total computation time for the entire targets pipeline was approximately 14.25 hours. A complete record of the R environment and packages used in this study can be found in Tables B1 and B2 in Appendix B. All code used in this study is openly available, licensed under the MIT

License, and can be accessed at the study's GitHub repository https://github.com/mccarthy-mg/mccarthy_EEGNetworkVariants_2024 or Open Science Framework (OSF) repository <https://osf.io/xztdk/> (DOI: <https://doi.org/10.5281/zenodo.6578410>). A copy of this licence and its terms can be found in the study's GitHub or OSF repository.

EEG preprocessing

Raw EEG data was preprocessed to remove noise and non-neural artifacts from the data using the following steps. First, following recommendations by Widmann, Schröger, & Maess (2015), a two-pass forward and reverse, zero-phase, non-causal band-pass finite impulse response filter was used to remove slow drift potentials at infraslow frequencies less than 0.10 Hz, line noise at 60.00 Hz, and irrelevant noise fluctuations greater than 60.00 Hz (de Cheveigné & Nelken, 2019; Widmann et al., 2015). The finite impulse response filter used a Hamming window with 0.0194 passband ripple and 53 dB stopband attenuation. The lower passband edge and transition bandwidth were set at 0.10 Hz (-12 dB cutoff frequency: 0.05 Hz), and the upper passband edge and transition bandwidth were set at 50.00 Hz (-12 dB cutoff frequency: 56.25 Hz). The filter length was 16501 samples (33.002 seconds). These filter parameters were selected after exploring the difference between raw and filtered signals and verifying that the selected filter parameters improved signal quality over alternative filter parameters or the raw signal (Widmann et al., 2015). Second, the data was downsampled from 500 to 200 Hz in order to reduce the size of the data and speed up computations operating on the data. Third, data was rereferenced to the common average reference in order to reduce spatial biases in the signal amplitude of channels caused by their distance to the original reference electrode (Nunez & Srinivasan, 2006). Fourth, bad channels and segments were manually marked and removed to prepare the data for ICA decomposition. Channels were marked as bad if they contained

excessive noise or drift for a significant portion of the recording. Bad channels were marked in 26.19% of recordings, ranging from 1 to 7 bad channels marked per recording with a mode of 1. Segments were marked as bad if they contained excessive noise or drift that (1) could interfere with fitting the ICA decomposition due to the amount of variance their component would capture, or (2) was unlikely to be repaired by ICA decomposition. Bad segments were marked in 94.05% of the recordings, ranging from 0 to 11 bad segments marked per recording with a mode of 1. The total duration of bad segments per recording across the entire sample ranged from 0.97 to 124.81 seconds long ($M = 17.89$, $SD = 18.30$). Fifth, ICA decomposition fitted using the Picard algorithm (Ablin, Cardoso, & Gramfort, 2017, 2018) was performed to remove components carrying muscle artifacts or ocular artifacts (eye blinks, saccades, or horizontal eye movements) from the data. Components carrying artifacts were manually selected and then removed. Finally, bad channels were interpolated using spherical splines (Perrin, Pernier, Bertrand, & Echallier, 1989) and put back into the data.

After artifact rejection, the continuous data was divided into 5 second epochs and filtered into five frequency bands to prepare for functional connectivity analysis. This was a three-step process. First, the epochs with an 8 second duration were created at 5 second intervals such that an epoch occurred from 0-8 seconds, 5-13 seconds, 10-18 seconds, and so forth, until the end of the recording. Epochs that contained a bad segment were removed. Second, the epoched data was filtered into five frequency bands—delta (δ , 1-4 Hz), theta (θ , 4-8 Hz), alpha (α , 8-13 Hz), beta (β , 13-30 Hz), and gamma (γ , 30-50 Hz)—using a two-pass forward and reverse, zero-phase, non-causal band-pass finite impulse response filter. Third, epochs were cropped to a 5 second duration starting 1 second into each epoch such that an epoch then occurred from 1-6 seconds, 6-11 seconds, 11-16 seconds, and so forth. We used this three-step process in order to avoid

distorting the true signal, as filtering epoched data creates edge artifacts at the start and end of each epoch that distort the true signal. Creating longer epochs in the first step provided padding around the edges of each epoch that could be cropped in the third step to remove these edge artifacts; and overlapping epochs in the first step made it possible for the cropped epochs in the third step to be non-overlapping and contiguous with reference to the continuous data, preserving the true signal across the length of the recording. The final 5 second duration was selected in order to have a sufficient number of oscillatory cycles per epoch to get reliable functional connectivity estimates across all five frequency bands.

Analyses

Functional connectivity

Functional connectivity was estimated between all pairs of EEG channels using the phase lag index (PLI; Stam et al., 2007) and the orthogonalized amplitude envelope correlation (AEC; Hipp et al., 2012), which measure phase coupling and amplitude coupling, respectively. Both the phase lag index and the orthogonalized amplitude envelope correlation account for the effects of field spread and volume conduction, reducing the possibility of spurious coupling between channels from influencing our functional connectivity estimates (Bastos & Schoffelen, 2016). Beyond basic concerns of validity, we selected the phase lag index because it is one of if not the most popular phase coupling metrics that accounts for volume conduction, and thus, is likely to be used in future EEG network variant studies; on the other hand, the orthogonalized amplitude envelope correlation was selected out of necessity, as it is currently the only available metric for estimating amplitude coupling while accounting for volume conduction. After estimating functional connectivity between all pairs of EEG channels, the resulting estimates from each recording were collected into twelve symmetrical 64×64 matrices (functional connectomes) per frequency band and measure, which reflected

electrophysiological cortical functional networks derived from averaged phase or amplitude coupling between each pair of channels. These functional connectomes were the basic unit of observation for subsequent analyses.

Phase coupling The average amount of phase coupling between pairs of sensors was estimated in each recording using the phase lag index (PLI; Stam et al., 2007). The phase lag index estimates the asymmetry of the distribution of phase angle differences between two signals x and y (Stam et al., 2007; Vinck, Oostenveld, van Wingerden, Battaglia, & Pennartz, 2011), given by:

$$\text{PLI}(x, y) = \frac{1}{n} \sum_{f=1}^n \left| \frac{1}{N} \sum_{i=1}^N \text{sign}(\text{imag}(S_{xyfi})) \right|,$$

where n is the number of frequency bins in each frequency band, N is the number of epochs, $\text{sign}(\cdot)$ is the signum operator, $\text{imag}(\cdot)$ is the imaginary operator, and S_{xyi} is the complex-valued cross spectral density between two sensors x and y at the individual frequency bins f in the i th epoch, from which we extract the phase angle differences at each frequency bin.

We estimated the cross spectral density between two signals x and y using multitaper spectral estimation (Babadi & Brown, 2014; Thomson, 1982) with digital prolate spheroidal sequence (DPSS) (Slepian & Pollak, 1961) windows. Seven tapers were used for each frequency band. The individual frequency bins used for each frequency band was determined by calculating the Discrete Fourier Transform sample frequencies for a 1001 sample window (corresponding to a 5 second epoch) and a sample space of 0.005 (the inverse of the 200 Hz sampling rate). This resulted in 501 frequency bins spaced at roughly 0.2 Hz intervals between zero and 100 Hz. Then

for each frequency band we simply selected the frequency bins that were equal to or between the minimum and maximum frequencies of each frequency band.

The phase lag index takes values between 0 and 1. A value of 0 indicates either no phase coupling or phase coupling with a phase angle difference centred around 0 or 180 degrees, and a value of 1 indicates perfect phase coupling with a consistent nonzero phase angle difference. By only considering consistent nonzero phase angle differences as indicators of phase coupling between two sensors, the phase lag index ignores phase coupling that could be explained by volume conduction from a single common source (at the cost of also ignoring non-spurious zero lag coupling), making it a sound measure of the interactions between different underlying neural sources (Stam et al., 2007).

Finally, to examine the sensitivity of our analyses to different spectral analysis approaches (cf. Bruns, 2004), we also estimated the phase lag index using the Hilbert transform method (Stam et al., 2007). The results of these analyses are shown in Figures A7-A11 in Appendix A.

Amplitude coupling The average amount of amplitude coupling between pairs of sensors was estimated in each recording using the orthogonalized amplitude envelope correlation (AEC; Hipp et al., 2012). The orthogonalized amplitude envelope correlation estimates the absolute Pearson correlation coefficient of the amplitude envelopes between two orthogonalized complex-valued analytic signals x and y (Hipp et al., 2012), given by:

$$\text{AEC}(x, y) = \left| \frac{1}{N} \sum_{i=1}^N \frac{\sum_{t=1}^n (x_{it} - \bar{x}_i)(y_{it} - \bar{y}_i)}{\sqrt{\sum_{t=1}^n (x_{it} - \bar{x}_i)^2 \sum_{t=1}^n (y_{it} - \bar{y}_i)^2}} \right|,$$

where N is the number of epochs, n is the number of samples in each epoch, x_{ij} and y_{ij} are the individual sample points t of the amplitude envelopes in the i th epoch, and \bar{x}_j and \bar{y}_j are the sample means of the amplitude envelopes in the i th epoch.

We extracted the analytic signal from each channel's time-course using the Hilbert transform (Stam et al., 2007). Following this, the complex-valued analytic signals $X(a, b)$ and $Y(a, b)$ for each pair of channels were orthogonalized by removing signal components that shared the same phase between the two signals (Hipp et al., 2012), given by:

$$X_{\perp Y}(a, b) = \text{Im} \left(X(a, b) \frac{Y(a, b)^*}{|Y(a, b)|} \right),$$

where $Y(a, b)^*$ is the complex conjugate of $X(a, b)$. This orthogonalization procedure allowed us to ignore the parts of each signal that could be explained by volume conduction from a single common source, making the subsequent amplitude envelope correlations a sound measure of the interactions between different underlying neural sources (Hipp et al., 2012). After orthogonalization, the amplitude envelopes of the two analytic signals were computed by taking the absolute value of each signal, then the amplitude envelope correlation between them was estimated. We computed amplitude envelope correlations for both directions of the orthogonalization (X to Y , and Y to X), then averaged the values to get the final amplitude envelope correlation estimate for each pair.

The amplitude envelope correlation takes values between 0 and 1. A value of 0 indicates no amplitude coupling between the orthogonalized signals, and a value of 1 indicates perfect amplitude coupling with a consistent amplitude envelope correlation between the orthogonalized signals.

Interpreting functional connectivity

We use connectivity profile matrices (Demuru et al., 2017) to compactly display the phase and amplitude coupling functional connectome from each recording. These plots serve as a supplement to our similarity analyses, providing a broad idea of what aspects of functional connectivity are being summarized by a given similarity estimate. Each row shows the vectorized lower triangle of the phase or amplitude coupling functional connectome from a given recording (i.e., all unique pairs in the connectome), and each column represents a pair of sensors. The strength of coupling between any pair of sensors corresponds to their phase lag index or amplitude envelope correlation estimate and is represented by the colour of that cell in the matrix, with darker colours representing less coupling and brighter colours representing more coupling.

Functional connectome similarity

The similarity of phase- and amplitude-based functional connectomes was next quantified by estimating the RV coefficient (Robert & Escoufier, 1976) between all pairs of functional connectomes from a given individual, session, and state within each frequency band (14,028 pairs total). The RV coefficient estimates the similarity between the patterns of observations in two positive semi-definite matrices \mathbf{X} and \mathbf{Y} based on the closeness of the relative position of the observations in each set (Abdi, Hervé, 2007; Escoufier, 1973; Josse & Holmes, 2016; Robert & Escoufier, 1976), given by:

$$RV(\mathbf{X}, \mathbf{Y}) = \frac{\text{trace}(\mathbf{ST})}{\sqrt{\text{trace}(\mathbf{SS}) \times \text{trace}(\mathbf{TT})}},$$

where the relative positions of the observations in each set are represented by the cross product matrices $\mathbf{S} = \mathbf{XX}^T$ and $\mathbf{T} = \mathbf{YY}^T$, and where \mathbf{X} and \mathbf{Y} have first been mean centred. The RV coefficient is a standard measurement in many fields, including neuroscience (e.g., Shahhosseini & Miranda, 2022), that can be thought of as a multivariate generalization of the

squared Pearson correlation coefficient between two variables to the case of two sets of variables, where two sets of variables are correlated if the relative position (in Hilbert space) of the observations in one set is similar to the relative position of the observations in the other set (Josse & Holmes, 2016; Mayer et al., 2011). More generally, the RV coefficient can be seen as a unifying tool for several linear multivariate statistical methods (such as multivariate linear models, principal components analysis, discriminant analysis, and canonical analysis), which can all be understood as processes that maximize the RV coefficient of various matrices under specific constraints (Josse & Holmes, 2016; Kherif, 2003; Robert & Escoufier, 1976).⁷

The RV coefficient takes values between 0 (no linear relationship) and 1 (perfect linear relationship). For our data, this defines a scale of similarity between two functional connectomes based on their patterns of connectivity strength that can be interpreted in much the same way as the familiar squared Pearson correlation coefficient; that is, a value close to one indicates a high degree of similarity between the patterns of connectivity strength in \mathbf{X} and \mathbf{Y} , whereas a value close to zero indicates a low degree of similarity. We chose the RV coefficient here given its ability to reduce the dimensionality of the relationship between functional connectomes to a single number with a familiar interpretation, facilitating further comparisons of how much and in which ways patterns of connectivity strength varied within and between individuals across sessions and states. For self-evident reasons, we chose this measure over its univariate counterpart, the Pearson correlation coefficient, because of the multivariate nature of functional

⁷ Mathematical details and discussion of the relationship between the RV coefficient and the squared Pearson correlation coefficient, as well as its relationship to other multivariate statistical methods, can be found in articles by Josse & Holmes (2016), and Robert & Escoufier (1976).

connectome data, which we did not want to ignore when quantifying functional connectome similarity. Although we do note that the Pearson correlation coefficient has also been used to successfully quantify similarity between pairs of functional connectomes in previous fMRI network variant studies, by vectorizing the lower triangle of each connectivity matrix then estimating the correlation between the two vectors (Finn et al., 2017, e.g., 2015; Gordon, Laumann, Gilmore, et al., 2017; Gratton et al., 2018).

Interpreting functional connectome similarities

We use similarity matrices to examine the similarities of functional connectomes between and within individuals, sessions, and states. When interpreting a similarity matrix, the two most important features are the *strength* and *pattern* of similarities. The strength of similarity between any pair of functional connectomes corresponds to their RV coefficient estimate and is represented by the colour of that cell in the matrix, with darker colours representing less similarity and brighter colours representing more similarity. To interpret the pattern of similarities we first need to consider the ordering of functional connectomes in the matrix. The boxes on the diagonal show within-participant similarities between all twelve functional connectomes from a given participant, the boxes on the off-diagonal show between-participant functional connectome similarities. With this organization in mind, we can examine the similarity matrix for visually obvious patterns of low and high similarity, such as those depicted in Figure 5 in the introduction.

Group-level functional connectome similarity contrasts

We used a mixed beta regression to model how functional connectome similarity varied between and within individuals, sessions, and states at the group-level for each frequency band (for an accessible overview of mixed beta regression, see Douma & Weedon, 2019; Heiss, 2021). The unit of observation was the pair of functional connectomes used for a given similarity estimate. The response variable

was the RV coefficient estimated for each pair, which was modelled with a beta distribution and related to the predictors with the logit link function following the parameterization of Cribari-Neto & Zeileis (2010) and Ferrari & Cribari-Neto (2004). The predictors were binary indicators (where 0 = No and 1 = Yes) for whether a pair was within participant, within session, or within state, and their interactions. Because the RV coefficient estimates are based on the similarity of pairs of functional connectomes, we accounted for statistical dependencies between observations by adding random intercepts to the model. All random effects were assumed to be normally distributed (Brooks et al., 2017).

We fit two versions of this model, which differed slightly in their random effects specification: A *maximal model* (Barr, Levy, Scheepers, & Tily (2013)) with random intercepts for both the **X** and **Y** connectome that each observation came from to account for statistical dependencies between observations that had a connectome in common, and a random intercept for the participant pair to account for the repeated observation of the same participant pairs; and a *reduced model* with only random intercepts for both the **X** and **Y** connectome that each observation came from. The reduced models were fit for pragmatic reasons, due to convergence problems with several of the maximal models where the estimate for the variance of the participant pair parameter was zero (i.e., the fit was singular). The effect of not including participant pair was negligible for point estimates, which were similar or equivalent between models where it was and was not included; but was noticeable for interval estimates, which were generally wider by a factor of two to four when it was included compared to when it was not included. This difference did not meaningfully change the conclusions drawn from our results, however. Results from the reduced models are presented in the results section of this manuscript

for parsimony across sections, and results from the maximal models are shown in Figures A12–A21 in Appendix A.

The fit of the model was assessed using the following diagnostics: Posterior predictive checks—wherein we simulated replicated data under the fitted model and compared these to the observed data—were used to check for systematic differences between the fitted model and observed data (Gelman et al., 2013; Gelman & Hill, 2006; Gelman, Hill, & Vehtari, 2020). Randomized quantile residuals plotted against uniform distribution quantiles were used to check for signs of model misspecification (Dunn & Smyth, 1996; Hartig & Lohse, 2022). Quantiles of the random effects plotted against standard normal distribution quantiles were used to check if the random effects were normally distributed; however, generalized linear mixed effects models have a large degree of robustness against misspecifying the shape of the random effects distribution (see McCulloch & Neuhaus, 2011). Variance Inflation Factors were used to check for multicollinearity between the predictors (J. Fox & Monette, 1992; Marcoulides & Raykov, 2019; O'brien, 2007), where a value of less than five as indicated low multicollinearity between the predictors, values between five and ten moderate, and values greater than ten high and not tolerable (James, Witten, Hastie, & Tibshirani, 2021).

After fitting the model, we constructed a reference grid using estimated marginal means (Lenth et al., 2022; Searle, Speed, & Milliken, 1980), which were backtransformed to the response scale [0-1] for interpretability. The estimated marginal means were then used to estimate the difference in functional connectome similarity within and between participants using pairwise contrasts, as we illustrated in the introduction. Differences were estimated for (1) the overall difference in similarity within and between participants, which we term the *main effect*; (2) the difference in similarity within and between participants for each level of one predictor

(e.g., within session similarity) while averaging over levels of the other predictor (e.g., within and between state similarity); (3) the difference in similarity within and between participants for the unique combinations within and between session and state. For any of these contrasts: A difference of zero indicated equal amounts of functional connectome similarity within and between participants, a positive difference indicated more similarity within than between participants, and a negative difference indicated more similarity between than within participants.

Interpreting group-level contrasts

We use interval plots to report the group-level contrasts estimating the difference in functional connectome similarity within and between participants at various levels of the session and state predictors. To interpret these contrasts, we report compatibility intervals (CIs), which are equivalent to classical confidence intervals (Amrhein & Greenland, 2022). An $x\%$ compatibility interval shows the effect sizes most compatible with our data, given the correctness of the set of procedural and statistical assumptions used to compute the interval, which we call the *background model* (see Amrhein & Greenland, 2022). As discussed by Amrhein et al. (2019), there are two important points to keep in mind when interpreting compatibility intervals. First, although interval shows the values most compatible with our data, it does not mean values outside the interval are incompatible; they are merely less compatible, given our background model. Indeed, there are many values outside the interval that will also be compatible with our data, which have not been included due to (known and unknown) assumptions that we have not modelled (Amrhein et al., 2019). Second, the point estimate and values near it are more compatible with our data than values near the limits of the interval; we use both 95% and 66% compatibility intervals in our plots to highlight this. Additionally, given that the correctness of *all* assumptions used to compute our estimates was doubtful (e.g., we knowingly misspecified the random effects of the reduced mixed beta

regression models, the absence of measurement errors in our procedure is unlikely, etc.), we emphasize that our estimates likely understate uncertainty about the effect sizes most compatible with our data, and should not be taken as showing some general truth (Amrhein et al., 2019).

In addition, to assist readers unfamiliar with the analytic approach we have taken here, for each contrast we also report the observed *p*-value corresponding to a targeted hypothesis test of zero difference in functional connectome similarity within and between participants. Just as we discussed for compatibility intervals, we emphasize that each *p*-value merely provides a measure of the degree of statistical compatibility between the targeted hypothesis and our data, given the background model—referring to a targeted hypothesis test of *every* assumption used to compute the test, including procedural and statistical assumptions as well as the targeted hypothesis of zero difference (Greenland, 2017, 2019; Greenland et al., 2016). Thus, a small *p*-value only suggests that there may be a problem with at least one assumption used to compute the test, without indicating which one; and a large *p*-value only suggests that the test did not detect a problem, without indicating whether this was because there were no problems or because the test was insensitive to them (Amrhein et al., 2019; Greenland, 2017).

Individual-level functional connectome similarity contrasts To explore how well the group-level model and contrasts represented individual differences in our sample, we also fit a mixed beta regression for each participant, following the same parameterization as both the reduced and maximal group-level models. These individual-level models were followed-up using the same pairwise contrasts as in the group-level model, and comparisons between the group-level and individual-level contrasts were done visually. Results from the individual-level models are briefly summarized in the results section of this manuscript, and results from each individual-

level model are shown in Appendix A (for reduced models, see Figures A1-A6; for maximal models, see Figures A12-A21).

Interpreting individual-level contrasts

We use ridge plots to report the individual-level contrasts estimating the difference in functional connectome similarity within and between participants at various levels of the session and state predictors. To interpret these contrasts, we report 95% compatibility distributions, which are equivalent to classical confidence distributions (Schweder & Hjort, 2016; Xie & Singh, 2013). Like with a compatibility interval, a 95% compatibility distribution shows the effect sizes most compatible with our data, given the background model, and is a sample-dependent distribution representing compatibility intervals of all levels for a parameter (Xie & Singh, 2013). We used scaled and shifted t distributions as the sampling distribution for the individual-level contrasts, using the point estimate, standard error, and degrees of freedom as parameters for the distribution. The peak of the distribution corresponds to the point estimate, and changes in the density of the distribution correspond to differences in compatibility values have with our data.

Results

The results section is split into three parts. In the first part, we provide a brief summary of our functional connectivity analyses, which serves to demonstrate that both of our functional connectivity metrics gave reasonable results in each frequency band that were in agreement with previous published work. In the second part, we investigate differences in functional connectome

similarity within and between participants at the group-level.⁸ In the final part, we investigate outcome variability in differences in functional connectome similarity within and between participants at the individual-level.

Functional connectivity analyses

Figure 8 shows the results from the functional connectivity analyses for a single illustrative recording. Note that although the strength of coupling differs between the phase lag index (Figure 8A) and the amplitude envelope correlation (Figure 8B), the two coupling modes are qualitatively similar in their spatial organization. This level of spatial correspondence between phase coupling and amplitude coupling functional connectomes during resting state is in agreement with previous published work (Mostame & Sadaghiani, 2020). We selected this recording for illustrative purposes because the spatial correspondence between its phase coupling and amplitude coupling functional connectome was particularly obvious; however, we emphasize that this observation was generally consistent across recordings and frequency bands for all participants (see Phase Coupling Functional Connectomes, Amplitude Coupling Functional Connectomes, and Phase Coupling Functional Connectomes [Hilbert transform] in the Supplementary Material available online).

⁸ For accessibility, larger versions of the figures in this section are available in the online supplement (see Similarity Matrices in the Supplementary Material available online).

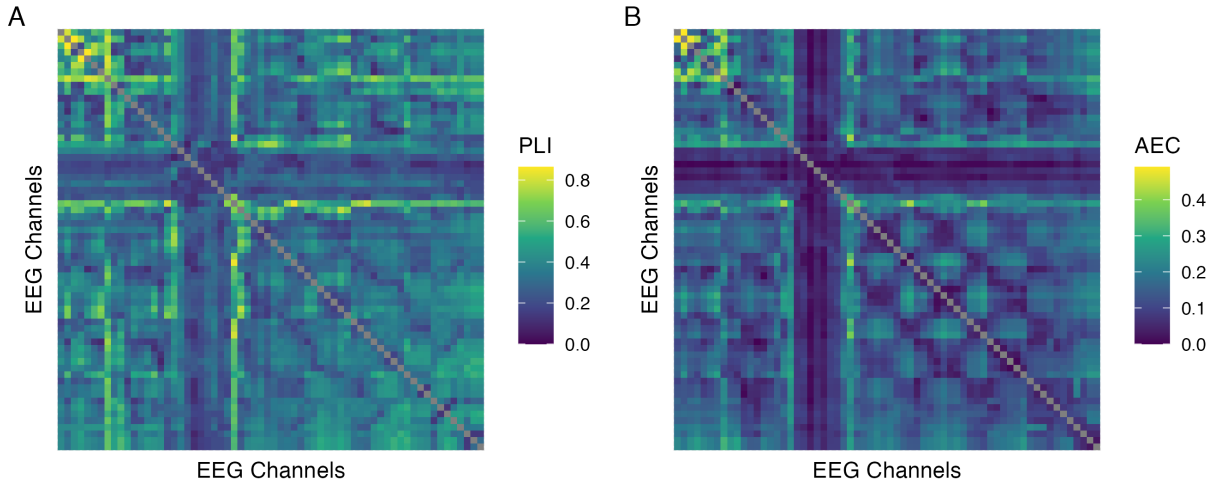


Figure 8. Results of the phase coupling (A) and amplitude coupling (B) functional connectivity analyses for a single illustrative recording (participant P16, session 3, eyes open 2, delta band). For each functional connectome, EEG channels are ordered as follows (from left to right, and from top to bottom): Fp1, Fp2, AF7, AF3, AFz, AF4, AF8, F7, F5, F3, F1, Fz, F2, F4, F6, F8, FT9, FT7, FC5, FC3, FC1, FCz, FC2, FC4, FC6, FT8, FT10, T7, C5, C3, C1, Cz, C2, C4, C6, T8, TP9, TP7, CP5, CP3, CP1, CPz, CP2, CP4, CP6, TP8, TP10, P7, P5, P3, P1, Pz, P2, P4, P6, P8, PO7, PO3, POz, PO4, PO8, O1, Oz, O2.

Figure 9 shows the distribution of coupling magnitudes in each frequency band across all recordings and EEG channel pairs, organized by participant. Descriptive statistics summarizing each of these distributions are shown in Table 1. The small mean, wide range, and right-skew of phase lag index (Figure 9A) and amplitude envelope correlation (Figure 9B) estimates in each frequency band were in agreement with previous published work (e.g., Fraschini, Pani, Didaci, & Marcialis, 2019; Lai et al., 2018; Mehrkanoon, Breakspear, Britz, & Boonstra, 2014), and can be explained in part by the underestimation of true connectivity inherent to each of these metrics due to their discounting of true zero lag interactions (Cohen, 2015; Fraschini et al., 2019;

Hipp et al., 2012; Stam et al., 2007). Additionally, a clear frequency band response was observed for both coupling modes, with the strongest coupling occurring in the alpha band for each metric. This was unsurprising, as alpha oscillations are known to play a prominent role in intrinsic connectivity networks (Mantini et al., 2007; Marino, Arcara, Porcaro, & Mantini, 2019; Sadaghiani & Kleinschmidt, 2016; Samogin et al., 2020), and greater coupling in the alpha band relative to other frequency bands during resting state has been reported in previously published work using both the phase lag index (Hardmeier et al., 2014; Mehrkanoon et al., 2014; Van Der Molen, Stam, & Van Der Molen, 2014) and the orthogonalized amplitude envelope correlation (Hipp et al., 2012; Mehrkanoon et al., 2014; Samogin et al., 2020; Samogin, Rueda Delgado, Taberna, Swinnen, & Mantini, 2022; Taberna et al., 2021).

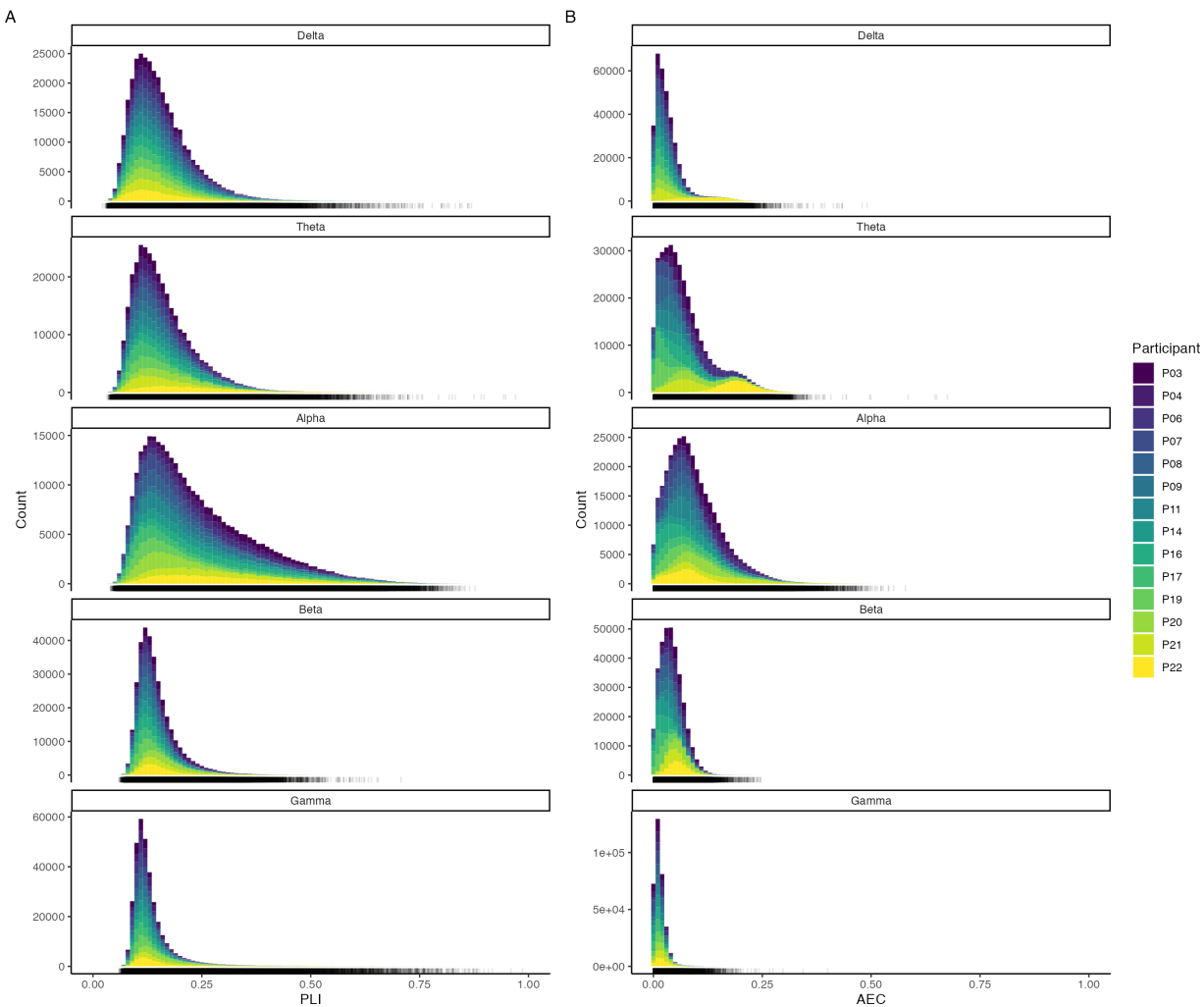


Figure 9. Distribution of phase lag index (A) and amplitude envelope correlation (B) estimates across all recordings and EEG channel pairs in each frequency band. Note that the scale of the y-axis is free across panels. The marginal rug beneath each histogram shows the observed coupling estimates.

Table 1

Summary statistics describing the distribution of phase lag index and amplitude envelope correlation estimates across all functional connectomes and EEG channel pairs in each frequency band.

Coupling Mode	Frequency Band	Minimum	Maximum	Mean	SD	Skewness	Kurtosis
Phase							
	Delta	0.022	0.869	0.156	0.069	1.474	3.997
	Theta	0.031	0.970	0.162	0.072	1.497	3.721
	Alpha	0.040	0.877	0.243	0.129	1.076	0.819
	Beta	0.058	0.707	0.147	0.048	2.010	6.637
	Gamma	0.060	0.986	0.136	0.060	4.125	25.201
Amplitude							
	Delta	0.000	0.491	0.035	0.035	2.311	7.135
	Theta	0.000	0.675	0.072	0.058	1.252	1.377
	Alpha	0.000	0.579	0.093	0.063	1.145	1.958
	Beta	0.000	0.247	0.042	0.026	0.743	0.852
	Gamma	0.000	0.400	0.015	0.013	2.872	20.428
SD = Standard Deviation							

Finally, note that although amplitude envelope correlation estimates were generally smaller than phase lag index estimates in a given frequency band, we caution against a neurophysiological interpretation of these differences in terms of the relative degree of phase to amplitude coupling. Although both metrics provide an indication of coupling consistency and share the same possible range of 0 to 1, they are mathematically and conceptually distinct from one another. Because of this, quantitative comparisons between the two metrics in terms of

coupling magnitudes are nebulous at best, and there is no reason to believe these metrics would give similar estimates when the relative degree of phase to amplitude coupling was equal.

Instead, we reiterate that both metrics performed as expected based on what has been reported in previous work; thus, we proceeded with our full analysis plan for both coupling modes across all frequency bands, under the assumption that our estimates provided a sound representation of underlying (non-zero lag) global network activity for each participant.

Phase coupling functional connectome similarity analyses

Delta

Figure 10A shows the connectivity profiles for all phase coupling functional connectomes in the delta band, organized by participant and recording. Plots and summary statistics of the distribution of coupling magnitudes across all recordings and EEG channel pairs are shown above in Figure 9 and Table 1, respectively.

Figure 10B shows the functional connectome similarity estimates between all pairs of phase coupling functional connectomes in the delta band. There was a visually obvious group effect, with high similarity between functional connectomes regardless of participant, session, or state. This was supported by the group-level contrast results in Figure 10C, which showed that although functional connectomes were more similar within participants than between participants at all levels of the session and state predictors, on average, the effect sizes most compatible with our data, given the background model, ranged from practically nil to at most small. Table 2 shows the estimated marginal means and targeted hypothesis tests of zero difference within and between participants corresponding to each of these contrasts. Note that the between-participant functional connectome similarity means were stable across contexts, whereas the within-participant means were more variable, indicating that the (at most) small positive differences in

functional connectome similarity can be attributed to individual-dependent factors with slight modulations by session and state. Jointly, these results suggest that, on average, the phase coupling dynamics of underlying global network activity in the delta band was differentiated between individuals across contexts, but with only a slight, negligible influence of individual-dependent factors over and above the influence of stable group-dependent factors.

These results remained largely consistent when the phase lag index was estimated using the Hilbert transform method instead of the multitaper method (Figure A7), with some minor differences: (1) phase coupling was generally weaker, but individual patterns of coupling were similar or the same; (2) functional connectome similarity was generally higher, but patterns of similarity were similar or the same; and (3) differences in functional connectome similarity were generally smaller, but were still positive with a similar pattern of variation across contexts. Likewise, the contrast results remained consistent between the reduced and maximal models of functional connectome similarity when the phase lag index was estimated using the Hilbert transform method (Figure A17), but with slightly more uncertainty in the estimates. The maximal model of functional connectome similarity did not converge when the phase lag index was estimated using the multitaper method (Table A1).

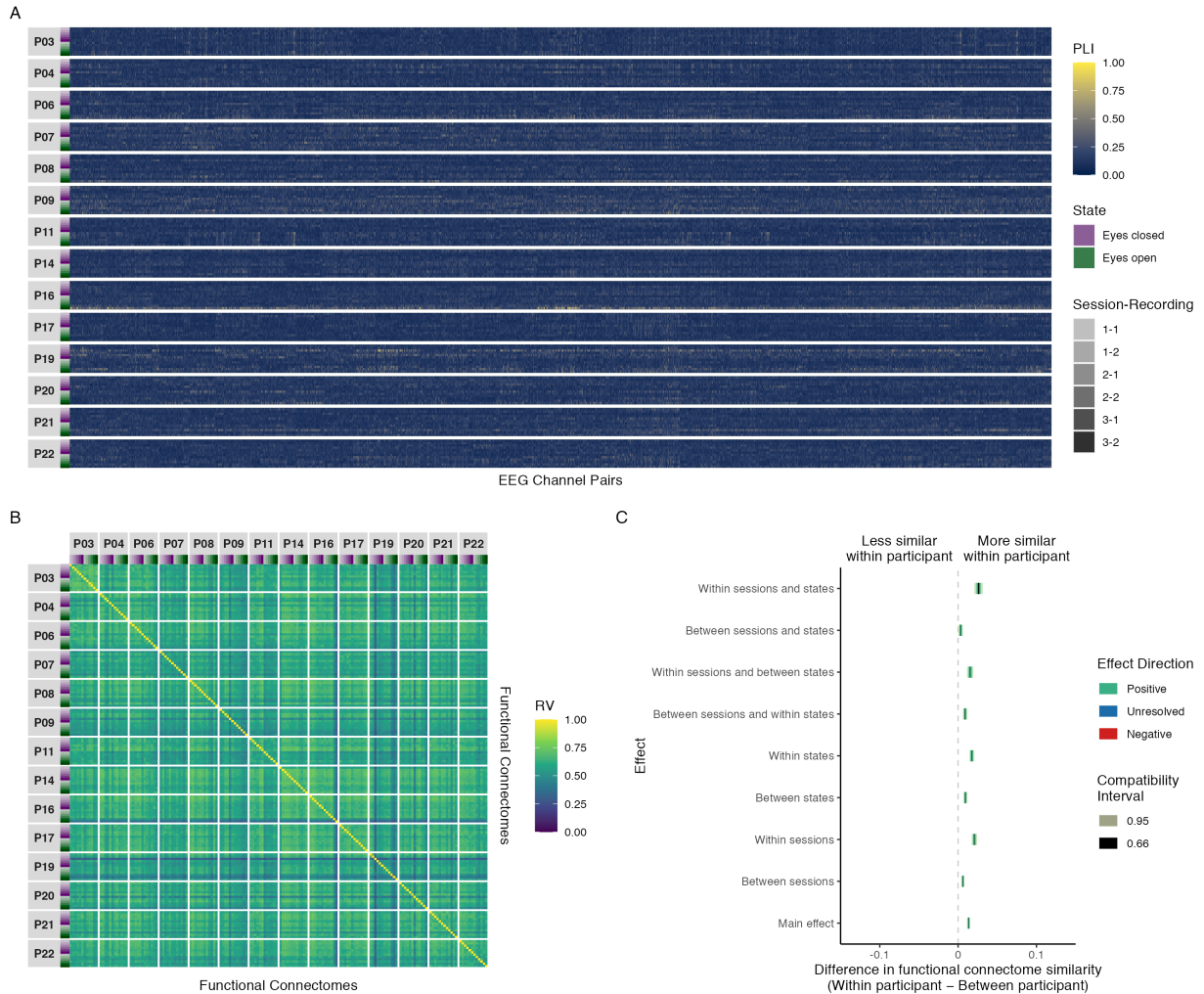


Figure 10. Results of phase coupling analyses in the delta band: (A) connectivity profiles for all functional connectomes, organized by participant and recording; (B) estimates of functional connectome similarity between all pairs of functional connectomes, organized by participant and recording; and (C) group-level contrasts estimating the average difference in functional connectome similarity within and between participants across contexts.

Table 2

Estimated marginal means, mean differences, and targeted hypothesis tests of zero difference in delta band phase coupling functional connectome similarity within and between participants across contexts.

Contrast	Within Participant	Between Participant	Mean Difference			
	Mean (SE)	Mean (SE)	ΔRV (SE)	95% CI	t(14,017)	p
Main effect ¹	0.606 (0.006)	0.593 (0.006)	0.013 (0.001)	0.011, 0.016	12.613	< .001
Between sessions ²	0.599 (0.006)	0.593 (0.006)	0.006 (0.001)	0.004, 0.008	5.681	< .001
Within sessions ²	0.614 (0.006)	0.593 (0.006)	0.021 (0.002)	0.017, 0.024	12.217	< .001
Between states ³	0.601 (0.006)	0.592 (0.006)	0.009 (0.001)	0.007, 0.012	7.132	< .001
Within states ³	0.612 (0.006)	0.594 (0.006)	0.018 (0.002)	0.015, 0.021	11.215	< .001
Between sessions and within states	0.603 (0.006)	0.594 (0.006)	0.009 (0.001)	0.006, 0.012	6.220	< .001
Within sessions and between states	0.608 (0.006)	0.592 (0.006)	0.015 (0.002)	0.012, 0.019	7.814	< .001
Between sessions and states	0.595 (0.006)	0.591 (0.006)	0.003 (0.001)	0.000, 0.006	2.169	.030
Within sessions and states	0.621 (0.007)	0.595 (0.006)	0.026 (0.003)	0.021, 0.031	9.693	< .001

SE = Standard Error, CI = Compatibility Interval

¹Results are averaged over the levels of session and state.

²Results are averaged over the levels of state.

³Results are averaged over the levels of session.

Theta Figure 11A shows the connectivity profiles for all phase coupling functional connectomes in the theta band, organized by participant and recording. Plots and summary statistics of the distribution of coupling magnitudes across all recordings and EEG channel pairs are shown above in Figure 9 and Table 1, respectively.

Figure 11B shows the functional connectome similarity estimates between all pairs of phase coupling functional connectomes in the theta band. There was a visually obvious group effect, with high similarity between functional connectomes regardless of participant, session, or state. This was supported by the group-level contrast results in Figure 11C, which showed that although functional connectomes were more similar within participants than between participants at all levels of the session and state predictors, on average, the effect sizes most compatible with our data, given the background model, were at most small. Table 3 shows the estimated marginal means and targeted hypothesis tests of zero difference within and between participants corresponding to each of these contrasts. Note that the between-participant functional connectome similarity means were stable across contexts, whereas the within-participant means were more variable, indicating that the (at most) small positive differences in functional connectome similarity can be attributed to individual-dependent factors with slight modulations by session and state. Jointly, these results suggest that, on average, the phase coupling dynamics of underlying global network activity in the theta band was differentiated between individuals across contexts, but with only a slight influence of individual-dependent factors over and above the influence of stable group-dependent factors.

These results remained largely consistent when the phase lag index was estimated using the Hilbert transform method instead of the multitaper method (Figure A8), with some minor differences: (1) phase coupling was generally weaker, but individual patterns of coupling were

similar or the same; (2) functional connectome similarity was generally higher, but patterns of similarity were similar or the same; and (3) differences in functional connectome similarity were generally of similar magnitudes, with the exception of the within sessions and between states contrast which was visibly smaller. Likewise, the contrast results remained consistent between the reduced and maximal mixed beta regression models of functional connectome similarity when the phase lag index was estimated using both the multitaper method (Figure A12) and the Hilbert transform method (Figure A18), but with slightly more uncertainty in the estimates.

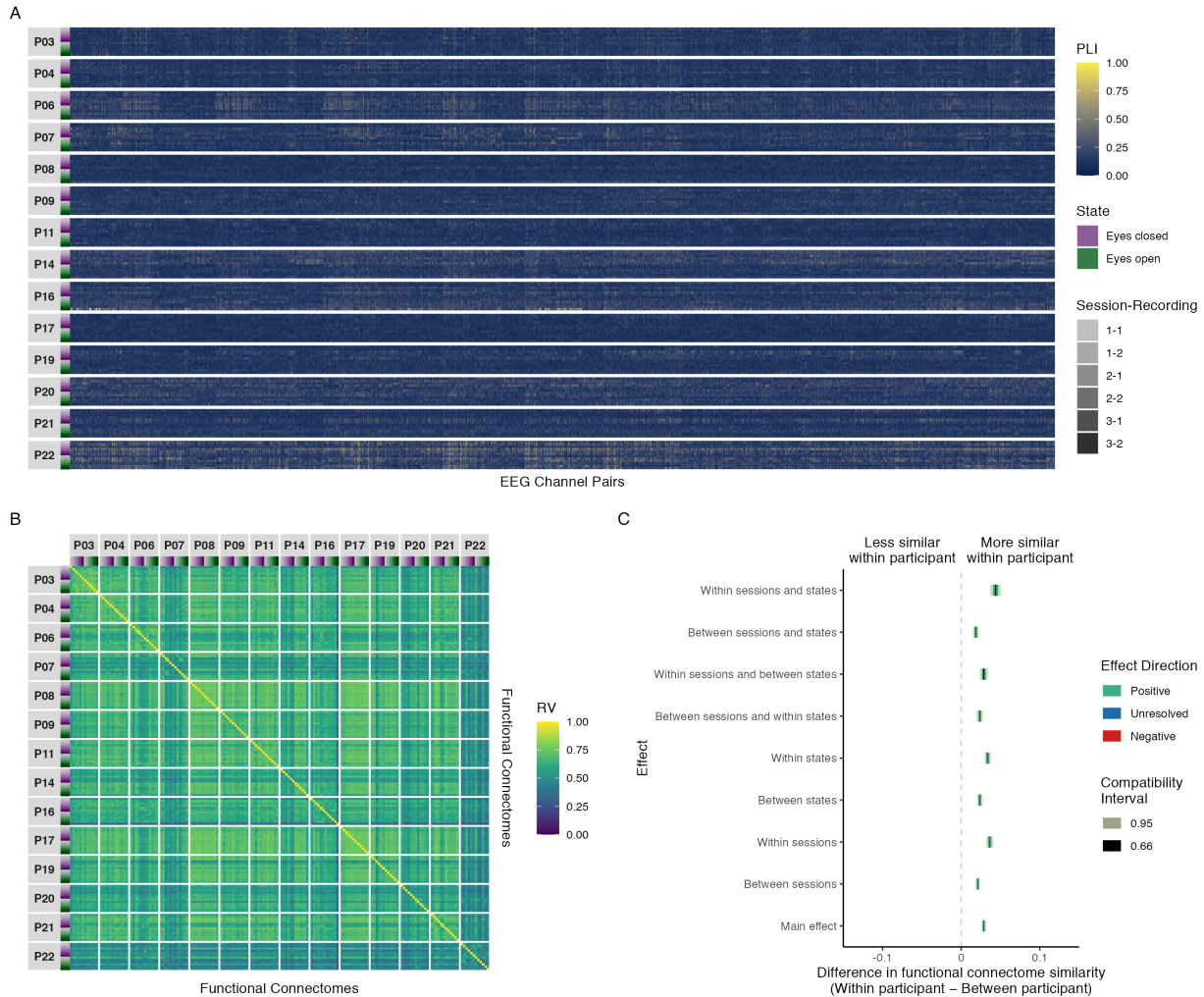


Figure 11. Results of phase coupling analyses in the theta band: (A) connectivity profiles for all functional connectomes, organized by participant and recording; (B) estimates of functional connectome similarity between all pairs of functional connectomes, organized by participant and recording; and (C) group-level contrasts estimating the average difference in functional connectome similarity within and between participants across contexts.

Table 3

Estimated marginal means, mean differences, and targeted hypothesis tests of zero difference in theta band phase coupling functional connectome similarity within and between participants across contexts.

Contrast	Within Participant	Between Participant	Mean Difference			
	Mean (SE)	Mean (SE)	ΔRV (SE)	95% CI	t(14,017)	p
Main effect ¹	0.643 (0.006)	0.614 (0.006)	0.029 (0.001)	0.026, 0.031	20.371	< .001
Between sessions ²	0.635 (0.006)	0.614 (0.006)	0.021 (0.001)	0.018, 0.024	14.854	< .001
Within sessions ²	0.651 (0.006)	0.615 (0.006)	0.036 (0.002)	0.032, 0.041	16.244	< .001
Between states ³	0.637 (0.006)	0.614 (0.006)	0.024 (0.002)	0.020, 0.027	13.776	< .001
Within states ³	0.648 (0.006)	0.615 (0.006)	0.034 (0.002)	0.030, 0.038	16.378	< .001
Between sessions and within states	0.638 (0.006)	0.614 (0.006)	0.024 (0.002)	0.020, 0.027	12.331	< .001
Within sessions and between states	0.644 (0.006)	0.615 (0.006)	0.029 (0.003)	0.024, 0.034	11.077	< .001
Between sessions and states	0.631 (0.006)	0.613 (0.006)	0.019 (0.002)	0.015, 0.022	9.647	< .001
Within sessions and states	0.659 (0.007)	0.615 (0.006)	0.044 (0.004)	0.037, 0.051	12.440	< .001

SE = Standard Error, CI = Compatibility Interval

¹Results are averaged over the levels of session and state.

²Results are averaged over the levels of state.

³Results are averaged over the levels of session.

Alpha Figure 12A shows the connectivity profiles for all phase coupling functional connectomes in the alpha band, organized by participant and recording. Plots and summary statistics of the distribution of coupling magnitudes across all recordings and EEG channel pairs are shown above in Figure 9 and Table 1, respectively.

Figure 12B shows the functional connectome similarity estimates between all pairs of phase coupling functional connectomes in the alpha band. There were no visually obvious patterns of similarity consistent across participants, but there were some individual differences worth highlighting: Participant P03 showed high similarity across sessions and states, corresponding to an individual effect; Participants P14, P17, and P19 showed moderate to high similarity in the eyes open state across sessions, and moderate similarity between participants, corresponding to a partial state effect; and participants P07, P08, P11, and P20 showed moderate similarity across sessions and states with themselves and each other, corresponding to a partial group effect. The remaining participants showed no distinctive patterns. Additionally, unlike the delta, theta, beta, and gamma bands, the amount of similarity between participants was generally moderate and considerably more variable; not consistently high.

However, despite the presence of more visually apparent individual effects, there was still a strong group effect. This was supported by the group-level contrast results in Figure 12C, which showed that although functional connectomes were more similar within participants than between participants at all levels of the session and state predictors, on average, the effect sizes most compatible with our data, given the background model, were still at most small. Table 4 shows the estimated marginal means and targeted hypothesis tests of zero difference within and between participants corresponding to each of these contrasts. Note that the between-participant functional connectome similarity means were stable across contexts, whereas the within-participant means

were more variable, indicating that the (at most) small positive differences in functional connectome similarity can be attributed to individual-dependent factors with small modulations by session and state. Jointly, these results suggest that, on average, the phase coupling dynamics of underlying global network activity in the alpha band was differentiated between individuals across contexts, but with only a small influence of individual-dependent factors over and above the influence of stable group-dependent factors.

These results remained largely consistent when the phase lag index was estimated using the Hilbert transform method instead of the multitaper method (Figure A9), with some minor differences: (1) phase coupling was generally weaker, but individual patterns of coupling were similar or the same; and (2) functional connectome similarity was generally higher, but patterns of similarity were similar or the same; however, differences in functional connectome similarity were generally of similar magnitudes. Likewise, the contrast results remained consistent between the reduced and maximal mixed beta regression models of functional connectome similarity when the phase lag index was estimated using both the multitaper method (Figure A13) and the Hilbert transform method (Figure A19), but with slightly more uncertainty in the estimates.

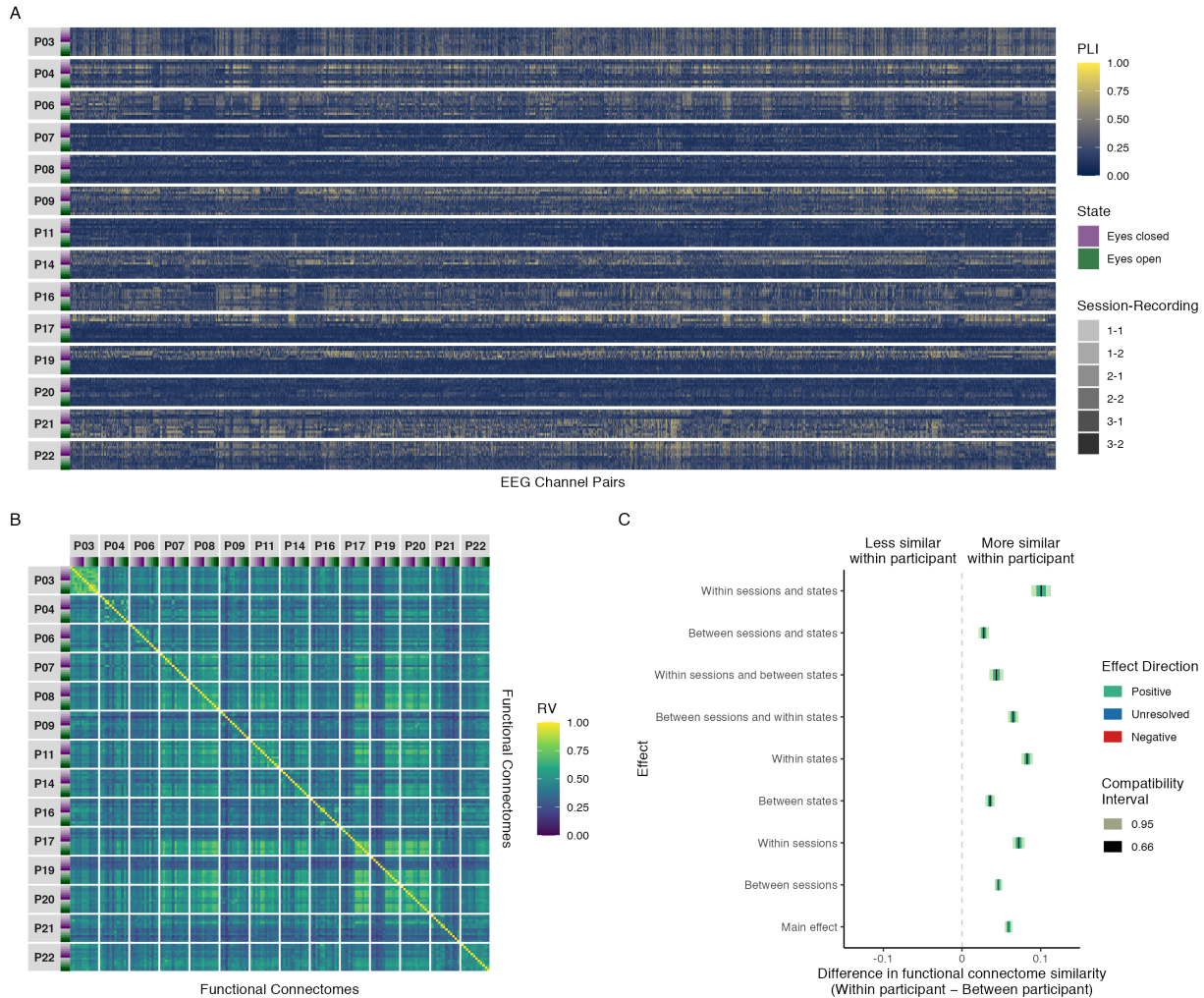


Figure 12. Results of phase coupling analyses in the alpha band: (A) connectivity profiles for all functional connectomes, organized by participant and recording; (B) estimates of functional connectome similarity between all pairs of functional connectomes, organized by participant and recording; and (C) group-level contrasts estimating the average difference in functional connectome similarity within and between participants across contexts.

Table 4

Estimated marginal means, mean differences, and targeted hypothesis tests of zero difference in alpha band phase coupling functional connectome similarity within and between participants across contexts.

Contrast	Within Participant	Between Participant	Mean Difference			
	Mean (SE)	Mean (SE)	ΔRV (SE)	95% CI	t(14,017)	p
Main effect ¹	0.490 (0.009)	0.431 (0.008)	0.059 (0.002)	0.054, 0.064	24.025	< .001
Between sessions ²	0.477 (0.009)	0.431 (0.008)	0.046 (0.002)	0.041, 0.051	18.638	< .001
Within sessions ²	0.503 (0.009)	0.431 (0.008)	0.072 (0.004)	0.064, 0.080	18.267	< .001
Between states ³	0.463 (0.009)	0.428 (0.008)	0.036 (0.003)	0.030, 0.042	11.886	< .001
Within states ³	0.517 (0.009)	0.434 (0.008)	0.083 (0.004)	0.076, 0.090	22.665	< .001
Between sessions and within states	0.500 (0.009)	0.435 (0.008)	0.065 (0.003)	0.058, 0.072	19.192	< .001
Within sessions and between states	0.471 (0.009)	0.428 (0.008)	0.044 (0.005)	0.035, 0.053	9.601	< .001
Between sessions and states	0.455 (0.009)	0.427 (0.008)	0.028 (0.003)	0.021, 0.034	8.212	< .001
Within sessions and states	0.535 (0.010)	0.434 (0.008)	0.101 (0.006)	0.088, 0.113	15.975	< .001

SE = Standard Error, CI = Compatibility Interval

¹Results are averaged over the levels of session and state.

²Results are averaged over the levels of state.

³Results are averaged over the levels of session.

Beta Figure 13A shows the connectivity profiles for all phase coupling functional connectomes in the beta band, organized by participant and recording. Plots and summary statistics of the distribution of coupling magnitudes across all recordings and EEG channel pairs are shown above in Figure 9 and Table 1, respectively.

Figure 13B shows the functional connectome similarity estimates between all pairs of phase coupling functional connectomes in the beta band. There was a visually obvious group effect, with high similarity between functional connectomes regardless of participant, session, or state. This was supported by the group-level contrast results in Figure 13C, which showed that although functional connectomes were more similar within participants than between participants at all levels of the session and state predictors, on average, the effect sizes most compatible with our data, given the background model, were at most small. Table 5 shows the estimated marginal means and targeted hypothesis tests of zero difference within and between participants corresponding to each of these contrasts. Note that the between-participant functional connectome similarity means were stable across contexts, whereas the within-participant means were more variable, indicating that the (at most) small positive differences in functional connectome similarity can be attributed to individual-dependent factors with slight modulations by session and state. Jointly, these results suggest that, on average, the phase coupling dynamics of underlying global network activity in the beta band was differentiated between individuals across contexts, but with only a slight influence of individual-dependent factors over and above the influence of stable group-dependent factors.

These results remained largely consistent when the phase lag index was estimated using the Hilbert transform method instead of the multitaper method (Figure A10), with some minor differences: (1) phase coupling was generally weaker, but individual patterns of coupling were

similar or the same; (2) functional connectome similarity was generally higher, but patterns of similarity were similar or the same; and (3) differences in functional connectome similarity were generally smaller, but were still positive with a similar pattern of variation across contexts. Likewise, the contrast results remained consistent between the reduced and maximal mixed beta regression models of functional connectome similarity when the phase lag index was estimated using both the multitaper method (Figure A14) and the Hilbert transform method (Figure A20), but with slightly more uncertainty in the estimates.

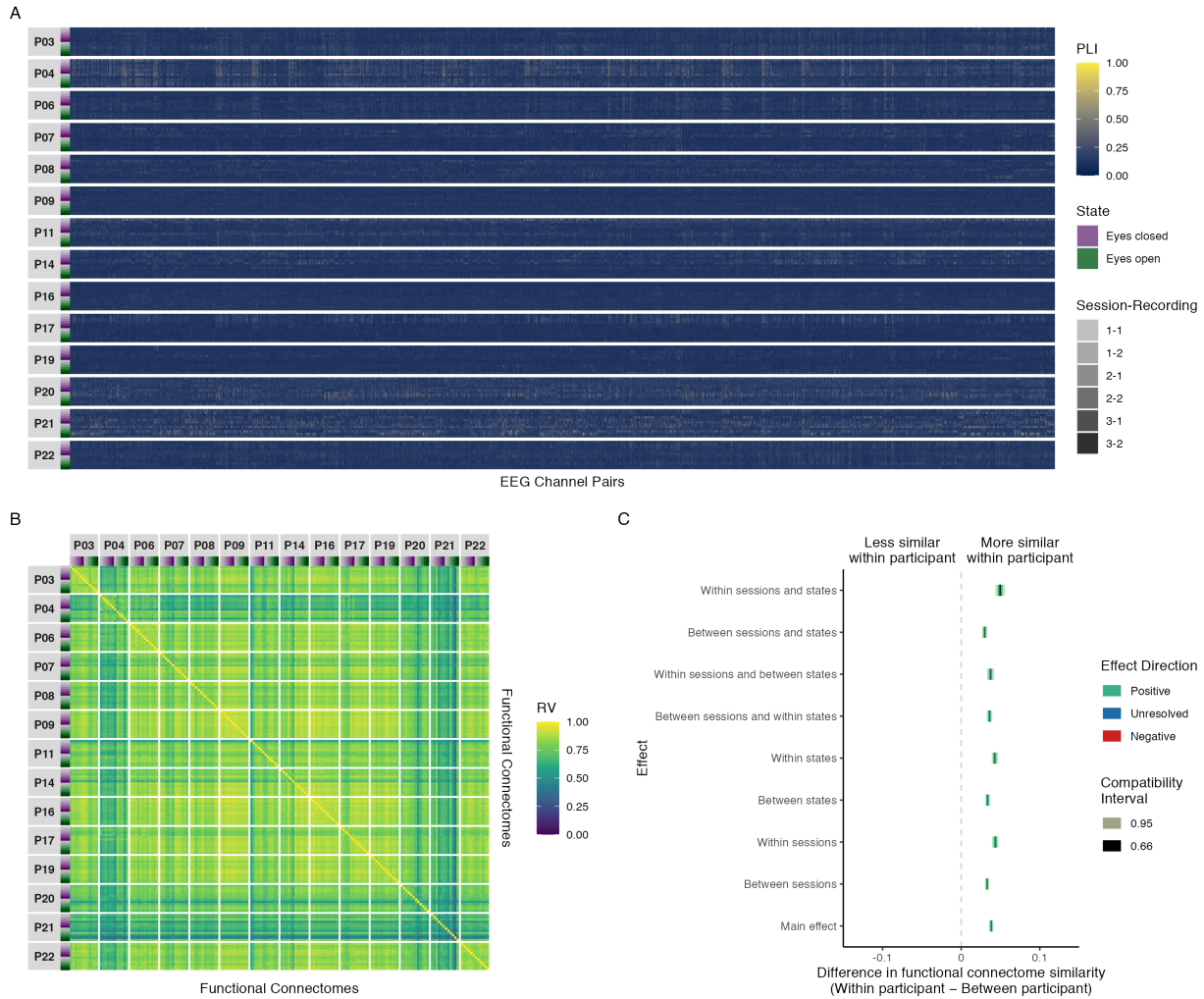


Figure 13. Results of phase coupling analyses in the beta band: (A) connectivity profiles for all functional connectomes, organized by participant and recording; (B) estimates of functional connectome similarity between all pairs of functional connectomes, organized by participant and recording; and (C) group-level contrasts estimating the average difference in functional connectome similarity within and between participants across contexts.

Table 5

Estimated marginal means, mean differences, and targeted hypothesis tests of zero difference in beta band phase coupling functional connectome similarity within and between participants across contexts.

Contrast	Within Participant	Between Participant	Mean Difference			
	Mean (SE)	Mean (SE)	ΔRV (SE)	95% CI	t(14,017)	p
Main effect ¹	0.812 (0.006)	0.774 (0.007)	0.038 (0.001)	0.035, 0.041	25.835	< .001
Between sessions ²	0.807 (0.006)	0.774 (0.007)	0.033 (0.001)	0.030, 0.036	23.045	< .001
Within sessions ²	0.818 (0.006)	0.774 (0.007)	0.043 (0.002)	0.039, 0.047	20.599	< .001
Between states ³	0.807 (0.006)	0.774 (0.007)	0.034 (0.002)	0.030, 0.037	20.374	< .001
Within states ³	0.817 (0.006)	0.774 (0.007)	0.043 (0.002)	0.039, 0.047	21.638	< .001
Between sessions and within states	0.811 (0.006)	0.775 (0.007)	0.036 (0.002)	0.032, 0.040	19.772	< .001
Within sessions and between states	0.811 (0.006)	0.774 (0.007)	0.037 (0.002)	0.033, 0.042	15.922	< .001
Between sessions and states	0.804 (0.006)	0.774 (0.007)	0.030 (0.002)	0.026, 0.033	16.774	< .001
Within sessions and states	0.824 (0.006)	0.774 (0.007)	0.049 (0.003)	0.043, 0.056	15.915	< .001

SE = Standard Error, CI = Compatibility Interval

¹Results are averaged over the levels of session and state.

²Results are averaged over the levels of state.

³Results are averaged over the levels of session.

Gamma Figure 14A shows the connectivity profiles for all phase coupling functional connectomes in the gamma band, organized by participant and recording. Plots and summary statistics of the distribution of coupling magnitudes across all recordings and EEG channel pairs are shown above in Figure 9 and Table 1, respectively.

Figure 14B shows the functional connectome similarity estimates between all pairs of phase coupling functional connectomes in the gamma band. There was a visually obvious group effect, with high similarity between functional connectomes regardless of participant, session, or state. This was supported by the group-level contrast results in Figure 14C, which showed that although functional connectomes were more similar within participants than between participants at all levels of the session and state predictors, on average, the effect sizes most compatible with our data, given the background model, ranged from practically nil to at most small. Table 6 shows the estimated marginal means and targeted hypothesis tests of zero difference within and between participants corresponding to each of these contrasts. Note that the between-participant functional connectome similarity means were stable across contexts, whereas the within-participant means were more variable, indicating that the (at most) small positive differences in functional connectome similarity can be attributed to individual-dependent factors with slight modulations by session and state. Jointly, these results suggest that, on average, the phase coupling dynamics of underlying global network activity in the gamma band was differentiated between individuals across contexts, but with only a slight, negligible influence of individual-dependent factors over and above the influence of stable group-dependent factors.

These results remained largely consistent when the phase lag index was estimated using the Hilbert transform method instead of the multitaper method (Figure A11), with some minor differences: (1) phase coupling was generally weaker, but individual patterns of coupling were

similar or the same; (2) functional connectome similarity was generally higher, but patterns of similarity were similar or the same; and (3) differences in functional connectome similarity were generally smaller, but were still positive with a similar pattern of variation across contexts. Likewise, the contrast results remained largely consistent between the reduced and maximal mixed beta regression models of functional connectome similarity when the phase lag index was estimated using both the multitaper method (Figure A15) and the Hilbert transform method (Figure A21), but with slightly more uncertainty in the estimates. This increased uncertainty resulted in the direction of the between sessions, between sessions and within states, and between sessions and states contrasts to become unresolved. However, the difference in interpretation between the maximal model and reduced model results here was minor: The maximal model simply requires the qualification that the differences in functional connectome similarity within and between participants most compatible with our data for these contrasts, given the background model, also included the possibility of (essentially) zero difference.

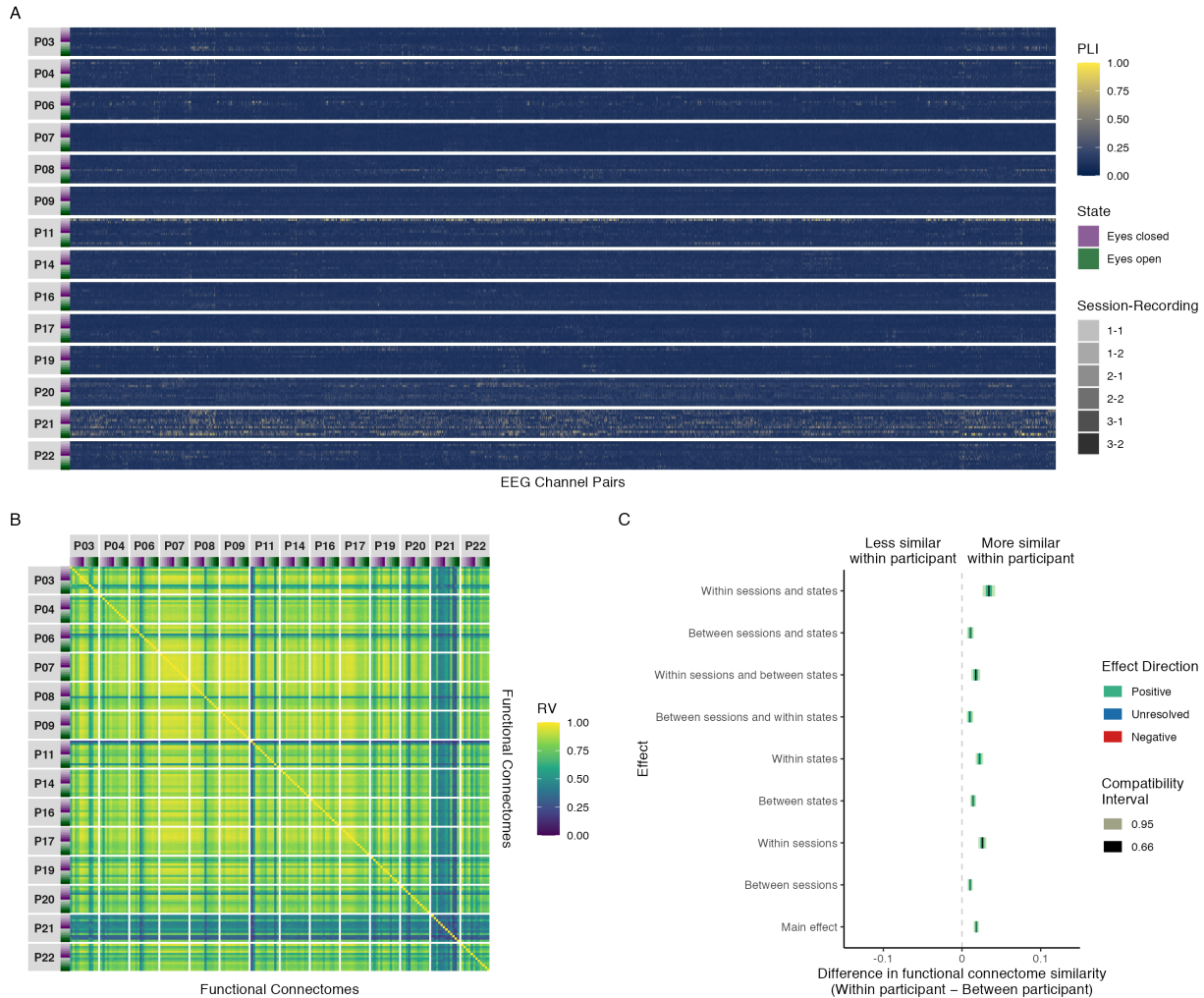


Figure 14. Results of phase coupling analyses in the gamma band: (A) connectivity profiles for all functional connectomes, organized by participant and recording; (B) estimates of functional connectome similarity between all pairs of functional connectomes, organized by participant and recording; and (C) group-level contrasts estimating the average difference in functional connectome similarity within and between participants across contexts.

Table 6

Estimated marginal means, mean differences, and targeted hypothesis tests of zero difference in gamma band phase coupling functional connectome similarity within and between participants across contexts.

Contrast	Within Participant	Between Participant	Mean Difference			
	Mean (SE)	Mean (SE)	ΔRV (SE)	95% CI	t(14,017)	p
Main effect ¹	0.786 (0.011)	0.768 (0.011)	0.018 (0.002)	0.015, 0.021	10.809	< .001
Between sessions ²	0.779 (0.011)	0.769 (0.011)	0.010 (0.002)	0.007, 0.014	6.475	< .001
Within sessions ²	0.794 (0.011)	0.768 (0.011)	0.026 (0.003)	0.021, 0.031	9.895	< .001
Between states ³	0.783 (0.011)	0.768 (0.011)	0.014 (0.002)	0.010, 0.018	7.275	< .001
Within states ³	0.790 (0.011)	0.768 (0.011)	0.022 (0.002)	0.017, 0.027	9.215	< .001
Between sessions and within states	0.779 (0.011)	0.768 (0.011)	0.010 (0.002)	0.006, 0.014	4.729	< .001
Within sessions and between states	0.786 (0.011)	0.768 (0.011)	0.018 (0.003)	0.012, 0.023	6.093	< .001
Between sessions and states	0.779 (0.011)	0.769 (0.011)	0.011 (0.002)	0.006, 0.015	4.986	< .001
Within sessions and states	0.802 (0.011)	0.768 (0.011)	0.034 (0.004)	0.026, 0.042	8.409	< .001

SE = Standard Error, CI = Compatibility Interval

¹Results are averaged over the levels of session and state.

²Results are averaged over the levels of state.

³Results are averaged over the levels of session.

Amplitude coupling functional connectome similarity analyses

Alpha

Figure 15A shows the connectivity profiles for all amplitude coupling functional connectomes in the alpha band, organized by participant and recording. Plots and summary statistics of the distribution of coupling magnitudes across all recordings and EEG channel pairs are shown above in Figure 9 and Table 1, respectively.

Figure 15B shows the functional connectome similarity estimates between all pairs of amplitude coupling functional connectomes in the alpha band. Interestingly—although perhaps not surprisingly given the spatial correspondence between phase coupling and amplitude coupling functional connectomes (Figure 8)—similar patterns of individual differences in functional connectome similarity were observed here in relation to the phase coupling similarities observed in the alpha band (Figure 12B). However, there was also a visually obvious group effect, with high similarity between functional connectomes regardless of participant, session, or state.

This was supported by the group-level contrast results in Figure 15C, which showed that although functional connectomes were more similar within participants than between participants at all levels of the session and state predictors, on average, the effect sizes most compatible with our data, given the background model, ranged from practically nil to at most small. Table 7 shows the estimated marginal means and targeted hypothesis tests of zero difference within and between participants corresponding to each of these contrasts. Note that the between-participant functional connectome similarity means were stable across contexts, whereas the within-participant means were more variable, indicating that the (at most) small positive differences in functional connectome similarity can be attributed to individual-dependent factors with small modulations by session and state. Jointly, these results suggest that, on average, the amplitude

coupling dynamics of underlying global network activity in the alpha band was differentiated between individuals across contexts, but with only a slight, negligible influence of individual-dependent factors over and above the influence of stable group-dependent factors.

The contrast results remained largely consistent between the reduced and maximal mixed beta regression models of functional connectome similarity, but with slightly more uncertainty in the estimates (Figure A16). This increased uncertainty resulted in the direction of the between sessions and states contrast to become unresolved. However, the difference in interpretation between the maximal model and reduced model results here was minor: The maximal model simply requires the qualification that the differences in functional connectome similarity within and between participants most compatible with our data for this contrast, given the background model, also included the possibility of (essentially) zero difference.

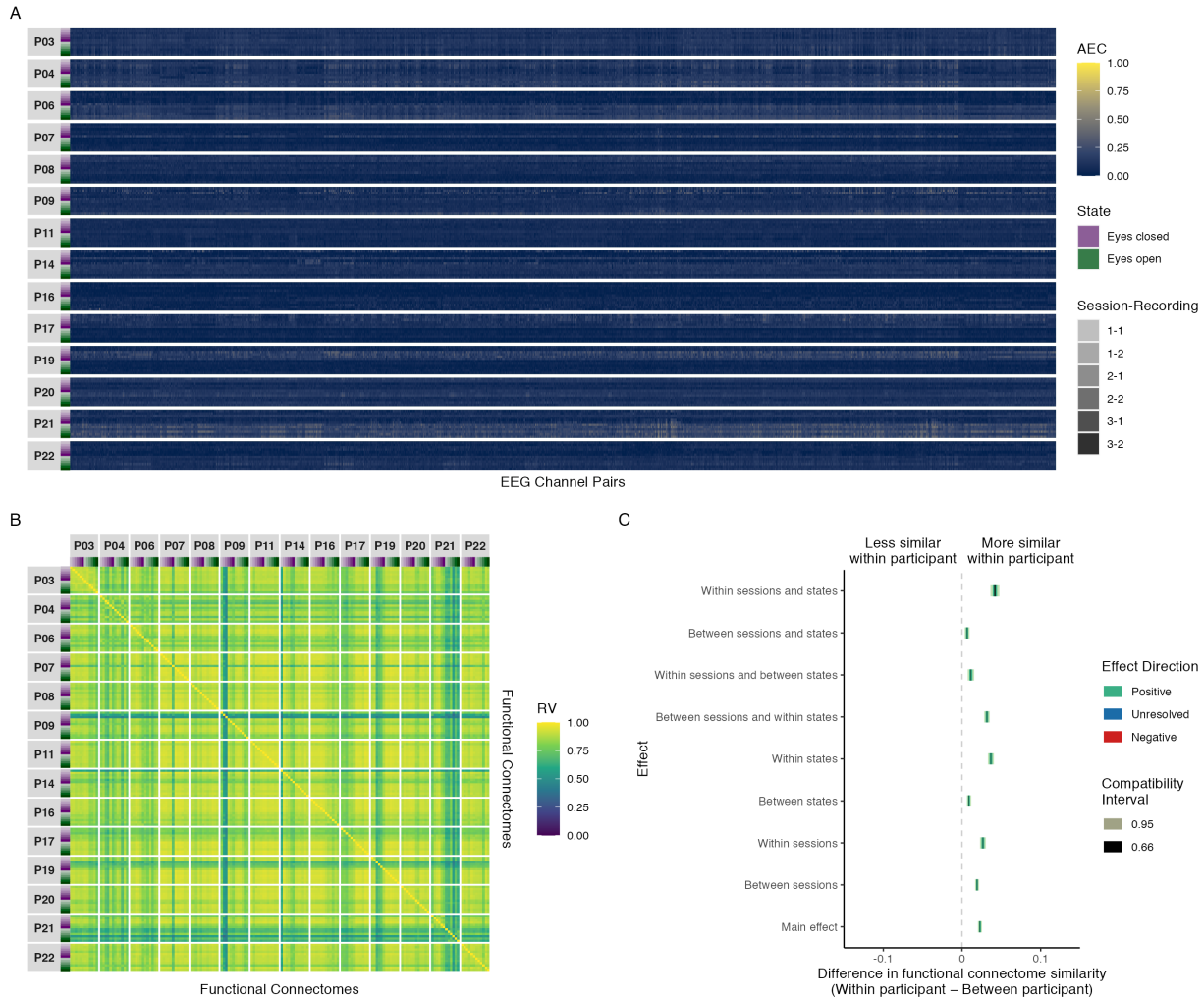


Figure 15. Results of amplitude coupling analyses in the alpha band: (A) connectivity profiles for all functional connectomes, organized by participant and recording; (B) estimates of functional connectome similarity between all pairs of functional connectomes, organized by participant and recording; and (C) group-level contrasts estimating the average difference in functional connectome similarity within and between participants across contexts.

Table 7

Estimated marginal means, mean differences, and targeted hypothesis tests of zero difference in alpha band amplitude coupling functional connectome similarity within and between participants across contexts.

Contrast	Within Participant	Between Participant	Mean Difference			
	Mean (SE)	Mean (SE)	ΔRV (SE)	95% CI	t(14,017)	p
Main effect ¹	0.865 (0.005)	0.842 (0.006)	0.023 (0.001)	0.020, 0.025	17.478	< .001
Between sessions ²	0.862 (0.005)	0.843 (0.006)	0.019 (0.001)	0.017, 0.022	15.005	< .001
Within sessions ²	0.869 (0.005)	0.842 (0.006)	0.027 (0.002)	0.023, 0.030	14.096	< .001
Between states ³	0.852 (0.006)	0.843 (0.006)	0.009 (0.001)	0.006, 0.012	6.386	< .001
Within states ³	0.879 (0.005)	0.842 (0.006)	0.037 (0.002)	0.033, 0.041	18.996	< .001
Between sessions and within states	0.874 (0.005)	0.842 (0.006)	0.032 (0.002)	0.028, 0.035	17.770	< .001
Within sessions and between states	0.854 (0.006)	0.843 (0.006)	0.011 (0.002)	0.007, 0.015	5.448	< .001
Between sessions and states	0.849 (0.006)	0.843 (0.006)	0.007 (0.002)	0.004, 0.010	4.192	< .001
Within sessions and states	0.884 (0.005)	0.842 (0.006)	0.042 (0.003)	0.036, 0.048	14.396	< .001

SE = Standard Error, CI = Compatibility Interval

¹Results are averaged over the levels of session and state.

²Results are averaged over the levels of state.

³Results are averaged over the levels of session.

Delta, Theta, Beta, and Gamma

Although we conducted all analyses for the delta, theta, beta, and gamma bands, we refrain from interpreting the results of these analyses here based on a post-hoc suggestion from a committee member; however, for transparency, the functional connectome similarity results for these frequency bands are shown in Figure A22 in Appendix A. In short, the rationale behind this decision was that the functional connectome similarity analyses for these frequency bands appeared misleading, due to an unforeseen limitation of our approach to quantifying functional connectome similarity. Specifically—although the distribution of amplitude envelope correlation estimates in each of these frequency bands was in agreement with previous published work (e.g., Fraschini et al., 2019; Lai et al., 2018; Mehrkanoon et al., 2014)—any qualitatively distinct differences in spatial organization between any pair of functional connectomes was overshadowed by the fact that the relative position of the observations in each connectome were very close together in space, resulting in very high to near-perfect estimates of functional connectome similarity across participants, sessions, and states. While these estimates are a statistically valid reflection of the data, we felt that they were neurophysiologically unrealistic, greatly exaggerating the magnitude of similarity between any pair of functional connectomes and failing to capture the intended nuance across participants, sessions, and states.

Outcome variability of functional connectome similarity contrasts

Figure 16 summarizes the results of the individual-level phase coupling and amplitude coupling functional connectome similarity contrasts in each frequency band, respectively, showing the proportion of participants whose 95% compatibility intervals for a given contrast were positive, unresolved, or negative. The effect sizes corresponding to these results are shown in Figures A1-A6 in Appendix A. Note that across all frequency bands and contrasts there was a

mixture of participants whose most compatible effect sizes, given the background model, were unresolved or positive, with a smaller portion of negative effect sizes. Thus, although the group-level contrast results for both phase coupling and amplitude coupling functional connectomes across all frequency bands suggested that, on average, differences in functional connectome similarity may have been influenced to a slight or at most small extent by individual-dependent factors—this relationship was not necessarily true at an individual-level for all participants.⁹

⁹ Note that this statement would hold true even if we only considered the direction of the point estimates for each individual-level contrast. This is shown in Figures 1 to 6 in Appendix A, where it can be seen that although the majority of point estimates were positive across all contrasts, a small but not insignificant proportion of participants had negative point estimates for most contrasts across all frequency bands and coupling modes.

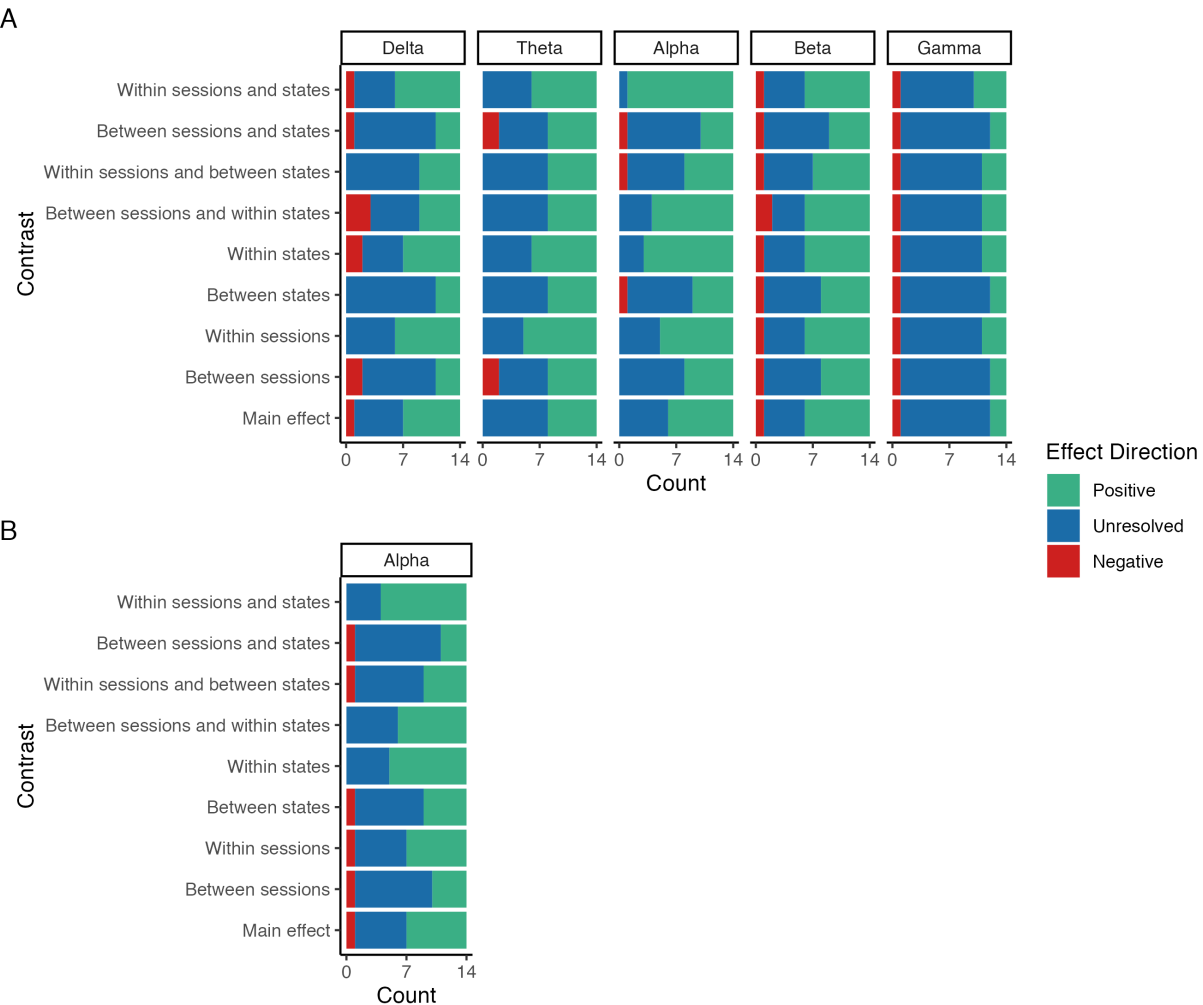


Figure 16. Stacked bar plots showing the proportion of individual participants whose 95% compatibility intervals for the phase coupling (A) and amplitude coupling (B) functional connectome similarity contrasts were positive, unresolved, or negative in each frequency band.

Discussion

In this study, we explored the feasibility of using EEG to study network variants by examining whether or not EEG phase coupling and amplitude coupling functional connectomes showed similar evidence of stable individual differences across contexts to what has been

described in the fMRI literature. To address this question, we used pairwise contrasts to estimate how much and in which ways functional connectome similarity differed within and between individuals across sessions and states, using eyes open and eyes closed resting state EEG data collected across three sessions over the course of approximately three months. Based on the findings of previous fMRI network variant research (e.g., Gratton et al., 2018; Seitzman et al., 2019), we hypothesized that functional connectomes would be more similar within than between individuals across all contrasts, on average, with smaller variations in similarity related to session or state (see Figure 7).

Overall, our results were inconclusive. In support of our primary scientific hypothesis, the group-level effect sizes most compatible with our data, given the background model, showed that, on average, both phase coupling and amplitude coupling functional connectomes were more similar within than between individuals across contexts and frequency bands (Figures 10-15); that our data were incompatible with a model that assumed zero difference in functional connectome similarity within and between individuals across contexts (Tables 2-7); and that these differences were attributable to individual-dependent factors with small modulations by session and state (Tables 2-7). Moreover, the magnitude of these differences varied across contexts in an expected way, with the largest differences in similarity within and between individuals occurring for functional connectomes from the same sessions and states, the smallest differences occurring for functional connectomes from the different sessions and states, and relatively smaller increases and decreases in similarity across other contexts. At this level of description, our results were broadly consistent with the findings of methodologically similar fMRI studies (e.g., Gratton et al., 2018). These results remained largely consistent for phase coupling functional connectomes when the phase lag index was estimated using the Hilbert

transform method instead of the multitaper method (Figures A7-A11); and with few exceptions, these results were consistent between the reduced and maximal models of functional connectome similarity for both phase coupling and amplitude coupling functional connectomes (Figures A12-A16).

However, in general, the group-level effect sizes most compatible with our data, given the background model, ranged from practically nil to at most small, depending on the contrast, coupling mode, and frequency band in question (Figures 10-15). Thus, although our results suggested that, on average, the phase coupling and amplitude coupling dynamics of underlying global network activity in each frequency band was differentiated between individuals across contexts *in our sample*, the influence of individual-dependent factors over and above the influence of stable group-dependent factors was negligible or small at best. This is a clear departure from what has been described in the fMRI literature, where differences in functional connectome similarity within and between individuals have been reported to be stable, relatively large, and visually obvious, indicative of “a clear influence of individual features over and above common organizational principles at the network level,” (Marek et al., 2018) such that fMRI functional connectomes may be well-suited for measuring and identifying the neural causes of variation in human behaviour, cognition, and their dysfunction (Gratton et al., 2018). Our results do not inspire such confidence. Indeed, given the inherent limitations of EEG functional connectivity analysis, it is unclear to what extent our results reflect genuinely small interindividual differences in electrophysiological connectivity across contexts, versus methodological limitations, selection bias, or random variation in our sample that may have caused us to underestimate or overestimate the magnitude of interindividual differences relative to the (unknown) true effects.

Finally, we note that although the group-level effect sizes most compatible with our data, given the background model, were more similar within than between individuals, on average, this relationship was not true for all participants. Indeed, there was a notable degree of outcome variability in the direction (Figure 16) and magnitude (for reduced models, see Figures A1-A6; for maximal models, see Figures A12-A16) of these effects when differences in functional connectome similarity were analyzed at an individual level. These results were also a clear departure from what has been described in the fMRI literature, where differences in functional connectome similarity within and between individuals have been found to be consistently positive at an individual-level, with relatively little outcome variability in the magnitude of these differences (Gratton et al., 2018). Moreover, because of the outcome variability in our sample, we caution against confusing the positive and precise estimates of average effects for the group-level contrasts with the predictability of individual outcomes, which were more variable in both their direction and magnitude. However, equally, we also caution against confusing the individual-level contrasts whose direction was unresolved with precise zero effects or evidence of no positive difference in functional connectome similarity. For many of these contrasts, the effect sizes most compatible with our data, given the background model, included a range of effects that—although generally still small—were not negligible; thus, even though they leave open the possibility of negative, zero, or positive but negligible effects, they also leave open the possibility of small effects that may be worth investigating further.

Considered together, given the background model used to investigate our research question, our results did not generally demonstrate the feasibility of using EEG to study network variants due to the inconsistencies observed across participants in our sample. At best our findings leave open the possibility that EEG functional connectomes may be suitable measures of

stable individual differences in whole brain functional network organization, given that both the group-level results and a subset of individual-level results showed consistently positive differences in functional connectome similarity within versus between individuals across contexts and frequency bands; however, it is apparent that if the phase coupling and/or amplitude coupling dynamics of underlying global network activity across frequency bands are indeed influenced by stable individual-dependent factors, further work identifying and developing methods to reliably measure and quantify these stable individual differences is necessary.

Consistency with related neurophysiological connectomics literature

As we noted in the results section, both our phase coupling and amplitude coupling functional connectivity analyses performed as expected based on what has been reported in previous work using the phase lag index and orthogonalized amplitude envelope correlation with resting state EEG; thus, we assumed that our estimates were able to provide a sound representation of underlying (non-zero lag) global network activity for each participant and coupling mode. Specifically, consistent with previous work, we found (1) a high level of spatial correspondence between phase coupling and amplitude coupling functional connectomes (Figure 8) (Mostame & Sadaghiani, 2020); (2) typical distributions of coupling magnitudes in each frequency band for both coupling modes that were right-skewed with a small mean and wide range (Figure 9) (Fraschini et al., 2019; Lai et al., 2018; Mehrkanoon et al., 2014); and (3) a clear frequency band response was observed for both coupling modes (Figure 9), with the strongest coupling occurring in the alpha band for both the phase lag index (Hardmeier et al., 2014; Mehrkanoon et al., 2014; Van Der Molen et al., 2014) and the orthogonalized amplitude envelope correlation (Hipp et al., 2012; Mehrkanoon et al., 2014; Samogin et al., 2020, 2022; Taberna et al., 2021).

Notably, the prominence of alpha band functional connectivity coincided with the strongest differences in functional connectome similarity within versus between individuals observed in our study (Figure 12C), which may indicate that EEG network variants are more sensitive to brain state than fMRI network variants (cf. Gratton et al., 2018), given the well-documented relationship between brain state, spectral power, and coupling strength observed with neurophysiological recording methods (e.g., Barry et al., 2007; Siegel, Donner, & Engel, 2012; Vidaurre et al., 2018). From this perspective, the clear frequency band response in our functional connectome similarity results may be unsurprising, as alpha oscillations are the most dominant rhythm during resting state and are known to play a prominent role in intrinsic connectivity networks (Mantini et al., 2007; Marino et al., 2019; Sadaghiani & Kleinschmidt, 2016; Samogin et al., 2020). In support of this point, although we found that the relative strength of both within individual and between individual similarities generally shifted in the same direction from one frequency band to another, the magnitude of group-level differences in phase coupling functional connectome similarity within versus between individuals was not equivalent across frequency bands, indicating that functional connectomes became less or more differentiated between individuals as a function of frequency band.

Furthermore, the pattern of group-level contrast results for phase coupling functional connectome similarities in the alpha band (Figure 12C) appeared to be influenced more by an individual-state effect than an individual-session effect (Figure 7, fourth plot); whereas (although subtle) the delta, theta, beta, and gamma bands (Figures 10C, 11C, 13C, 14C) appeared to be influenced more by an individual-session effect than an individual-state effect (Figure 7, third plot). Although we did not predict this outcome, it may also be unsurprising, given that the typical widespread reduction in alpha band oscillations between eyes-closed and eyes-open

resting state and associated changes in functional connectivity would be expected to produce such a pattern of results given that, within individuals, functional connectomes would be noticeably dissimilar between these states, on average, but similar within them; whereas the more subtle differences between eyes-closed and eyes-open resting state for other frequency bands would be less likely to produce such noticeable changes.

Our results are also conceptually consistent with a recent study by Nentwich et al. (2020), who investigated the relationship between twelve phenotypic variables (age, sex, socioeconomic status, intelligence, and diagnostic assessments for sleep disturbance, behavioural and emotional problems, attention-deficit/hyperactivity disorder, anxiety, inattention, mood, internet addiction, distress tolerance) and phase coupling functional connectome similarities in a large sample of typically and atypically developing children and adolescents during resting in the delta, theta, alpha, and beta bands. They found that all twelve variables were unable to explain variation in functional connectome similarities between and among individuals in the delta, theta, alpha, and beta bands: with the exception of sex and age in the beta band. Although our study did not examine the relationship between any variables of interest and functional connectome similarity, the findings of Nentwich et al. (2020) indicate—similar to our findings—that (1) functional connectomes may become more differentiated between individuals as a function of frequency band, given they only found phenotype-connectome relationships in the beta band; and (2) network variants may be harder to detect with EEG. Regarding the latter point, Nentwich et al. (2020) also investigated the relationship between the aforementioned twelve variables and fMRI functional connectome similarities in the same sample. Here they found that four variables (age, sex, intelligence, and the assessment for behavioural and emotional problems) were able to explain variation in functional connectome similarities between and among individuals,

suggesting that fMRI functional connectomes may better capture practically relevant information compared to EEG.

Finally, the smaller variations in within-individual functional connectome similarity across sessions and states observed in our sample were also consistent with previous EEG (Nentwich et al., 2020), electrocorticography (ECoG; Mostame & Sadaghiani, 2021), and magnetoencephalography (MEG; Colclough et al., 2016) research, which found that phase coupling and amplitude coupling functional connectomes were generally stable within individuals, showing moderate to high similarity within and between sessions and states across frequency bands. Additionally, in agreement with Colclough et al. (2016), we found that within-individual functional connectome similarity was generally higher when functional connectivity was estimated with the orthogonalized amplitude envelope correlation than with the phase lag index.

Differences between phase and amplitude coupling

Across all frequency bands, we found that functional connectivity estimated with the orthogonalized amplitude envelope correlation was generally smaller than with the phase lag index (Figure 9). As we discussed in the results section, we expected the estimates from these metrics to differ, given that the phase lag index and orthogonalized amplitude envelope correlation measure different aspects of functional connectivity in mathematically distinct ways. However, we also note that this difference is likely partially due to differences in the frequency specificity of the two methods, with the phase lag index having greater specificity than the orthogonalized amplitude envelope correlation. This difference in frequency specificity is attributable to the phase lag index being estimated and averaged over multiple frequency bins in

each frequency band when using the multitaper method, versus the orthogonalized amplitude envelope correlation being estimated with a single analytic signal in each frequency band when using the Hilbert transform method. In Figures A7-A11 in Appendix A we show how the results change when the phase lag index is estimated using the Hilbert transform method. Across all five frequency bands we found that (1) functional connectivity was generally lower than we found with the multitaper method, but individual patterns of connectivity were similar or the same; and (2) functional connectome similarity was generally higher than we found with the multitaper method, but patterns of similarity and contrast effect sizes were similar or the same. Thus, although these changes were not great enough to change our conclusions, they did make the differences observed between the phase lag index and orthogonalized amplitude envelope correlation results less stark, highlighting how different spectral analysis methods can influence functional connectivity estimates if analysis parameters cannot be matched (cf. Bruns, 2004).

Another factor possibly contributing to the differences observed between the phase lag index and orthogonalized amplitude envelope correlation was the effect of epoch length on the two methods. Fraschini et al. (2016) compared the effect of non-overlapping epochs with variable length (1, 2, 4, 6, 8, 10, 12, 14 and 16 seconds) on broadband (1-20 Hz) functional connectivity estimates in a small sample of middle-aged adults during resting eyes-closed resting state. They found that epoch length affected both the magnitude of group-averaged mean functional connectivity and the distinctiveness of functional connectivity patterns. Specifically, group-averaged global functional connectivity was higher for the phase lag index than the orthogonalized amplitude envelope correlation at 1-6 second long epochs, with more comparable estimates between the two methods with 8-16 second long epochs; that group-averaged global functional connectivity decreased as a function of epoch length, with the phase lag index and

orthogonalized amplitude envelope correlation stabilizing at 12 and 6 second long epochs, respectively; and that the distinctiveness of group-averaged functional connectivity patterns increased as a function of epoch length, with shorter epochs showing blurrier patterns relative to longer epochs where patterns became more distinct. Because Fraschini et al.'s (2016) results were based on broadband group-averaged global functional connectivity, they are not directly comparable to our own findings; however, they do highlight how preprocessing decisions can (differentially) influence functional connectivity estimates. In the context of our study, we emphasize the need for future work to explore how preprocessing decisions can influence individual-level functional connectivity and functional connectome similarity estimates, with a focus on identifying approaches that can achieve both high within-individual and low between-individual functional connectome similarity.

Factors that may contribute to differences between EEG and fMRI

Factors that could explain the differences between our findings and what has been reported in the fMRI literature are the spatial and temporal resolutions of the two modalities, and the methods used to estimate functional connectivity.

Network variants are likely sensitive to the spatial resolution of the neuroimaging system used to study them, as this influences the precision with which individual differences in functional connectivity can be measured. For EEG, the number of electrodes and distance between them determines spatial resolution, with higher electrode density corresponding to higher spatial resolution (Ferree, Clay, & Tucker, 2001; Robinson et al., 2017; Ryynanen et al., 2004; Ryynanen et al., 2006). With low electrode density, as in the 10-20 system, EEG typically has a spatial resolution of approximately 5 to 9 centimetres (Burle et al., 2015; Srinivasan,

Tucker, & Murias, 1998). Higher density EEG systems can achieve a spatial resolution of up to 1 to 2 centimetres, but this still falls short of the spatial resolution of fMRI, which typically ranges from 500 microns to 4 millimetres (Glover, 2011). Because EEG functional connectomes are naturally spatially blurrier than fMRI functional connectomes, network variants may be harder to detect or less pronounced in EEG, leading to smaller, less consistent, differences in functional connectome similarity within versus between individuals.¹⁰ Future work might address this possibility either by testing how individual differences in functional connectome similarity vary as a function of electrode density, or by using simultaneous (source-space) EEG and fMRI (Mulert, 2013) to compare the strength and consistency of network variants between the two modalities in the same sample.

Network variants are also likely sensitive to the methods used to estimate functional connectivity. There are two assumptions related to this that are important to consider when

¹⁰ EEG biometrics research has demonstrated that resting state (eyes open and closed) functional connectomes from the same individual can be accurately matched when comparing a given individual's connectome against all other connectomes in small samples (up to and around 100 participants; e.g., La Rocca et al., 2014). However, although findings like this do suggest that EEG functional connectomes are more similar within than between individuals—to a degree that allows for accurate matching—they do not address the magnitude of these individual differences. Thus, future work may find that EEG has sufficient spatial resolution for biometrics (where the size of individual differences do not matter, so long as they are consistent), but insufficient spatial resolution for studying network variants (where the size of individual differences are a focal interest).

evaluating our results, and which may be worth investigating in future research. First, we assumed that five-minute recordings would be sufficient to get stable functional connectivity estimates with EEG given that (1) the longer scanning times needed to reliably detect network variants with fMRI is related to its low sampling rate (Seitzman et al., 2019), and not to the actual timeframe at which neural processes occur; and (2) EEG samples a substantially larger number of time points than fMRI in a much shorter timeframe. Because we found that functional connectomes were generally stable within individuals, showing moderate to high similarity within and between sessions and states across timescales, we believe this assumption was justified. However, we do note that longer recordings have been found to improve the stability of fMRI functional connectivity estimates in a qualitatively distinct way from higher sampling rates (Birn et al., 2013), likely due to slow network changes being more fully captured by longer recordings. Future work may benefit from testing if the stability of EEG functional connectivity estimates gain a similar improvement from longer recordings, particularly at lower frequencies such as the delta band; such work would pair nicely with the identifying the optimal epoch length(s) for band-limited, individual-level functional connectivity analysis (cf. Fraschini et al., 2016), as we discussed in the previous section.

Second, we assumed that network variants could be observed when considering only phase coupling and amplitude coupling with non-zero lag, discounting the true zero-lag coupling that occurs in functional networks. However, this discounting leads to an underestimation of true connectivity for both the phase lag index and amplitude envelope correlation by a non-trivial amount (Hipp et al., 2012; Stam et al., 2007), and might also remove or attenuate individual-specific features of the functional connectome (Fraschini et al., 2019). Given that we generally found the strongest similarities between functional connectomes with homogeneously low

patterns of coupling, non-zero lag phase and amplitude coupling methods may not be feasible for studying network variants in frequency bands where (1) the magnitude of coupling estimates is expected to be generally homogeneous for a given state, task, or functional connectivity metric; and (2) the chosen method of quantifying functional connectome similarity is sensitive to the distribution of coupling magnitudes. The most extreme examples of this in our study were with amplitude coupling functional connectomes in the delta, theta, beta, and gamma bands, where we found that unexpectedly high similarity within and between individuals was associated with functional connectomes with homogeneously low coupling estimates across EEG channel pairs for all connectomes (Figure A22). As we discussed in the results section, these estimates were a statistically valid reflection of the data, given our method for quantifying functional connectome similarity; however, equally, we felt that they were neurophysiologically unrealistic, greatly exaggerating the magnitude of similarity between any pair of functional connectomes and failing to capture the intended nuance across participants, sessions, and states due to the limitations of our chosen method.

One potential solution to avoid homogeneously low patterns of coupling would be to use phase coupling and amplitude coupling methods that include zero-lag coupling—supplemented with tests against volume conduction (Cohen, 2015)—as these methods tend to produce larger, more normally distributed, estimates of functional connectivity (e.g., Fraschini et al., 2019; Lai et al., 2018). However, although this approach is feasible in the context of ECoG studies where volume conduction is less of a concern (Mostame & Sadaghiani, 2021), it is impractical for EEG studies since it requires inspecting hundreds of thousands of individual connections to rule out possible contamination by volume conduction (Cohen, 2015). Another potential solution would be to use non-zero lag coupling methods that might underestimate true connectivity by a lesser

amount, such as the weighted phase lag index (Vinck et al., 2011) for phase coupling; and cokurtosis (or its normalized counterpart, the non-Gaussian power correlation) for amplitude coupling, which may be less sensitive to the signal orthogonalization procedure used to account for volume conduction (Hindriks & Tewarie, 2023). Finally, regardless of the chose functional connectivity metric, applying transformations to functional connectivity estimates, such as the square root or cube root transform, may broaden the circumstances under which functional connectome similarity analyses obtain reasonable estimates—as these transformations can reduce the right-skew of functional connectivity estimates, making them more amenable for analysis when the chosen method of quantifying functional connectome similarity is sensitive to the distribution of coupling magnitudes. Regardless of the potential solution, the spatial mixing caused by volume conduction poses a difficult problem, and future work may benefit from testing the robustness of different functional connectivity methods for studying network variants with EEG (for a related example using magnetoencephalography, see Colclough et al., 2016).

Limitations

In addition to the discussion above, the following methodological and statistical assumptions are important to consider when evaluating our results.

First, it is unclear how our results might generalize to more diverse, larger samples. In particular, our participants were healthy young adults in their twenties sampled from a western, educated, industrialized, rich, and democratic population, who have been shown to be outliers on a number of behavioural and cognitive measures in comparison with the rest of the human population (Henrich et al., 2010). Differences in functional connectivity have been found with ageing (e.g., Samogin et al., 2022), neurological disease or disorder (e.g., Engels et al., 2015),

mental illnesses such as depression (e.g., Shim, Im, Kim, & Lee, 2018), head trauma (e.g., C. Cao & Slobounov, 2010), and alcoholism (e.g., R. Cao, Wu, Li, Xiang, & Chen, 2014); thus, it might be reasonable to expect that our exclusion criteria removed meaningful variation from our sample. Additionally, given the size of our sample, and the inconsistencies we observed across participants, we caution against generalizing our results to samples with similar characteristics. Instead, we stress the importance of future work examining these relationships in larger, more representative samples, whose results can then be combined using meta-analytic studies and other cumulative approaches in order to come to more generalized scientific conclusions about electrophysiological network variants (Amrhein et al., 2019; Berner & Amrhein, 2021; Nichols et al., 2019, 2021). Based on the results of our study, at most we might conclude that—if network variants can be reliably detected with EEG—there is no guarantee that their presence can be detected in a given individual or data set, given the background models used to estimate functional connectivity, functional connectome similarity, and interindividual differences across contexts.

Second, we assumed that the connectivity structure in each frequency band was stationary over the length of the recording for both phase and amplitude coupling functional connectomes. Although neural oscillations are naturally non-stationary, varying from moment to moment (Faisal et al., 2008), stationary patterns of functional connectivity during resting state have been identified in EEG (e.g., Olguín-Rodríguez et al., 2018), fMRI (e.g., Laumann et al., 2017), and simultaneous EEG-fMRI studies (e.g., Daniel Arzate-Mena et al., 2022), with consistent positive or negative coupling occurring between sites or electrodes, even when averaging over multiple epochs. These stationary patterns are thought to be the substrate for effective brain function, permitting the adaptability and efficiency needed to optimize responses to our often-

unpredictable environment (Garrett et al., 2013), and thus reflect neuropsychologically relevant signals of interest. However, we do note that approaches accounting for nonlinear dynamics may provide complimentary insights to those that focus on the stable aspects of network variants. For example, Van De Ville, Farouj, Preti, Liégeois, & Amico (2021) found that fMRI functional connectomes exhibit short transient bursts of uniqueness even at short time windows, with different resting state networks becoming more or less unique between individuals as a function of time window length, suggesting that the dynamic aspects of network variants are worth exploring.

Third, we limited our investigation to within-frequency analyses of functional connectivity and network similarity. Although cross-frequency coupling is also considered to be a key mechanism by which the brain transmits and processes information, integrating functional systems across multiple spatiotemporal scales (Canolty & Knight, 2010), we did not explore for the presence of network variants in cross-frequency coupling functional connectomes given that most research on cross-frequency coupling focuses on coupling within brain regions or between a small number of regions of interest, rather than the entire connectome. Only a handful of studies have demonstrated that cross-frequency coupling also occurs in whole brain functional networks (Keitel, Thut, & Gross, 2017; Palva, 2005; Siebenhühner, Wang, Palva, & Palva, 2016; van der Meij, Kahana, & Maris, 2012), and the validity of these findings has recently come into question due to standard cross-frequency coupling analyses showing significant cross-frequency coupling in the absence of any underlying physiological coupling (Aru et al., 2015). Recently, however, Siebenhühner et al. (2020) were able to demonstrate the presence of true cross-frequency coupling in whole brain functional networks—ruling out the influence of spurious coupling—in both a small sample of presurgical epilepsy patients during eyes-closed resting state using stereo-

EEG, and a small sample of healthy controls during eyes-open resting state using magnetoencephalography. Moreover, they found that network strength was predictive of individual differences on several cognitive tasks in the healthy control sample (the other sample did not complete these tasks); thus, cross-frequency coupling may be a worthwhile avenue for future EEG network variant research if methods for estimating true cross-frequency coupling are validated, improved, and made more accessible (e.g., Idjadi et al., 2022).

Fourth, although our analyses focused solely on interindividual differences in connectivity strength across contexts (necessarily, given our data was in sensor-space), we emphasize that interindividual differences in the size and position of network nodes and network topography likely also influenced our results. Because each of these forms of variation can be present simultaneously, the effects of one form of variation can influence estimates of the others (Gordon & Nelson, 2021); thus, our estimates of phase coupling and amplitude coupling were likely driven by a mixture of each of these three forms of interindividual variability, rather than connectivity strength alone. Moreover, in the context of our functional connectome similarity analyses, the relative influence of each form of interindividual variability likely differed for within-participant and between-participant comparisons. Specifically, we would expect the size and position of network nodes and network topography to be more stable within individuals from recording to recording, given the relative stability of cortical organization over time (e.g., Laumann et al., 2015); thus, within-participant differences in functional connectivity and functional connectome similarity across contexts may be more influenced by true changes in coupling. However, we cannot assume such a dissociation for between-participant differences, therefore, any individual differences observed in our sample likely reflected an unknown mixture

of each of these forms of variation—whose relative influence likely varied across participants (Gordon & Nelson, 2021).

Fifth, building upon our discussion in both the results and the previous section, it is important to acknowledge that our approach to quantifying functional connectome similarity through a single summary statistic—although convenient for subsequent analyses and interpretation—cannot be expected to reflect the full complexity of our functional connectivity data. As with any summary statistic, there are circumstances where different summary statistics may be considered more or less useful, and likewise, where the obtained estimates may be considered more or less representative of the data they aim to summarize. In the context of our study, although the RV coefficient estimates we obtained across all coupling modes and frequency bands appeared to provide representative summaries of the similarity between functional connectomes, we also saw that these summaries became less useful under certain circumstances, due to the sensitivity of this metric to the distribution of coupling magnitudes resulting in neurophysiologically unrealistic estimates of functional connectome similarity. In future work, absent a gold-standard, it may be pertinent to quantify functional connectome similarity using multiple measures of association—both as a form of sensitivity analysis, and to better evaluate what features of the functional connectome best reflect interindividual differences across contexts (Venkatesh, Jaja, & Pessoa, 2020).

Sixth, we note that our approach to estimating individual differences in functional connectome similarity within and between participants was somewhat insensitive to the possibility that EEG network variants are not individually unique, but rather fall into unique subgroups or clusters. This was due to our use of pairwise contrasts comparing the degree of similarity within versus between participants, which would necessarily lead to larger effect sizes

in cases where a participant's functional connectomes were wholly unique versus cases where a participant's functional connectomes were similar to some participants but different from others. Thus, in some cases individual effect sizes may have been reduced as a consequence not of a group effect, but of a subgroup effect. Given this possibility, we emphasize the importance of interpreting outcome variability estimates in our sample in light of the patterns present in the similarity matrix those estimates were based on. One potential solution to control for possible subgroup effects in future studies using a pairwise contrast approach would be to add a *within subgroup* covariate to the model (denoting whether a pair came from the same or different subgroups), which could be derived from cluster analysis of functional connectome data (e.g., Tokuda, Yamashita, & Yoshimoto, 2021). Additionally, using more diverse and/or larger samples may further reduce the likelihood of possible subgroup effects skewing individual effect sizes towards zero, and improve the precision of uncertainty estimates for individual-level sub-models, reducing the likelihood of the data not resolving whether the most compatible effect sizes for a given individual are positive or negative.

Finally, because our study only involved resting state data, we caution against generalizing our results to other brain states or tasks. Although electrophysiological phase coupling and amplitude coupling functional connectomes have been reported to be stable across different brain states and tasks (Mostame & Sadaghiani, 2021), as we previously explained for fMRI functional connectomes, this is not to say that brain states or tasks have no influence on electrophysiological functional connectome organization. Indeed, the relative stability of electrophysiological functional connectome organization has been found to modulate across both tasks and frequency bands (Mostame & Sadaghiani, 2021), and it is likely that different state or task manipulations will bring out or otherwise mask meaningful differences between participants

(Finn, 2021; Finn & Bandettini, 2020; Finn et al., 2020; Finn et al., 2017). Likewise, although phase coupling and amplitude coupling functional connectomes have been found to be qualitatively similar in their spatial organization during resting state (which we observed in our data as well), in support of their status as two distinct modes of functional connectivity, the two coupling have also been found to exhibit task-evoked and stimulus-evoked divergences in their spatial organization (Mostame & Sadaghiani, 2020). Thus, although there were clear similarities between our phase coupling and amplitude coupling results, this does not imply that the results from one coupling mode are interchangeable with the other.

Conclusion

As the field begins to incorporate multimodal evidence towards our understanding of individual differences in whole brain functional network organization, we will inevitably encounter challenges while traversing similar research trends and advances previously observed and currently ongoing in the fMRI literature (Sadaghiani & Wirsich, 2020). In this study, we explored the feasibility of using EEG to study network variants by examining whether or not EEG phase coupling and amplitude coupling functional connectomes showed similar evidence of stable individual differences across contexts to what has been described in the fMRI literature (e.g., Gratton et al., 2018). Overall, our results were inconclusive, and did not generally demonstrate the feasibility of using EEG to study network variants due to the inconsistencies observed across participants in our sample. At best our findings left open the possibility that EEG functional connectomes may be suitable measures of stable individual differences in whole brain functional network organization, but also made clear that—if the phase coupling and/or amplitude coupling dynamics of underlying global network activity across frequency bands are indeed influenced by stable individual-dependent factors—further work identifying and

developing methods to reliably measure and quantify these stable individual differences is necessary.

References

- Abdi, Hervé. (2007). *RV Coefficient and Congruence Coefficient*.
- Ablin, P., Cardoso, J.-F., & Gramfort, A. (2017). Faster ICA under orthogonal constraint. *arXiv:1711.10873 [Stat]*. Retrieved from <http://arxiv.org/abs/1711.10873>
- Ablin, P., Cardoso, J.-F., & Gramfort, A. (2018). Faster independent component analysis by preconditioning with Hessian approximations. *IEEE Transactions on Signal Processing*, 66(15), 4040–4049. <https://doi.org/10.1109/TSP.2018.2844203>
- Adrian, E. D., & Mathews, B. H. C. (1934). The Berger Rhythm: Potential changes from the occipital lobes in man. *Brain*, 57(4), 355–385. <https://doi.org/10.1093/brain/57.4.355>
- Akalin Acar, Z., & Makeig, S. (2013). Effects of Forward Model Errors on EEG Source Localization. *Brain Topography*, 26(3), 378–396. <https://doi.org/10.1007/s10548-012-0274-6>
- Akam, T., & Kullmann, D. M. (2010). Oscillations and Filtering Networks Support Flexible Routing of Information. *Neuron*, 67(2), 308–320. <https://doi.org/10.1016/j.neuron.2010.06.019>
- Allaire, J., Xie, Y., McPherson, J., Luraschi, J., Ushey, K., Atkins, A., ... Iannone, R. (2022). *Rmarkdown: Dynamic documents for r*. Retrieved from <https://CRAN.R-project.org/package=rmarkdown>
- Amrhein, V., & Greenland, S. (2022). Discuss practical importance of results based on interval estimates and p-value functions, not only on point estimates and null p-values. *Journal of*

Information Technology, 02683962221105904.

<https://doi.org/10.1177/02683962221105904>

Amrhein, V., Greenland, S., & McShane, B. (2019). Scientists rise up against statistical significance. *Nature*, 567(7748), 305–307. <https://doi.org/10.1038/d41586-019-00857-9>

Amrhein, V., Trafimow, D., & Greenland, S. (2019). Inferential Statistics as Descriptive Statistics: There Is No Replication Crisis if We Don't Expect Replication. *The American Statistician*, 73(sup1), 262–270. <https://doi.org/10.1080/00031305.2018.1543137>

Anderson, J. S., Ferguson, M. A., Lopez-Larson, M., & Yurgelun-Todd, D. (2011). Reproducibility of Single-Subject Functional Connectivity Measurements. *American Journal of Neuroradiology*, 32(3), 548–555. <https://doi.org/10.3174/ajnr.A2330>

Aru, J., Aru, J., Priesemann, V., Wibral, M., Lana, L., Pipa, G., ... Vicente, R. (2015). Untangling cross-frequency coupling in neuroscience. *Current Opinion in Neurobiology*, 31, 51–61. <https://doi.org/10.1016/j.conb.2014.08.002>

Aust, F., & Barth, M. (2022). *Papaja: Prepare american psychological association journal articles with r markdown*. Retrieved from <https://github.com/crsh/papaja>

Azevedo, F. A. C., Carvalho, L. R. B., Grinberg, L. T., Farfel, J. M., Ferretti, R. E. L., Leite, R. E. P., ... Herculano-Houzel, S. (2009). Equal numbers of neuronal and nonneuronal cells make the human brain an isometrically scaled-up primate brain. *The Journal of Comparative Neurology*, 513(5), 532–541. <https://doi.org/10.1002/cne.21974>

Babadi, B., & Brown, E. N. (2014). A review of multitaper spectral analysis. *IEEE transactions on bio-medical engineering, 61*(5), 1555–1564.

<https://doi.org/10.1109/TBME.2014.2311996>

Barch, D. M., Burgess, G. C., Harms, M. P., Petersen, S. E., Schlaggar, B. L., Corbetta, M., ...

WU-Minn HCP Consortium. (2013). Function in the human connectome: task-fMRI and individual differences in behavior. *NeuroImage, 80*, 169–189.

<https://doi.org/10.1016/j.neuroimage.2013.05.033>

Barr, D. J., Levy, R., Scheepers, C., & Tily, H. J. (2013). Random effects structure for confirmatory hypothesis testing: Keep it maximal. *Journal of Memory and Language, 68*(3), 255–278. <https://doi.org/10.1016/j.jml.2012.11.001>

Barry, R. J., Clarke, A. R., Johnstone, S. J., & Brown, C. R. (2009). EEG differences in children between eyes-closed and eyes-open resting conditions. *Clinical Neurophysiology, 120*(10), 1806–1811. <https://doi.org/10.1016/j.clinph.2009.08.006>

Barry, R. J., Clarke, A. R., Johnstone, S. J., Magee, C. A., & Rushby, J. A. (2007). EEG differences between eyes-closed and eyes-open resting conditions. *Clinical Neurophysiology, 118*(12), 2765–2773. <https://doi.org/10.1016/j.clinph.2007.07.028>

Barry, R. J., & De Blasio, F. M. (2017). EEG differences between eyes-closed and eyes-open resting remain in healthy ageing. *Biological Psychology, 129*, 293–304.
<https://doi.org/10.1016/j.biopsych.2017.09.010>

- Bastos, A. M., & Schoffelen, J.-M. (2016). A Tutorial Review of Functional Connectivity Analysis Methods and Their Interpretational Pitfalls. *Frontiers in Systems Neuroscience*, 9. <https://doi.org/10.3389/fnsys.2015.00175>
- Bateson, P. (2017). Robustness and plasticity in development. *WIREs Cognitive Science*, 8(1-2), e1386. <https://doi.org/10.1002/wcs.1386>
- Battel, L., Cunegatto, F., Viduani, A., Fisher, H. L., Kohrt, B. A., Mondelli, V., ... Kieling, C. (2021). Mind the brain gap: The worldwide distribution of neuroimaging research on adolescent depression. *NeuroImage*, 231, 117865.
<https://doi.org/10.1016/j.neuroimage.2021.117865>
- Beckmann, C. F., DeLuca, M., Devlin, J. T., & Smith, S. M. (2005). Investigations into resting-state connectivity using independent component analysis. *Philosophical Transactions of the Royal Society B: Biological Sciences*, 360(1457), 1001–1013.
<https://doi.org/10.1098/rstb.2005.1634>
- Berger, H. (1929). Über das Elektrenkephalogramm des Menschen. *Archiv für Psychiatrie und Nervenkrankheiten*, 87(1), 527–570. <https://doi.org/10.1007/BF01797193>
- Berner, D., & Amrhein, V. (2021). *Why and How We Should Join the Shift From Significance Testing to Estimation*. <https://doi.org/10.20944/preprints202112.0235.v1>
- Bijsterbosch, J. D. (2017). *Introduction to resting state fMRI functional connectivity* (First edition). Oxford, United Kingdom ; New York, NY: Oxford University Press.
- Bijsterbosch, J. D., Woolrich, M. W., Glasser, M. F., Robinson, E. C., Beckmann, C. F., Van Essen, D. C., ... Smith, S. M. (2018). The relationship between spatial configuration and

functional connectivity of brain regions. *eLife*, 7, e32992.

<https://doi.org/10.7554/eLife.32992>

Birn, R. M., Molloy, E. K., Patriat, R., Parker, T., Meier, T. B., Kirk, G. R., ... Prabhakaran, V. (2013). The effect of scan length on the reliability of resting-state fMRI connectivity estimates. *NeuroImage*, 83, 550–558. <https://doi.org/10.1016/j.neuroimage.2013.05.099>

Birn, R. M., Smith, M. A., Jones, T. B., & Bandettini, P. A. (2008). The respiration response function: the temporal dynamics of fMRI signal fluctuations related to changes in respiration. *NeuroImage*, 40(2), 644–654.

<https://doi.org/10.1016/j.neuroimage.2007.11.059>

Biswal, B., Yetkin, F. Z., Haughton, V. M., & Hyde, J. S. (1995). Functional connectivity in the motor cortex of resting human brain using echo-planar MRI. *Magnetic Resonance in Medicine*, 34(4), 537–541. <https://doi.org/10.1002/mrm.1910340409>

Bitta, M., Kariuki, S. M., Abubakar, A., & Newton, C. R. J. C. (2017). Burden of neurodevelopmental disorders in low and middle-income countries: A systematic review and meta-analysis. *Wellcome Open Research*, 2, 121.

<https://doi.org/10.12688/wellcomeopenres.13540.3>

Blankenburg, S., Wu, W., Lindner, B., & Schreiber, S. (2015). Information filtering in resonant neurons. *Journal of Computational Neuroscience*, 39(3), 349–370.

<https://doi.org/10.1007/s10827-015-0580-6>

Braga, R. M., & Buckner, R. L. (2017). Parallel Interdigitated Distributed Networks within the Individual Estimated by Intrinsic Functional Connectivity. *Neuron*, 95(2), 457–471.e5.
<https://doi.org/10.1016/j.neuron.2017.06.038>

Braga, R. M., Van Dijk, K. R. A., Polimeni, J. R., Eldaief, M. C., & Buckner, R. L. (2019). Parallel distributed networks resolved at high resolution reveal close juxtaposition of distinct regions. *Journal of Neurophysiology*, 121(4), 1513–1534.
<https://doi.org/10.1152/jn.00808.2018>

Breakspear, M. (2017). Dynamic models of large-scale brain activity. *Nature Neuroscience*, 20(3), 340–352. <https://doi.org/10.1038/nn.4497>

Brett, M., Johnsrude, I. S., & Owen, A. M. (2002). The problem of functional localization in the human brain. *Nature Reviews Neuroscience*, 3(3), 243–249.
<https://doi.org/10.1038/nrn756>

Brookes, M. J., Hale, J. R., Zumer, J. M., Stevenson, C. M., Francis, S. T., Barnes, G. R., ... Nagarajan, S. S. (2011). Measuring functional connectivity using MEG: methodology and comparison with fcMRI. *NeuroImage*, 56(3), 1082–1104.
<https://doi.org/10.1016/j.neuroimage.2011.02.054>

Brooks, M., E., Kristensen, K., Benthem, K., J., van, Magnusson, A., Berg, C., W., Nielsen, A., ... Bolker, B., M. (2017). glmmTMB Balances Speed and Flexibility Among Packages for Zero-inflated Generalized Linear Mixed Modeling. *The R Journal*, 9(2), 378.
<https://doi.org/10.32614/RJ-2017-066>

Brown, T. T. (2017). Individual differences in human brain development. *WIREs Cognitive Science*, 8(1-2), e1389. <https://doi.org/10.1002/wcs.1389>

Bruns, A. (2004). Fourier-, Hilbert- and wavelet-based signal analysis: are they really different approaches? *Journal of Neuroscience Methods*, 137(2), 321–332.
<https://doi.org/10.1016/j.jneumeth.2004.03.002>

Bruns, A., Eckhorn, R., Jokeit, H., & Ebner, A. (2000). Amplitude envelope correlation detects coupling among incoherent brain signals. *Neuroreport*, 11(7), 1509–1514.

Bullmore, E., & Sporns, O. (2009). Complex brain networks: graph theoretical analysis of structural and functional systems. *Nature Reviews. Neuroscience*, 10(3), 186–198.
<https://doi.org/10.1038/nrn2575>

Burle, B., Spieser, L., Roger, C., Casini, L., Hasbroucq, T., & Vidal, F. (2015). Spatial and temporal resolutions of EEG: Is it really black and white? A scalp current density view. *International Journal of Psychophysiology*, 97(3), 210–220.
<https://doi.org/10.1016/j.ijpsycho.2015.05.004>

Buxton, R. B. (2013). The physics of functional magnetic resonance imaging (fMRI). *Reports on Progress in Physics*, 76(9), 096601. <https://doi.org/10.1088/0034-4885/76/9/096601>

Buzsáki, G. (2011). *Rhythms of the Brain* (Illustrated edition). Oxford ; New York: Oxford University Press.

Buzsáki, G., Anastassiou, C. A., & Koch, C. (2012). The origin of extracellular fields and currents — EEG, ECoG, LFP and spikes. *Nature Reviews Neuroscience*, 13(6), 407–420.
<https://doi.org/10.1038/nrn3241>

- Buzsáki, G., & Draguhn, A. (2004). Neuronal Oscillations in Cortical Networks. *Science*, 304(5679), 1926–1929. <https://doi.org/10.1126/science.1099745>
- Buzsáki, G., & Wang, X.-J. (2012). Mechanisms of Gamma Oscillations. *Annual Review of Neuroscience*, 35(1), 203–225. <https://doi.org/10.1146/annurev-neuro-062111-150444>
- Buzsáki, G., & Watson, B. O. (2012). Brain rhythms and neural syntax: implications for efficient coding of cognitive content and neuropsychiatric disease. *Dialogues in Clinical Neuroscience*, 14(4), 345–367. <https://doi.org/10.31887/DCNS.2012.14.4/gbuzsaki>
- Cadwell, C. R., Bhaduri, A., Mostajo-Radji, M. A., Keefe, M. G., & Nowakowski, T. J. (2019). Development and Arealization of the Cerebral Cortex. *Neuron*, 103(6), 980–1004. <https://doi.org/10.1016/j.neuron.2019.07.009>
- Campbell, M. C., & Tishkoff, S. A. (2008). African Genetic Diversity: Implications for Human Demographic History, Modern Human Origins, and Complex Disease Mapping. *Annual Review of Genomics and Human Genetics*, 9(1), 403–433. <https://doi.org/10.1146/annurev.genom.9.081307.164258>
- Campitelli, E. (2022). *Ggnewscale: Multiple fill and colour scales in ggplot2*. Retrieved from <https://CRAN.R-project.org/package=ggnewscale>
- Canolty, R. T., & Knight, R. T. (2010). The functional role of cross-frequency coupling. *Trends in Cognitive Sciences*, 14(11), 506–515. <https://doi.org/10.1016/j.tics.2010.09.001>
- Cao, C., & Slobounov, S. (2010). Alteration of Cortical Functional Connectivity as a Result of Traumatic Brain Injury Revealed by Graph Theory, ICA, and sLORETA Analyses of EEG

Signals. *IEEE Transactions on Neural Systems and Rehabilitation Engineering*, 18(1), 11–19. <https://doi.org/10.1109/TNSRE.2009.2027704>

Cao, R., Wu, Z., Li, H., Xiang, J., & Chen, J. (2014). Disturbed Connectivity of EEG Functional Networks in Alcoholism: A Graph-Theoretic Analysis. *Bio-Medical Materials and Engineering*, 24(6), 2927–2936. <https://doi.org/10.3233/BME-141112>

Caramazza, A. (1986). On drawing inferences about the structure of normal cognitive systems from the analysis of patterns of impaired performance: The case for single-patient studies. *Brain and Cognition*, 5(1), 41–66. [https://doi.org/10.1016/0278-2626\(86\)90061-8](https://doi.org/10.1016/0278-2626(86)90061-8)

Chang, C., & Glover, G. H. (2009). Relationship between respiration, end-tidal CO₂, and BOLD signals in resting-state fMRI. *NeuroImage*, 47(4), 1381–1393. <https://doi.org/10.1016/j.neuroimage.2009.04.048>

Chatrian, G. E., Lettich, E., & Nelson, P. L. (1985). Ten Percent Electrode System for Topographic Studies of Spontaneous and Evoked EEG Activities. *American Journal of EEG Technology*, 25(2), 83–92. <https://doi.org/10.1080/00029238.1985.11080163>

Chatrian, G. E., Lettich, E., & Nelson, P. L. (1988). Modified nomenclature for the “10%” electrode system. *Journal of Clinical Neurophysiology: Official Publication of the American Electroencephalographic Society*, 5(2), 183–186.

Chella, F., Pizzella, V., Zappasodi, F., & Marzetti, L. (2016). Impact of the reference choice on scalp EEG connectivity estimation. *Journal of Neural Engineering*, 13(3), 036016. <https://doi.org/10.1088/1741-2560/13/3/036016>

- Cnudde, K., van Hees, S., Brown, S., van der Wijk, G., Pexman, P. M., & Protzner, A. B. (2021). Increased Neural Efficiency in Visual Word Recognition: Evidence from Alterations in Event-Related Potentials and Multiscale Entropy. *Entropy*, 23(3), 304. <https://doi.org/10.3390/e23030304>
- Cohen, M. X. (2014). *Analyzing neural time series data: theory and practice*. Cambridge, Massachusetts: The MIT Press.
- Cohen, M. X. (2015). Effects of time lag and frequency matching on phase-based connectivity. *Journal of Neuroscience Methods*, 250, 137–146. <https://doi.org/10.1016/j.jneumeth.2014.09.005>
- Cohen, M. X. (2017). Where Does EEG Come From and What Does It Mean? *Trends in Neurosciences*, 40(4), 208–218. <https://doi.org/10.1016/j.tins.2017.02.004>
- Colclough, G. L., Woolrich, M. W., Tewarie, P. K., Brookes, M. J., Quinn, A. J., & Smith, S. M. (2016). How reliable are MEG resting-state connectivity metrics? *NeuroImage*, 138, 284–293. <https://doi.org/10.1016/j.neuroimage.2016.05.070>
- Cole, Michael W., Bassett, Danielle S., Power, J. D., Braver, Todd S., & Petersen, Steven E. (2014). Intrinsic and Task-Evoked Network Architectures of the Human Brain. *Neuron*, 83(1), 238–251. <https://doi.org/10.1016/j.neuron.2014.05.014>
- Cribari-Neto, F., & Zeileis, A. (2010). Beta Regression in R. *Journal of Statistical Software*, 34(2). <https://doi.org/10.18637/jss.v034.i02>
- Cronbach, L. J. (1957). The two disciplines of scientific psychology. *American Psychologist*, 12(11), 671–684. <https://doi.org/10.1037/h0043943>

- Daniel Arzate-Mena, J., Abela, E., Olguín-Rodríguez, P. V., Ríos-Herrera, W., Alcauter, S., Schindler, K., ... Rummel, C. (2022). Stationary EEG pattern relates to large-scale resting state networks – An EEG-fMRI study connecting brain networks across time-scales. *NeuroImage*, 246, 118763. <https://doi.org/10.1016/j.neuroimage.2021.118763>
- de Cheveigné, A., & Nelken, I. (2019). Filters: When, Why, and How (Not) to Use Them. *Neuron*, 102(2), 280–293. <https://doi.org/10.1016/j.neuron.2019.02.039>
- Deco, G., & Corbetta, M. (2011). The dynamical balance of the brain at rest. *The Neuroscientist: A Review Journal Bringing Neurobiology, Neurology and Psychiatry*, 17(1), 107–123. <https://doi.org/10.1177/1073858409354384>
- Demuru, M., Gouw, A. A., Hillebrand, A., Stam, C. J., van Dijk, B. W., Scheltens, P., ... Visser, P. J. (2017). Functional and effective whole brain connectivity using magnetoencephalography to identify monozygotic twin pairs. *Scientific Reports*, 7(1), 9685. <https://doi.org/10.1038/s41598-017-10235-y>
- DiNicola, L. M., Braga, R. M., & Buckner, R. L. (2020). Parallel distributed networks dissociate episodic and social functions within the individual. *Journal of Neurophysiology*, 123(3), 1144–1179. <https://doi.org/10.1152/jn.00529.2019>
- Douma, J. C., & Weedon, J. T. (2019). Analysing continuous proportions in ecology and evolution: A practical introduction to beta and Dirichlet regression. *Methods in Ecology and Evolution*, 10(9), 1412–1430. <https://doi.org/10.1111/2041-210X.13234>
- Drew, P. J. (2022). Neurovascular coupling: motive unknown. *Trends in Neurosciences*, 45(11), 809–819. <https://doi.org/10.1016/j.tins.2022.08.004>

- Dubois, J., & Adolphs, R. (2016). Building a science of individual differences from fMRI. *Trends in Cognitive Sciences*, 20(6), 425–443. <https://doi.org/10.1016/j.tics.2016.03.014>
- Dunn, P. K., & Smyth, G. K. (1996). Randomized Quantile Residuals. *Journal of Computational and Graphical Statistics*, 5(3), 236. <https://doi.org/10.2307/1390802>
- Dworetzky, A., Seitzman, B. A., Adeyemo, B., Neta, M., Coalson, R. S., Petersen, S. E., & Gratton, C. (2021). Probabilistic mapping of human functional brain networks identifies regions of high group consensus. *NeuroImage*, 237, 118164. <https://doi.org/10.1016/j.neuroimage.2021.118164>
- Elam, J. S., Glasser, M. F., Harms, M. P., Sotiroopoulos, S. N., Andersson, J. L. R., Burgess, G. C., ... Van Essen, D. C. (2021). The Human Connectome Project: A retrospective. *NeuroImage*, 244, 118543. <https://doi.org/10.1016/j.neuroimage.2021.118543>
- Elliott, M. L., Knodt, A. R., Cooke, M., Kim, M. J., Melzer, T. R., Keenan, R., ... Hariri, A. R. (2019). General functional connectivity: Shared features of resting-state and task fMRI drive reliable and heritable individual differences in functional brain networks. *NeuroImage*, 189, 516–532. <https://doi.org/10.1016/j.neuroimage.2019.01.068>
- Elliott, M. L., Knodt, A. R., Ireland, D., Morris, M. L., Poulton, R., Ramrakha, S., ... Hariri, A. R. (2020). What Is the Test-Retest Reliability of Common Task-Functional MRI Measures? New Empirical Evidence and a Meta-Analysis. *Psychological Science*, 1–15. <https://doi.org/10.1177/0956797620916786>

Engel, A. K., Gerloff, C., Hilgetag, C. C., & Nolte, G. (2013). Intrinsic Coupling Modes: Multiscale Interactions in Ongoing Brain Activity. *Neuron*, 80(4), 867–886.
<https://doi.org/10.1016/j.neuron.2013.09.038>

Engels, M. M., Stam, C. J., van der Flier, W. M., Scheltens, P., de Waal, H., & van Straaten, E. C. (2015). Declining functional connectivity and changing hub locations in Alzheimer's disease: an EEG study. *BMC Neurology*, 15(1), 145. <https://doi.org/10.1186/s12883-015-0400-7>

Escoufier, Y. (1973). Le Traitement des Variables Vectorielles. *Biometrics*, 29(4), 751.
<https://doi.org/10.2307/2529140>

Faisal, A. A., Selen, L. P. J., & Wolpert, D. M. (2008). Noise in the nervous system. *Nature Reviews Neuroscience*, 9(4), 292–303. <https://doi.org/10.1038/nrn2258>

Falk, E. B., Hyde, L. W., Mitchell, C., Faul, J., Gonzalez, R., Heitzeg, M. M., ... Schulenberg, J. (2013). What is a representative brain? Neuroscience meets population science. *Proceedings of the National Academy of Sciences*, 110(44), 17615–17622.
<https://doi.org/10.1073/pnas.1310134110>

Fedorenko, E. (2021). The early origins and the growing popularity of the individual-subject analytic approach in human neuroscience. *Current Opinion in Behavioral Sciences*, 40, 105–112. <https://doi.org/10.1016/j.cobeha.2021.02.023>

Fedorenko, E., & Blank, I. A. (2020). Broca's Area Is Not a Natural Kind. *Trends in Cognitive Sciences*, 24(4), 270–284. <https://doi.org/10.1016/j.tics.2020.01.001>

Ferrari, S., & Cribari-Neto, F. (2004). Beta Regression for Modelling Rates and Proportions. *Journal of Applied Statistics*, 31(7), 799–815.

<https://doi.org/10.1080/0266476042000214501>

Ferree, T. C., Clay, M. T., & Tucker, D. M. (2001). The spatial resolution of scalp EEG. *Neurocomputing*, 38-40, 1209–1216. [https://doi.org/10.1016/S0925-2312\(01\)00568-9](https://doi.org/10.1016/S0925-2312(01)00568-9)

Finn, E. S. (2021). Is it time to put rest to rest? *Trends in Cognitive Sciences*, 25(12), 1021–1032.

<https://doi.org/10.1016/j.tics.2021.09.005>

Finn, E. S., & Bandettini, P. A. (2020, August 24). *Movie-watching outperforms rest for functional connectivity-based prediction of behavior* (p. 2020.08.23.263723). p. 2020.08.23.263723. Cold Spring Harbor Laboratory.

<https://doi.org/10.1101/2020.08.23.263723>

Finn, E. S., Glerean, E., Khojandi, A. Y., Nielson, D., Molfese, P. J., Handwerker, D. A., & Bandettini, P. A. (2020). Idiosynchrony: From shared responses to individual differences during naturalistic neuroimaging. *NeuroImage*, 215, 116828.

<https://doi.org/10.1016/j.neuroimage.2020.116828>

Finn, E. S., & Rosenberg, M. D. (2021). Beyond fingerprinting: Choosing predictive connectomes over reliable connectomes. *NeuroImage*, 239, 118254.

<https://doi.org/10.1016/j.neuroimage.2021.118254>

Finn, E. S., Scheinost, D., Finn, D. M., Shen, X., Papademetris, X., & Constable, R. T. (2017). Can brain state be manipulated to emphasize individual differences in functional

connectivity? *NeuroImage*, 160, 140–151.
<https://doi.org/10.1016/j.neuroimage.2017.03.064>

Finn, E. S., Shen, X., Scheinost, D., Rosenberg, M. D., Huang, J., Chun, M. M., ... Constable, R. T. (2015). Functional connectome fingerprinting: identifying individuals using patterns of brain connectivity. *Nature Neuroscience*, 18(11), 1664–1671.
<https://doi.org/10.1038/nn.4135>

Fox, J., & Monette, G. (1992). Generalized Collinearity Diagnostics. *Journal of the American Statistical Association*, 87(417), 178–183.
<https://doi.org/10.1080/01621459.1992.10475190>

Fox, M. D., & Greicius, M. (2010). Clinical applications of resting state functional connectivity. *Frontiers in Systems Neuroscience*, 4. <https://doi.org/10.3389/fnsys.2010.00019>

Fox, M. D., Snyder, A. Z., Vincent, J. L., Corbetta, M., Van Essen, D. C., & Raichle, M. E. (2005). The human brain is intrinsically organized into dynamic, anticorrelated functional networks. *Proceedings of the National Academy of Sciences of the United States of America*, 102(27), 9673–9678. <https://doi.org/10.1073/pnas.0504136102>

Fraschini, M., Demuru, M., Crobe, A., Marrosu, F., Stam, C. J., & Hillebrand, A. (2016). The effect of epoch length on estimated EEG functional connectivity and brain network organisation. *Journal of Neural Engineering*, 13(3), 036015. <https://doi.org/10.1088/1741-2560/13/3/036015>

Fraschini, M., Pani, S. M., Didaci, L., & Marcialis, G. L. (2019). Robustness of functional connectivity metrics for EEG-based personal identification over task-induced intra-class

and inter-class variations. *Pattern Recognition Letters*, 125, 49–54.

<https://doi.org/10.1016/j.patrec.2019.03.025>

Fries, P. (2015). Rhythms for Cognition: Communication through Coherence. *Neuron*, 88(1), 220–235. <https://doi.org/10.1016/j.neuron.2015.09.034>

Friston, K. J. (2002). Functional integration and inference in the brain. *Progress in Neurobiology*, 68(2), 113–143. [https://doi.org/10.1016/S0301-0082\(02\)00076-X](https://doi.org/10.1016/S0301-0082(02)00076-X)

Friston, K. J. (2011). Functional and Effective Connectivity: A Review. *Brain Connectivity*, 1(1), 13–36. <https://doi.org/10.1089/brain.2011.0008>

Friston, K. J., & Price, C. J. (2003). Degeneracy and redundancy in cognitive anatomy. *Trends in Cognitive Sciences*, 7(4), 151–152. [https://doi.org/10.1016/S1364-6613\(03\)00054-8](https://doi.org/10.1016/S1364-6613(03)00054-8)

Frost, M. A., & Goebel, R. (2012). Measuring structural-functional correspondence: Spatial variability of specialised brain regions after macro-anatomical alignment. *NeuroImage*, 59(2), 1369–1381. <https://doi.org/10.1016/j.neuroimage.2011.08.035>

Garrett, D. D., Samanez-Larkin, G. R., MacDonald, S. W. S., Lindenberger, U., McIntosh, A. R., & Grady, C. L. (2013). Moment-to-moment brain signal variability: A next frontier in human brain mapping? *Neuroscience and Biobehavioral Reviews*, 37(4), 610–624. <https://doi.org/10.1016/j.neubiorev.2013.02.015>

Gelman, A., Carlin, J. B., Stern, H. S., Dunson, D. B., Vehtari, A., & Rubin, D. B. (2013). *Bayesian Data Analysis* (3rd edition). Boca Raton: Chapman and Hall/CRC. Retrieved from <http://www.stat.columbia.edu/~gelman/book/>

- Gelman, A., & Hill, J. (2006). *Data Analysis Using Regression and Multilevel/Hierarchical Models* (1st edition). Cambridge; New York: Cambridge University Press. Retrieved from <http://www.stat.columbia.edu/~gelman/arm/>
- Gelman, A., Hill, J., & Vehtari, A. (2020). *Regression and Other Stories* (1st ed.). Cambridge University Press. <https://doi.org/10.1017/9781139161879>
- Gigerenzer, G. (2018). Statistical Rituals: The Replication Delusion and How We Got There. *Advances in Methods and Practices in Psychological Science*, 1(2), 198–218. <https://doi.org/10.1177/2515245918771329>
- Glasser, M. F., Coalson, T. S., Robinson, E. C., Hacker, C. D., Harwell, J., Yacoub, E., ... Van Essen, D. C. (2016). A multi-modal parcellation of human cerebral cortex. *Nature*, 536(7615), 171–178. <https://doi.org/10.1038/nature18933>
- Glover, G. H. (2011). Overview of Functional Magnetic Resonance Imaging. *Neurosurgery Clinics of North America*, 22(2), 133–139. <https://doi.org/10.1016/j.nec.2010.11.001>
- Gohel, D., & Ross, N. (2023). *Officedown: Enhanced r markdown format for word and PowerPoint*. Retrieved from <https://CRAN.R-project.org/package=officedown>
- Gohel, D., & Skintzos, P. (2023). *Flextable: Functions for tabular reporting*. Retrieved from <https://CRAN.R-project.org/package=flextable>
- Gollo, L. L., Mirasso, C., Sporns, O., & Breakspear, M. (2014). Mechanisms of Zero-Lag Synchronization in Cortical Motifs. *PLoS Computational Biology*, 10(4), e1003548. <https://doi.org/10.1371/journal.pcbi.1003548>

Gordon, E. M., Laumann, T. O., Adeyemo, B., Gilmore, A. W., Nelson, S. M., Dosenbach, N. U. F., & Petersen, S. E. (2017). Individual-specific features of brain systems identified with resting state functional correlations. *NeuroImage*, 146, 918–939.

<https://doi.org/10.1016/j.neuroimage.2016.08.032>

Gordon, E. M., Laumann, T. O., Adeyemo, B., & Petersen, S. E. (2017). Individual Variability of the System-Level Organization of the Human Brain. *Cerebral Cortex (New York, N.Y.: 1991)*, 27(1), 386–399. <https://doi.org/10.1093/cercor/bhv239>

Gordon, E. M., Laumann, T. O., Gilmore, A. W., Newbold, D. J., Greene, D. J., Berg, J. J., ... Dosenbach, N. U. F. (2017). Precision functional mapping of individual human brains. *Neuron*, 95(4), 791–807.e7. <https://doi.org/10.1016/j.neuron.2017.07.011>

Gordon, E. M., Laumann, T. O., Marek, S., Raut, R. V., Gratton, C., Newbold, D. J., ... Nelson, S. M. (2020). Default-mode network streams for coupling to language and control systems. *Proceedings of the National Academy of Sciences*, 117(29), 17308–17319. <https://doi.org/10.1073/pnas.2005238117>

Gordon, E. M., & Nelson, S. M. (2021). Three types of individual variation in brain networks revealed by single-subject functional connectivity analyses. *Current Opinion in Behavioral Sciences*, 40, 79–86. <https://doi.org/10.1016/j.cobeha.2021.02.014>

Gramfort, A., Luessi, M., Larson, E., Engemann, D., Strohmeier, D., Brodbeck, C., ... Hämäläinen, M. (2013). MEG and EEG data analysis with MNE-Python. *Frontiers in Neuroscience*, 7, 267. <https://doi.org/10.3389/fnins.2013.00267>

Gratton, C., Kraus, B. T., Greene, D. J., Gordon, E. M., Laumann, T. O., Nelson, S. M., ...

Petersen, S. E. (2020). Defining Individual-Specific Functional Neuroanatomy for Precision Psychiatry. *Biological Psychiatry*, 88(1), 28–39.

<https://doi.org/10.1016/j.biopsych.2019.10.026>

Gratton, C., Laumann, T. O., Nielsen, A. N., Greene, D. J., Gordon, E. M., Gilmore, A. W., ...

Petersen, S. E. (2018). Functional Brain Networks Are Dominated by Stable Group and Individual Factors, Not Cognitive or Daily Variation. *Neuron*, 98(2), 439–452.e5.

<https://doi.org/10.1016/j.neuron.2018.03.035>

Gratton, C., Nelson, S. M., & Gordon, E. M. (2022). Brain-behavior correlations: Two paths toward reliability. *Neuron*, 110(9), 1446–1449.

<https://doi.org/10.1016/j.neuron.2022.04.018>

Grech, R., Cassar, T., Muscat, J., Camilleri, K. P., Fabri, S. G., Zervakis, M., ... Vanrumste, B. (2008). Review on solving the inverse problem in EEG source analysis. *Journal of NeuroEngineering and Rehabilitation*, 5(1), 25. <https://doi.org/10.1186/1743-0003-5-25>

Greene, A. S., Gao, S., Scheinost, D., & Constable, R. T. (2018). Task-induced brain state manipulation improves prediction of individual traits. *Nature Communications*, 9(1), 2807. <https://doi.org/10.1038/s41467-018-04920-3>

Greenland, S. (2017). Invited Commentary: The Need for Cognitive Science in Methodology. *American Journal of Epidemiology*, 186(6), 639–645. <https://doi.org/10.1093/aje/kwx259>

- Greenland, S. (2019). Valid P-Values Behave Exactly as They Should: Some Misleading Criticisms of P-Values and Their Resolution With S-Values. *The American Statistician*, 73(sup1), 106–114. <https://doi.org/10.1080/00031305.2018.1529625>
- Greenland, S., Senn, S. J., Rothman, K. J., Carlin, J. B., Poole, C., Goodman, S. N., & Altman, D. G. (2016). Statistical tests, P values, confidence intervals, and power: a guide to misinterpretations. *European Journal of Epidemiology*, 31(4), 337–350. <https://doi.org/10.1007/s10654-016-0149-3>
- Greicius, M. D., Krasnow, B., Reiss, A. L., & Menon, V. (2003). Functional connectivity in the resting brain: A network analysis of the default mode hypothesis. *Proceedings of the National Academy of Sciences*, 100(1), 253–258. <https://doi.org/10.1073/pnas.0135058100>
- Greicius, M. D., & Menon, V. (2004). Default-Mode Activity during a Passive Sensory Task: Uncoupled from Deactivation but Impacting Activation. *Journal of Cognitive Neuroscience*, 16(9), 1484–1492. <https://doi.org/10.1162/0898929042568532>
- Gu, J., & Kanai, R. (2014). What contributes to individual differences in brain structure? *Frontiers in Human Neuroscience*, 8. <https://doi.org/10.3389/fnhum.2014.00262>
- Hacker, C. D., Laumann, T. O., Szrama, N. P., Baldassarre, A., Snyder, A. Z., Leuthardt, E. C., & Corbetta, M. (2013). Resting state network estimation in individual subjects. *NeuroImage*, 82, 616–633. <https://doi.org/10.1016/j.neuroimage.2013.05.108>
- Hagmann, P., Cammoun, L., Gigandet, X., Meuli, R., Honey, C. J., Wedeen, V. J., & Sporns, O. (2008). Mapping the Structural Core of Human Cerebral Cortex. *PLOS Biology*, 6(7), e159. <https://doi.org/10.1371/journal.pbio.0060159>

Hall, C. N., Howarth, C., Kurth-Nelson, Z., & Mishra, A. (2016). Interpreting BOLD: towards a dialogue between cognitive and cellular neuroscience. *Philosophical Transactions of the Royal Society B: Biological Sciences*, 371(1705), 20150348.

<https://doi.org/10.1098/rstb.2015.0348>

Hall, E. L., Robson, S. E., Morris, P. G., & Brookes, M. J. (2014). The relationship between MEG and fMRI. *NeuroImage*, 102, 80–91.

<https://doi.org/10.1016/j.neuroimage.2013.11.005>

Hardmeier, M., Hatz, F., Bousleiman, H., Schindler, C., Stam, C. J., & Fuhr, P. (2014). Reproducibility of Functional Connectivity and Graph Measures Based on the Phase Lag Index (PLI) and Weighted Phase Lag Index (wPLI) Derived from High Resolution EEG. *PLoS ONE*, 9(10), e108648. <https://doi.org/10.1371/journal.pone.0108648>

Harrison, S. J., Woolrich, M. W., Robinson, E. C., Glasser, M. F., Beckmann, C. F., Jenkinson, M., & Smith, S. M. (2015). Large-scale Probabilistic Functional Modes from resting state fMRI. *NeuroImage*, 109, 217–231. <https://doi.org/10.1016/j.neuroimage.2015.01.013>

Hartig, F. (2022). *DHARMA: Residual diagnostics for hierarchical (multi-level / mixed) regression models*. Retrieved from <http://florianhartig.github.io/DHARMA/>

Hartig, F., & Lohse, L. (2022). *DHARMA: Residual Diagnostics for Hierarchical (Multi-Level / Mixed) Regression Models*. Retrieved from <https://CRAN.R-project.org/package=DHARMA>

Hatlestad-Hall, C., Bruña, R., Liljeström, M., Renvall, H., Heuser, K., Taubøll, E., ... Haraldsen, I. H. (2023). Reliable evaluation of functional connectivity and graph theory measures in

source-level EEG: How many electrodes are enough? *Clinical Neurophysiology*, 150, 1–16. <https://doi.org/10.1016/j.clinph.2023.03.002>

Haufe, S., Nikulin, V. V., Müller, K.-R., & Nolte, G. (2013). A critical assessment of connectivity measures for EEG data: a simulation study. *NeuroImage*, 64, 120–133. <https://doi.org/10.1016/j.neuroimage.2012.09.036>

He, B., Astolfi, L., Valdes-Sosa, P. A., Marinazzo, D., Palva, S. O., Benar, C.-G., ... Koenig, T. (2019). Electrophysiological Brain Connectivity: Theory and Implementation. *IEEE Transactions on Biomedical Engineering*, 66(7), 2115–2137. <https://doi.org/10.1109/TBME.2019.2913928>

Heiss, A. (2021, November 8). A guide to modeling proportions with Bayesian beta and zero-inflated beta regression models. Retrieved June 17, 2022, from <https://www.andrewheiss.com/blog/2021/11/08/beta-regression-guide/>

Henrich, J., Heine, S. J., & Norenzayan, A. (2010). The weirdest people in the world? *Behavioral and Brain Sciences*, 33(2-3), 61–83. <https://doi.org/10.1017/S0140525X0999152X>

Henry, C. E. (1941). Electroencephalographic individual differences and their constancy: I. During sleep. *Journal of Experimental Psychology*, 29(2), 117–132. <https://doi.org/10.1037/h0061342>

Henson, R. (2005). What can functional neuroimaging tell the experimental psychologist? *The Quarterly Journal of Experimental Psychology. A, Human Experimental Psychology*, 58(2), 193–233. <https://doi.org/10.1080/02724980443000502>

- Hillman, E. M. C. (2014). Coupling Mechanism and Significance of the BOLD Signal: A Status Report. *Annual Review of Neuroscience*, 37(1), 161–181. <https://doi.org/10.1146/annurev-neuro-071013-014111>
- Hindriks, R., & Tewarie, P. K. B. (2023). Dissociation between phase and power correlation networks in the human brain is driven by co-occurrent bursts. *Communications Biology*, 6(1), 286. <https://doi.org/10.1038/s42003-023-04648-x>
- Hipp, J. F., Hawellek, D. J., Corbetta, M., Siegel, M., & Engel, A. K. (2012). Large-scale cortical correlation structure of spontaneous oscillatory activity. *Nature Neuroscience*, 15(6), 884–890. <https://doi.org/10.1038/nn.3101>
- Honari, H., Choe, A. S., & Lindquist, M. A. (2021). Evaluating phase synchronization methods in fMRI: A comparison study and new approaches. *NeuroImage*, 228, 117704. <https://doi.org/10.1016/j.neuroimage.2020.117704>
- Honey, Christopher J., Kötter, R., Breakspear, M., & Sporns, O. (2007). Network structure of cerebral cortex shapes functional connectivity on multiple time scales. *Proceedings of the National Academy of Sciences*, 104(24), 10240–10245. <https://doi.org/10.1073/pnas.0701519104>
- Honey, C. J., Sporns, O., Cammoun, L., Gigandet, X., Thiran, J. P., Meuli, R., & Hagmann, P. (2009). Predicting human resting-state functional connectivity from structural connectivity. *Proceedings of the National Academy of Sciences*, 106(6), 2035–2040. <https://doi.org/10.1073/pnas.0811168106>

- Horien, C., Shen, X., Scheinost, D., & Constable, R. T. (2019). The individual functional connectome is unique and stable over months to years. *NeuroImage*, 189, 676–687.
<https://doi.org/10.1016/j.neuroimage.2019.02.002>
- Howarth, C., Gleeson, P., & Attwell, D. (2012). Updated energy budgets for neural computation in the neocortex and cerebellum. *Journal of Cerebral Blood Flow and Metabolism: Official Journal of the International Society of Cerebral Blood Flow and Metabolism*, 32(7), 1222–1232. <https://doi.org/10.1038/jcbfm.2012.35>
- Husson, F., Josse, J., Le, S., & Mazet, J. (2020). *FactoMineR: Multivariate exploratory data analysis and data mining*. Retrieved from <http://factominer.free.fr>
- Hutcheon, B., & Yarom, Y. (2000). Resonance, oscillation and the intrinsic frequency preferences of neurons. *Trends in Neurosciences*, 23(5), 216–222.
[https://doi.org/10.1016/s0166-2236\(00\)01547-2](https://doi.org/10.1016/s0166-2236(00)01547-2)
- Hutchison, R. M., Womelsdorf, T., Allen, E. A., Bandettini, P. A., Calhoun, V. D., Corbetta, M., ... Chang, C. (2013). Dynamic functional connectivity: Promise, issues, and interpretations. *NeuroImage*, 80, 360–378.
<https://doi.org/10.1016/j.neuroimage.2013.05.079>
- Idaji, M. J., Zhang, J., Stephani, T., Nolte, G., Müller, K.-R., Villringer, A., & Nikulin, V. V. (2022). Harmoni: A method for eliminating spurious interactions due to the harmonic components in neuronal data. *NeuroImage*, 252, 119053.
<https://doi.org/10.1016/j.neuroimage.2022.119053>

Jalbrzikowski, M., Liu, F., Foran, W., Klei, L., Calabro, F. J., Roeder, K., ... Luna, B. (2020).

Functional connectome fingerprinting accuracy in youths and adults is similar when examined on the same day and 1.5-years apart. *Human Brain Mapping*, 41(15), 4187–4199. <https://doi.org/10.1002/hbm.25118>

James, G., Witten, D., Hastie, T., & Tibshirani, R. (2021). *An introduction to statistical learning with applications in R* (2nd ed.). New York: Springer. Retrieved from <https://www.tandfonline.com/doi/full/10.1080/24754269.2021.1980261>

Josse, J., & Holmes, S. (2016). Measuring multivariate association and beyond. *Statistics Surveys*, 10, 132–167. <https://doi.org/10.1214/16-SS116>

Kaneko, K., & Tsuda, I. (2003). Chaotic itinerary. *Chaos: An Interdisciplinary Journal of Nonlinear Science*, 13(3), 926–936. <https://doi.org/10.1063/1.1607783>

Kay, M. (2022). *Ggdist: Visualizations of distributions and uncertainty*.

Keitel, C., Thut, G., & Gross, J. (2017). Visual cortex responses reflect temporal structure of continuous quasi-rhythmic sensory stimulation. *NeuroImage*, 146, 58–70. <https://doi.org/10.1016/j.neuroimage.2016.11.043>

Kherif, F. (2003). Group analysis in functional neuroimaging: selecting subjects using similarity measures. *NeuroImage*, 20(4), 2197–2208.

<https://doi.org/10.1016/j.neuroimage.2003.08.018>

Kong, R., Li, J., Orban, C., Sabuncu, M. R., Liu, H., Schaefer, A., ... Yeo, B. T. T. (2019). Spatial Topography of Individual-Specific Cortical Networks Predicts Human Cognition,

Personality, and Emotion. *Cerebral Cortex*, 29(6), 2533–2551.

<https://doi.org/10.1093/cercor/bhy123>

Kopell, N., Kramer, M. A., Malerba, P., & Whittington, M. A. (2010). Are Different Rhythms Good for Different Functions? *Frontiers in Human Neuroscience*, 4.

<https://doi.org/10.3389/fnhum.2010.00187>

Kraus, B. T., Perez, D., Ladwig, Z., Seitzman, B. A., Dworetzky, A., Petersen, S. E., & Gratton, C. (2021). Network variants are similar between task and rest states. *NeuroImage*, 229, 117743. <https://doi.org/10.1016/j.neuroimage.2021.117743>

Kraus, B. T., Zinbarg, R., Braga, R. M., Nusslock, R., Mittal, V. A., & Gratton, C. (2023). Insights from Personalized Models of Brain and Behavior for Identifying Biomarkers in Psychiatry. *Neuroscience & Biobehavioral Reviews*, 105259.

<https://doi.org/10.1016/j.neubiorev.2023.105259>

Krienen, F. M., Yeo, B. T. T., & Buckner, R. L. (2014). Reconfigurable task-dependent functional coupling modes cluster around a core functional architecture. *Philosophical Transactions of the Royal Society B: Biological Sciences*, 369(1653), 20130526.

<https://doi.org/10.1098/rstb.2013.0526>

Kuhn, T. S., & Hacking, I. (2012). *The structure of scientific revolutions* (Fourth edition). Chicago ; London: The University of Chicago Press.

La Rocca, D., Campisi, P., Vegso, B., Cserti, P., Kozmann, G., Babiloni, F., & Fallani, F. D. V. (2014). Human Brain Distinctiveness Based on EEG Spectral Coherence Connectivity.

IEEE Transactions on Biomedical Engineering, 61(9), 2406–2412.

<https://doi.org/10.1109/TBME.2014.2317881>

Lai, M., Demuru, M., Hillebrand, A., & Fraschini, M. (2018). A comparison between scalp- and source-reconstructed EEG networks. *Scientific Reports*, 8(1), 1–8.

<https://doi.org/10.1038/s41598-018-30869-w>

Landau, W. M. (2022). *Targets: Dynamic function-oriented make-like declarative workflows*.

Retrieved from <https://CRAN.R-project.org/package=targets>

Laumann, T. O., Gordon, E. M., Adeyemo, B., Snyder, A. Z., Joo, S. J., Chen, M.-Y., ...

Petersen, S. E. (2015). Functional System and Areal Organization of a Highly Sampled Individual Human Brain. *Neuron*, 87(3), 657–670.

<https://doi.org/10.1016/j.neuron.2015.06.037>

Laumann, T. O., Snyder, A. Z., Mitra, A., Gordon, E. M., Gratton, C., Adeyemo, B., ... Petersen,

S. E. (2017). On the Stability of BOLD fMRI Correlations. *Cerebral Cortex (New York, NY)*, 27(10), 4719–4732. <https://doi.org/10.1093/cercor/bhw265>

Lenth, R. V. (2022). *Emmeans: Estimated marginal means, aka least-squares means*. Retrieved

from <https://github.com/rvlenth/emmeans>

Lenth, R. V., Buerkner, P., Herve, M., Love, J., Miguez, F., Riebl, H., & Singmann, H. (2022).

emmeans: Estimated Marginal Means, aka Least-Squares Means. Retrieved from <https://CRAN.R-project.org/package=emmeans>

Lewis, M. D. (2005). Self-organizing individual differences in brain development.

Developmental Review, 25(3-4), 252–277. <https://doi.org/10.1016/j.dr.2005.10.006>

- Li, M., Wang, D., Ren, J., Langs, G., Stoecklein, S., Brennan, B. P., ... Liu, H. (2019). Performing group-level functional image analyses based on homologous functional regions mapped in individuals. *PLOS Biology*, 17(3), e2007032.
<https://doi.org/10.1371/journal.pbio.2007032>
- Liu, C., Downey, R. J., Mu, Y., Richer, N., Hwang, J., Shah, V. A., ... Ferris, D. P. (2023). Comparison of EEG Source Localization Using Simplified and Anatomically Accurate Head Models in Younger and Older Adults. *IEEE Transactions on Neural Systems and Rehabilitation Engineering*, 31, 2591–2602.
<https://doi.org/10.1109/TNSRE.2023.3281356>
- Liu, Q., Ganzetti, M., Wenderoth, N., & Mantini, D. (2018). Detecting Large-Scale Brain Networks Using EEG: Impact of Electrode Density, Head Modeling and Source Localization. *Frontiers in Neuroinformatics*, 12, 4.
<https://doi.org/10.3389/fninf.2018.00004>
- Liu, T. T., Nalci, A., & Falahpour, M. (2017). The global signal in fMRI: Nuisance or Information? *NeuroImage*, 150, 213–229.
<https://doi.org/10.1016/j.neuroimage.2017.02.036>
- Liu, Z., Fukunaga, M., De Zwart, J. A., & Duyn, J. H. (2010). Large-scale spontaneous fluctuations and correlations in brain electrical activity observed with magnetoencephalography. *NeuroImage*, 51(1), 102–111.
<https://doi.org/10.1016/j.neuroimage.2010.01.092>

Luck, S. J. (2014). *An introduction to the event-related potential technique* (Second edition). Cambridge, Massachusetts: The MIT Press.

Lüdecke, D., Makowski, D., Ben-Shachar, M. S., Patil, I., Waggoner, P., & Wiernik, B. M.

(2023). *Performance: Assessment of regression models performance*. Retrieved from <https://easystats.github.io/performance/>

Lundberg, I., Johnson, R., & Stewart, B. M. (2021). What Is Your Estimand? Defining the Target Quantity Connects Statistical Evidence to Theory. *American Sociological Review*, 86(3), 532–565. <https://doi.org/10.1177/00031224211004187>

Magnusson, A., Skaug, H., Nielsen, A., Berg, C., Kristensen, K., Maechler, M., ... Brooks, M. (2021). *glmmTMB: Generalized linear mixed models using template model builder*. Retrieved from <https://github.com/glmmTMB/glmmTMB>

Mahjoory, K., Nikulin, V. V., Botrel, L., Linkenkaer-Hansen, K., Fato, M. M., & Haufe, S. (2017). Consistency of EEG source localization and connectivity estimates. *NeuroImage*, 152, 590–601. <https://doi.org/10.1016/j.neuroimage.2017.02.076>

Mantini, D., Perrucci, M. G., Gratta, C. D., Romani, G. L., & Corbetta, M. (2007). Electrophysiological signatures of resting state networks in the human brain. *Proceedings of the National Academy of Sciences*, 104(32), 13170–13175. <https://doi.org/10.1073/pnas.0700668104>

Mantwill, M., Gell, M., Krohn, S., & Finke, C. (2022). Brain connectivity fingerprinting and behavioural prediction rest on distinct functional systems of the human connectome. *Communications Biology*, 5(1), 261. <https://doi.org/10.1038/s42003-022-03185-3>

- Marcoulides, K. M., & Raykov, T. (2019). Evaluation of Variance Inflation Factors in Regression Models Using Latent Variable Modeling Methods. *Educational and Psychological Measurement*, 79(5), 874–882. <https://doi.org/10.1177/0013164418817803>
- Marek, S., Siegel, J. S., Gordon, E. M., Raut, R. V., Gratton, C., Newbold, D. J., ... Dosenbach, N. U. F. (2018). Spatial and Temporal Organization of the Individual Human Cerebellum. *Neuron*, 100(4), 977–993.e7. <https://doi.org/10.1016/j.neuron.2018.10.010>
- Marek, S., Tervo-Clemmens, B., Calabro, F. J., Montez, D. F., Kay, B. P., Hatoum, A. S., ... Dosenbach, N. U. F. (2020). Towards Reproducible Brain-Wide Association Studies. *bioRxiv*, 2020.08.21.257758. <https://doi.org/10.1101/2020.08.21.257758>
- Marino, M., Arcara, G., Porcaro, C., & Mantini, D. (2019). Hemodynamic Correlates of Electrophysiological Activity in the Default Mode Network. *Frontiers in Neuroscience*, 13, 1060. <https://doi.org/10.3389/fnins.2019.01060>
- Matković, A., Anticevic, A., Murray, J. D., & Repovš, G. (2023). Static and dynamic fMRI-derived functional connectomes represent largely similar information. *Network Neuroscience*, 7(4), 1266–1301. https://doi.org/10.1162/netn_a_00325
- Mayer, C.-D., Lorent, J., & Horgan, G. W. (2011). Exploratory Analysis of Multiple Omics Datasets Using the Adjusted RV Coefficient. *Statistical Applications in Genetics and Molecular Biology*, 10(1). <https://doi.org/10.2202/1544-6115.1540>
- McCulloch, C. E., & Neuhaus, J. M. (2011). Misspecifying the Shape of a Random Effects Distribution: Why Getting It Wrong May Not Matter. *Statistical Science*, 26(3). <https://doi.org/10.1214/11-STS361>

Mehrkanoon, S., Breakspear, M., Britz, J., & Boonstra, T. W. (2014). Intrinsic Coupling Modes in Source-Reconstructed Electroencephalography. *Brain Connectivity*, 4(10), 812–825.
<https://doi.org/10.1089/brain.2014.0280>

Meyer, D. E., & Schvaneveldt, R. W. (1971). Facilitation in recognizing pairs of words: evidence of a dependence between retrieval operations. *Journal of Experimental Psychology*, 90(2), 227–234. <https://doi.org/10.1037/h0031564>

Michel, C. M., & Brunet, D. (2019). EEG Source Imaging: A Practical Review of the Analysis Steps. *Frontiers in Neurology*, 10. <https://doi.org/10.3389/fneur.2019.00325>

Michel, C. M., & Koenig, T. (2018). EEG microstates as a tool for studying the temporal dynamics of whole-brain neuronal networks: A review. *NeuroImage*, 180, 577–593.
<https://doi.org/10.1016/j.neuroimage.2017.11.062>

Miranda-Dominguez, O., Mills, B. D., Carpenter, S. D., Grant, K. A., Kroenke, C. D., Nigg, J. T., & Fair, D. A. (2014). Connectotyping: Model Based Fingerprinting of the Functional Connectome. *PLOS ONE*, 9(11), e111048. <https://doi.org/10.1371/journal.pone.0111048>

Moon, H. S., Jiang, H., Vo, T. T., Jung, W. B., Vazquez, A. L., & Kim, S.-G. (2021). Contribution of Excitatory and Inhibitory Neuronal Activity to BOLD fMRI. *Cerebral Cortex*, 31(9), 4053–4067. <https://doi.org/10.1093/cercor/bhab068>

Mostame, P., & Sadaghiani, S. (2020). Phase- and amplitude-coupling are tied by an intrinsic spatial organization but show divergent stimulus-related changes. *NeuroImage*, 219, 117051. <https://doi.org/10.1016/j.neuroimage.2020.117051>

Mostame, P., & Sadaghiani, S. (2021). Oscillation-Based Connectivity Architecture Is Dominated by an Intrinsic Spatial Organization, Not Cognitive State or Frequency. *Journal of Neuroscience*, 41(1), 179–192. <https://doi.org/10.1523/JNEUROSCI.2155-20.2020>

Mueller, S., Wang, D., Fox, M. D., Yeo, B. T. T., Sepulcre, J., Sabuncu, M. R., ... Liu, H. (2013). Individual variability in functional connectivity architecture of the human brain. *Neuron*, 77(3), 586–595. <https://doi.org/10.1016/j.neuron.2012.12.028>

Mulert, C. (2013). Simultaneous EEG and fMRI: towards the characterization of structure and dynamics of brain networks. *Dialogues in Clinical Neuroscience*, 15(3), 381–386. <https://doi.org/10.31887/DCNS.2013.15.3/cmulert>

Muthukrishna, M., Bell, A. V., Henrich, J., Curtin, C. M., Gedranovich, A., McInerney, J., & Thue, B. (2020). Beyond Western, Educated, Industrial, Rich, and Democratic (WEIRD) Psychology: Measuring and Mapping Scales of Cultural and Psychological Distance. *Psychological Science*, 31(6), 678–701. <https://doi.org/10.1177/0956797620916782>

Naselaris, T., Allen, E., & Kay, K. (2021). Extensive sampling for complete models of individual brains. *Current Opinion in Behavioral Sciences*, 40, 45–51. <https://doi.org/10.1016/j.cobeha.2020.12.008>

Nentwich, M., Ai, L., Madsen, J., Telesford, Q. K., Haufe, S., Milham, M. P., & Parra, L. C. (2020). Functional connectivity of EEG is subject-specific, associated with phenotype, and different from fMRI. *NeuroImage*, 218, 117001. <https://doi.org/10.1016/j.neuroimage.2020.117001>

Newbold, D. J., Laumann, T. O., Hoyt, C. R., Hampton, J. M., Montez, D. F., Raut, R. V., ...

Dosenbach, N. U. F. (2020). Plasticity and Spontaneous Activity Pulses in Disused Human Brain Circuits. *Neuron*, 107(3), 580–589.e6.

<https://doi.org/10.1016/j.neuron.2020.05.007>

Nichols, J. D., Kendall, W. L., & Boomer, G. S. (2019). Accumulating evidence in ecology: Once is not enough. *Ecology and Evolution*, 9(24), 13991–14004.

<https://doi.org/10.1002/ece3.5836>

Nichols, J. D., Oli, M. K., Kendall, William. L., & Boomer, G. S. (2021). A better approach for dealing with reproducibility and replicability in science. *Proceedings of the National Academy of Sciences*, 118(7), e2100769118. <https://doi.org/10.1073/pnas.2100769118>

Nielsen, J. D., Puonti, O., Xue, R., Thielscher, A., & Madsen, K. H. (2023). Evaluating the Influence of Anatomical Accuracy and Electrode Positions on EEG Forward Solutions. *NeuroImage*, 120259. <https://doi.org/10.1016/j.neuroimage.2023.120259>

Noble, S., Spann, M. N., Tokoglu, F., Shen, X., Constable, R. T., & Scheinost, D. (2017). Influences on the Test–Retest Reliability of Functional Connectivity MRI and its Relationship with Behavioral Utility. *Cerebral Cortex*, 27(11), 5415–5429.

<https://doi.org/10.1093/cercor/bhx230>

Nolte, G., Bai, O., Wheaton, L., Mari, Z., Vorbach, S., & Hallett, M. (2004). Identifying true brain interaction from EEG data using the imaginary part of coherency. *Clinical Neurophysiology*, 115(10), 2292–2307. <https://doi.org/10.1016/j.clinph.2004.04.029>

Nunez, P. L., & Srinivasan, R. (2006). *Electric Fields of the Brain*. Oxford University Press.

<https://doi.org/10.1093/acprof:oso/9780195050387.001.0001>

O'brien, R. M. (2007). A Caution Regarding Rules of Thumb for Variance Inflation Factors.

Quality & Quantity, 41(5), 673–690. <https://doi.org/10.1007/s11135-006-9018-6>

Ogawa, S., Lee, T. M., Kay, A. R., & Tank, D. W. (1990). Brain magnetic resonance imaging with contrast dependent on blood oxygenation. *Proceedings of the National Academy of Sciences of the United States of America*, 87(24), 9868–9872.

<https://doi.org/10.1073/pnas.87.24.9868>

Olguín-Rodríguez, P. V., Arzate-Mena, J. D., Corsi-Cabrera, M., Gast, H., Marín-García, A., Mathis, J., ... Müller, M. (2018). Characteristic Fluctuations Around Stable Attractor Dynamics Extracted from Highly Nonstationary Electroencephalographic Recordings. *Brain Connectivity*, 8(8), 457–474. <https://doi.org/10.1089/brain.2018.0609>

Palva, J. M. (2005). Phase Synchrony among Neuronal Oscillations in the Human Cortex.

Journal of Neuroscience, 25(15), 3962–3972. <https://doi.org/10.1523/JNEUROSCI.4250-04.2005>

Parra, M. A., Baez, S., Allegri, R., Nitrini, R., Lopera, F., Slachevsky, A., ... Ibanez, A. (2018). Dementia in Latin America: Assessing the present and envisioning the future. *Neurology*, 90(5), 222–231. <https://doi.org/10.1212/WNL.0000000000004897>

Pedersen, T. L. (2020). *Patchwork: The composer of plots*. Retrieved from <https://CRAN.R-project.org/package=patchwork>

- Penttonen, M., & Buzsáki, G. (2003). Natural logarithmic relationship between brain oscillators. *Thalamus and Related Systems*, 2(02), 145. <https://doi.org/10.1017/S1472928803000074>
- Perrin, F., Pernier, J., Bertrand, O., & Echallier, J. F. (1989). Spherical splines for scalp potential and current density mapping. *Electroencephalography and Clinical Neurophysiology*, 72(2), 184–187. [https://doi.org/10.1016/0013-4694\(89\)90180-6](https://doi.org/10.1016/0013-4694(89)90180-6)
- Pervaiz, U., Vidaurre, D., Woolrich, M. W., & Smith, S. M. (2020). Optimising network modelling methods for fMRI. *NeuroImage*, 211, 116604. <https://doi.org/10.1016/j.neuroimage.2020.116604>
- Pessoa, L. (2014). Understanding brain networks and brain organization. *Physics of Life Reviews*, 11(3), 400–435. <https://doi.org/10.1016/j.plrev.2014.03.005>
- Petersen, Steven E., & Sporns, O. (2015). Brain Networks and Cognitive Architectures. *Neuron*, 88(1), 207–219. <https://doi.org/10.1016/j.neuron.2015.09.027>
- Picchioni, D., Duyn, J. H., & Horovitz, S. G. (2013). Sleep and the functional connectome. *NeuroImage*, 80, 387–396. <https://doi.org/10.1016/j.neuroimage.2013.05.067>
- Poldrack, R. A., Laumann, T. O., Koyejo, O., Gregory, B., Hover, A., Chen, M.-Y., ... Mumford, J. A. (2015). Long-term neural and physiological phenotyping of a single human. *Nature Communications*, 6(1), 8885. <https://doi.org/10.1038/ncomms9885>
- Power, J. D., Barnes, K. A., Snyder, A. Z., Schlaggar, B. L., & Petersen, S. E. (2012). Spurious but systematic correlations in functional connectivity MRI networks arise from subject motion. *NeuroImage*, 59(3), 2142–2154. <https://doi.org/10.1016/j.neuroimage.2011.10.018>

- Power, J. D., Cohen, Alexander L., Nelson, Steven M., Wig, Gagan S., Barnes, K., Church, Jessica A., ... Petersen, Steven E. (2011). Functional Network Organization of the Human Brain. *Neuron*, 72(4), 665–678. <https://doi.org/10.1016/j.neuron.2011.09.006>
- Power, J. D., Lynch, C. J., Adeyemo, B., & Petersen, S. E. (2020). A Critical, Event-Related Appraisal of Denoising in Resting-State fMRI Studies. *Cerebral Cortex (New York, N.Y.: 1991)*, 30(10), 5544–5559. <https://doi.org/10.1093/cercor/bhaa139>
- Power, J. D., Mitra, A., Laumann, T. O., Snyder, A. Z., Schlaggar, B. L., & Petersen, S. E. (2014). Methods to detect, characterize, and remove motion artifact in resting state fMRI. *NeuroImage*, 84, 320–341. <https://doi.org/10.1016/j.neuroimage.2013.08.048>
- Price, C. J., & Friston, K. J. (2002). Degeneracy and cognitive anatomy. *Trends in Cognitive Sciences*, 6(10), 416–421. [https://doi.org/10.1016/S1364-6613\(02\)01976-9](https://doi.org/10.1016/S1364-6613(02)01976-9)
- R Core Team. (2021). *R: A language and environment for statistical computing*. Vienna, Austria: R Foundation for Statistical Computing. Retrieved from <https://www.R-project.org/>
- Raichle, M. E. (2010). Two views of brain function. *Trends in Cognitive Sciences*, 14(4), 180–190. <https://doi.org/10.1016/j.tics.2010.01.008>
- Raichle, M. E. (2015). The restless brain: how intrinsic activity organizes brain function. *Philosophical Transactions of the Royal Society B: Biological Sciences*, 370(1668). <https://doi.org/10.1098/rstb.2014.0172>
- Raichle, M. E., MacLeod, A. M., Snyder, A. Z., Powers, W. J., Gusnard, D. A., & Shulman, G. L. (2001). A default mode of brain function. *Proceedings of the National Academy of*

Sciences of the United States of America, 98(2), 676–682.

<https://doi.org/10.1073/pnas.98.2.676>

Raichle, M. E., & Mintun, M. A. (2006). Brain work and brain imaging. *Annual Review of Neuroscience*, 29, 449–476. <https://doi.org/10.1146/annurev.neuro.29.051605.112819>

Raichle, M. E., & Snyder, A. Z. (2007). A default mode of brain function: a brief history of an evolving idea. *NeuroImage*, 37(4), 1083-1090; discussion 1097-1099.

<https://doi.org/10.1016/j.neuroimage.2007.02.041>

Robert, P., & Escoufier, Y. (1976). A Unifying Tool for Linear Multivariate Statistical Methods: The RV- Coefficient. *Journal of the Royal Statistical Society. Series C (Applied Statistics)*, 25(3), 257–265. <https://doi.org/10.2307/2347233>

Robinson, A. K., Venkatesh, P., Boring, M. J., Tarr, M. J., Grover, P., & Behrmann, M. (2017). Very high density EEG elucidates spatiotemporal aspects of early visual processing. *Scientific Reports*, 7(1), 16248. <https://doi.org/10.1038/s41598-017-16377-3>

Roland, P. E., & Zilles, K. (1998). Structural divisions and functional fields in the human cerebral cortex. *Brain Research. Brain Research Reviews*, 26(2-3), 87–105.
[https://doi.org/10.1016/s0165-0173\(97\)00058-1](https://doi.org/10.1016/s0165-0173(97)00058-1)

Rosenberg, Monica D., Finn, E. S., Scheinost, D., Papademetris, X., Shen, X., Constable, R. T., & Chun, M. M. (2016). A neuromarker of sustained attention from whole-brain functional connectivity. *Nature Neuroscience*, 19(1), 165–171. <https://doi.org/10.1038/nn.4179>

- Rosenberg, Monica D., Martinez, S. A., Rapuano, K. M., Conley, M. I., Cohen, A. O., Cornejo, M. D., ... Casey, B. J. (2020). Behavioral and neural signatures of working memory in childhood. *Journal of Neuroscience*. <https://doi.org/10.1523/JNEUROSCI.2841-19.2020>
- Ryynanen, O. R. M., Hyttinen, J. A. K., Laarne, P. H., & Malmivuo, J. A. (2004). Effect of Electrode Density and Measurement Noise on the Spatial Resolution of Cortical Potential Distribution. *IEEE Transactions on Biomedical Engineering*, 51(9), 1547–1554.
<https://doi.org/10.1109/TBME.2004.828036>
- Ryynanen, O. R. M., Hyttinen, J. A. K., & Malmivuo, J. A. (2006). Effect of measurement noise and electrode density on the spatial resolution of cortical potential distribution with different resistivity values for the skull. *IEEE Transactions on Biomedical Engineering*, 53(9), 1851–1858. <https://doi.org/10.1109/TBME.2006.873744>
- Sadaghiani, S., & Kleinschmidt, A. (2016). Brain Networks and α -Oscillations: Structural and Functional Foundations of Cognitive Control. *Trends in Cognitive Sciences*, 20(11), 805–817. <https://doi.org/10.1016/j.tics.2016.09.004>
- Sadaghiani, S., & Wirsich, J. (2020). Intrinsic connectome organization across temporal scales: New insights from cross-modal approaches. *Network Neuroscience*, 4(1), 1–29.
https://doi.org/10.1162/netn_a_00114
- Samogin, J., Marino, M., Porcaro, C., Wenderoth, N., Dupont, P., Swinnen, S. P., & Mantini, D. (2020). Frequency-dependent functional connectivity in resting state networks. *Human Brain Mapping*, 41(18), 5187–5198. <https://doi.org/10.1002/hbm.25184>

Samogin, J., Rueda Delgado, L., Taberna, G. A., Swinnen, S. P., & Mantini, D. (2022). Age-Related Differences of Frequency-Dependent Functional Connectivity in Brain Networks and Their Link to Motor Performance. *Brain Connectivity*, brain.2021.0135.
<https://doi.org/10.1089/brain.2021.0135>

Satterthwaite, T. D., Wolf, D. H., Loughead, J., Ruparel, K., Elliott, M. A., Hakonarson, H., ... Gur, R. E. (2012). Impact of in-scanner head motion on multiple measures of functional connectivity: relevance for studies of neurodevelopment in youth. *NeuroImage*, 60(1), 623–632. <https://doi.org/10.1016/j.neuroimage.2011.12.063>

Sauce, B., & Matzel, L. D. (2013). The causes of variation in learning and behavior: why individual differences matter. *Frontiers in Psychology*, 4.
<https://doi.org/10.3389/fpsyg.2013.00395>

Schaworonkow, N., & Nikulin, V. V. (2022). Is sensor space analysis good enough? Spatial patterns as a tool for assessing spatial mixing of EEG/MEG rhythms. *NeuroImage*, 253, 119093. <https://doi.org/10.1016/j.neuroimage.2022.119093>

Schnitzler, A., & Gross, J. (2005). Normal and pathological oscillatory communication in the brain. *Nature Reviews Neuroscience*, 6(4), 285–296. <https://doi.org/10.1038/nrn1650>

Schoffelen, J.-M., & Gross, J. (2009). Source connectivity analysis with MEG and EEG. *Human Brain Mapping*, 30(6), 1857–1865. <https://doi.org/10.1002/hbm.20745>

Schweder, T., & Hjort, N. L. (2016). *Confidence, Likelihood, Probability: Statistical Inference with Confidence Distributions*. Cambridge: Cambridge University Press.
<https://doi.org/10.1017/CBO9781139046671>

- Searle, S. R., Speed, F. M., & Milliken, G. A. (1980). Population Marginal Means in the Linear Model: An Alternative to Least Squares Means. *The American Statistician*, 34(4), 216–221. <https://doi.org/10.1080/00031305.1980.10483031>
- Seeck, M., Koessler, L., Bast, T., Leijten, F., Michel, C., Baumgartner, C., ... Beniczky, S. (2017). The standardized EEG electrode array of the IFCN. *Clinical Neurophysiology*, 128(10), 2070–2077. <https://doi.org/10.1016/j.clinph.2017.06.254>
- Seeley, W. W., Menon, V., Schatzberg, A. F., Keller, J., Glover, G. H., Kenna, H., ... Greicius, M. D. (2007). Dissociable Intrinsic Connectivity Networks for Salience Processing and Executive Control. *The Journal of Neuroscience*, 27(9), 2349–2356. <https://doi.org/10.1523/JNEUROSCI.5587-06.2007>
- Seitzman, B. A., Gratton, C., Laumann, T. O., Gordon, E. M., Adeyemo, B., Dworetzky, A., ... Petersen, S. E. (2019). Trait-like variants in human functional brain networks. *Proceedings of the National Academy of Sciences*, 116(45), 22851–22861. <https://doi.org/10.1073/pnas.1902932116>
- Shahhosseini, Y., & Miranda, M. F. (2022). Functional Connectivity Methods and Their Applications in fMRI Data. *Entropy*, 24(3), 390. <https://doi.org/10.3390/e24030390>
- Shehzad, Z., Kelly, A. M. C., Reiss, P. T., Gee, D. G., Gotimer, K., Uddin, L. Q., ... Milham, M. P. (2009). The Resting Brain: Unconstrained yet Reliable. *Cerebral Cortex*, 19(10), 2209–2229. <https://doi.org/10.1093/cercor/bhn256>

Shim, M., Im, C.-H., Kim, Y.-W., & Lee, S.-H. (2018). Altered cortical functional network in major depressive disorder: A resting-state electroencephalogram study. *NeuroImage: Clinical*, 19, 1000–1007. <https://doi.org/10.1016/j.nicl.2018.06.012>

Siebenhühner, F., Wang, S. H., Arnulfo, G., Lampinen, A., Nobili, L., Palva, J. M., & Palva, S. (2020). Genuine cross-frequency coupling networks in human resting-state electrophysiological recordings. *PLOS Biology*, 18(5), e3000685. <https://doi.org/10.1371/journal.pbio.3000685>

Siebenhühner, F., Wang, S. H., Palva, J. M., & Palva, S. (2016). Cross-frequency synchronization connects networks of fast and slow oscillations during visual working memory maintenance. *eLife*, 5, e13451. <https://doi.org/10.7554/eLife.13451>

Siegel, M., Donner, T. H., & Engel, A. K. (2012). Spectral fingerprints of large-scale neuronal interactions. *Nature Reviews Neuroscience*, 13(2), 121–134. <https://doi.org/10.1038/nrn3137>

Siems, M., & Siegel, M. (2020). Dissociated neuronal phase- and amplitude-coupling patterns in the human brain. *NeuroImage*, 209, 116538. <https://doi.org/10.1016/j.neuroimage.2020.116538>

Singer, W. (2018). Neuronal oscillations: unavoidable and useful? *European Journal of Neuroscience*, 48(7), 2389–2398. <https://doi.org/10.1111/ejn.13796>

Sjoberg, D. D., Larmarange, J., Curry, M., Lavery, J., Whiting, K., & Zabor, E. C. (2023). *Gtsummary: Presentation-ready data summary and analytic result tables*. Retrieved from <https://CRAN.R-project.org/package=gtsummary>

Slepian, D., & Pollak, H. O. (1961). Prolate Spheroidal Wave Functions, Fourier Analysis and Uncertainty - I. *Bell System Technical Journal*, 40(1), 43–63.

<https://doi.org/10.1002/j.1538-7305.1961.tb03976.x>

Smith, D. M., Kraus, B. T., Dworetzky, A., Gordon, E. M., & Gratton, C. (2023). Brain hubs defined in the group do not overlap with regions of high inter-individual variability. *NeuroImage*, 120195. <https://doi.org/10.1016/j.neuroimage.2023.120195>

Smith, S. M., Vidaurre, D., Beckmann, C. F., Glasser, M. F., Jenkinson, M., Miller, K. L., ... Van Essen, D. C. (2013). Functional connectomics from resting-state fMRI. *Trends in Cognitive Sciences*, 17(12), 666–682. <https://doi.org/10.1016/j.tics.2013.09.016>

Speelman, C., & McGann, M. (2013). How Mean is the Mean? *Frontiers in Psychology*, 4. <https://doi.org/10.3389/fpsyg.2013.00451>

Sporns, O. (2022). The complex brain: connectivity, dynamics, information. *Trends in Cognitive Sciences*, 26(12), 1066–1067. <https://doi.org/10.1016/j.tics.2022.08.002>

Sporns, O., Tononi, G., & Kötter, R. (2005). The Human Connectome: A Structural Description of the Human Brain. *PLOS Computational Biology*, 1(4), e42. <https://doi.org/10.1371/journal.pcbi.0010042>

Srinivasan, R., Tucker, D. M., & Murias, M. (1998). Estimating the spatial Nyquist of the human EEG. *Behavior Research Methods, Instruments, & Computers*, 30(1), 8–19. <https://doi.org/10.3758/BF03209412>

Stam, C. J., Nolte, G., & Daffertshofer, A. (2007). Phase lag index: Assessment of functional connectivity from multi channel EEG and MEG with diminished bias from common

sources. *Human Brain Mapping*, 28(11), 1178–1193.

<https://doi.org/https://doi.org/10.1002/hbm.20346>

Stein, R. B., Gossen, E. R., & Jones, K. E. (2005). Neuronal variability: noise or part of the signal? *Nature Reviews. Neuroscience*, 6(5), 389–397. <https://doi.org/10.1038/nrn1668>

Stiles, J., & Jernigan, T. L. (2010). The Basics of Brain Development. *Neuropsychology Review*, 20(4), 327–348. <https://doi.org/10.1007/s11065-010-9148-4>

St-Onge, F., Javanray, M., Pichet Binette, A., Strikwerda-Brown, C., Remz, J., Spreng, R. N., ... Villeneuve, S. (2023). Functional connectome fingerprinting across the lifespan. *Network Neuroscience (Cambridge, Mass.)*, 7(3), 1206–1227.

https://doi.org/10.1162/netn_a_00320

Taberna, G. A., Samogin, J., Marino, M., & Mantini, D. (2021). Detection of Resting-State Functional Connectivity from High-Density Electroencephalography Data: Impact of Head Modeling Strategies. *Brain Sciences*, 11(6), 741.

<https://doi.org/10.3390/brainsci11060741>

Thomson, D. J. (1982). Spectrum estimation and harmonic analysis. *Proceedings of the IEEE*, 70(9), 1055–1096. <https://doi.org/10.1109/PROC.1982.12433>

Tokuda, T., Yamashita, O., & Yoshimoto, J. (2021). Multiple clustering for identifying subject clusters and brain sub-networks using functional connectivity matrices without vectorization. *Neural Networks*, 142, 269–287.

<https://doi.org/10.1016/j.neunet.2021.05.016>

- Tononi, G., Sporns, O., & Edelman, G. M. (1999). Measures of degeneracy and redundancy in biological networks. *Proceedings of the National Academy of Sciences of the United States of America*, 96(6), 3257–3262. Retrieved from <https://www.ncbi.nlm.nih.gov/pmc/articles/PMC15929/>
- Turkheimer, F. E., Leech, R., Expert, P., Lord, L.-D., & Vernon, A. C. (2015). The brain's code and its canonical computational motifs. From sensory cortex to the default mode network: A multi-scale model of brain function in health and disease. *Neuroscience & Biobehavioral Reviews*, 55, 211–222. <https://doi.org/10.1016/j.neubiorev.2015.04.014>
- Uddin, L. Q., Betzel, R. F., Cohen, J. R., Damoiseaux, J. S., De Brigard, F., Eickhoff, S. B., ... Spreng, R. N. (2023). Controversies and progress on standardization of large-scale brain network nomenclature. *Network Neuroscience*, 7(3), 864–905.
https://doi.org/10.1162/netn_a_00323
- Uddin, L. Q., Yeo, B. T. T., & Spreng, R. N. (2019). Towards a Universal Taxonomy of Macroscale Functional Human Brain Networks. *Brain Topography*, 32(6), 926–942.
<https://doi.org/10.1007/s10548-019-00744-6>
- Ushey, K. (2022). *Renv: Project environments*. Retrieved from <https://rstudio.github.io/renv/>
- Ushey, K., Allaire, J., & Tang, Y. (2022). *Reticulate: Interface to python*. Retrieved from <https://CRAN.R-project.org/package=reticulate>
- van den Brand, T. (2021). *ggh4x: Hacks for ggplot2*. Retrieved from <https://github.com/teunbrand/ggh4x>

- van der Meij, R., Kahana, M., & Maris, E. (2012). Phase-Amplitude Coupling in Human Electrocorticography Is Spatially Distributed and Phase Diverse. *Journal of Neuroscience*, 32(1), 111–123. <https://doi.org/10.1523/JNEUROSCI.4816-11.2012>
- Van De Ville, D., Farouj, Y., Preti, M. G., Liégeois, R., & Amico, E. (2021). When makes you unique: Temporality of the human brain fingerprint. *Science Advances*, 7(42), eabj0751. <https://doi.org/10.1126/sciadv.abj0751>
- Van Der Molen, M. J. W., Stam, C. J., & Van Der Molen, M. W. (2014). Resting-State EEG Oscillatory Dynamics in Fragile X Syndrome: Abnormal Functional Connectivity and Brain Network Organization. *PLoS ONE*, 9(2), e88451. <https://doi.org/10.1371/journal.pone.0088451>
- Van Dijk, K. R. A., Hedden, T., Venkataraman, A., Evans, K. C., Lazar, S. W., & Buckner, R. L. (2010). Intrinsic Functional Connectivity As a Tool For Human Connectomics: Theory, Properties, and Optimization. *Journal of Neurophysiology*, 103(1), 297–321. <https://doi.org/10.1152/jn.00783.2009>
- Van Dijk, K. R. A., Sabuncu, M. R., & Buckner, R. L. (2012). The influence of head motion on intrinsic functional connectivity MRI. *NeuroImage*, 59(1), 431–438. <https://doi.org/10.1016/j.neuroimage.2011.07.044>
- Van Essen, D. C., Glasser, M. F., Dierker, D. L., Harwell, J., & Coalson, T. (2012). Parcellations and Hemispheric Asymmetries of Human Cerebral Cortex Analyzed on Surface-Based Atlases. *Cerebral Cortex*, 22(10), 2241–2262. <https://doi.org/10.1093/cercor/bhr291>

Van Essen, D. C., Ugurbil, K., Auerbach, E., Barch, D., Behrens, T. E. J., Bucholz, R., ... WU-

Minn HCP Consortium. (2012). The Human Connectome Project: a data acquisition perspective. *NeuroImage*, 62(4), 2222–2231.

<https://doi.org/10.1016/j.neuroimage.2012.02.018>

Van Horn, J. D., Grafton, S. T., & Miller, M. B. (2008). Individual Variability in Brain Activity:

A Nuisance or an Opportunity? *Brain Imaging and Behavior*, 2(4), 327–334.

<https://doi.org/10.1007/s11682-008-9049-9>

Venkatesh, M., Jaja, J., & Pessoa, L. (2020). Comparing functional connectivity matrices: A

geometry-aware approach applied to participant identification. *NeuroImage*, 207, 116398.

<https://doi.org/10.1016/j.neuroimage.2019.116398>

Vidaurre, D., Hunt, L. T., Quinn, A. J., Hunt, B. A. E., Brookes, M. J., Nobre, A. C., & Woolrich,

M. W. (2018). Spontaneous cortical activity transiently organises into frequency specific phase-coupling networks. *Nature Communications*, 9(1), 2987.

<https://doi.org/10.1038/s41467-018-05316-z>

Vinck, M., Oostenveld, R., van Wingerden, M., Battaglia, F., & Pennartz, C. M. A. (2011). An

improved index of phase-synchronization for electrophysiological data in the presence of volume-conduction, noise and sample-size bias. *NeuroImage*, 55(4), 1548–1565.

<https://doi.org/10.1016/j.neuroimage.2011.01.055>

Viola, M. (2020). Beyond the Platonic Brain: facing the challenge of individual differences in

function-structure mapping. *Synthese*. <https://doi.org/10.1007/s11229-020-02875-x>

- Wang, D., Buckner, R. L., Fox, M. D., Holt, D. J., Holmes, A. J., Stoecklein, S., ... Liu, H. (2015). Parcellating cortical functional networks in individuals. *Nature Neuroscience*, 18(12), 1853–1860. <https://doi.org/10.1038/nn.4164>
- Ward, P. G. D., Orchard, E. R., Oldham, S., Arnatkevičiūtė, A., Sforazzini, F., Fornito, A., ... Jamadar, S. D. (2020). Individual differences in haemoglobin concentration influence bold fMRI functional connectivity and its correlation with cognition. *NeuroImage*, 221, 117196. <https://doi.org/10.1016/j.neuroimage.2020.117196>
- Wasserstein, R. L., & Lazar, N. A. (2016). The ASA Statement on p-Values: Context, Process, and Purpose. *The American Statistician*, 70(2), 129–133.
<https://doi.org/10.1080/00031305.2016.1154108>
- Wasserstein, R. L., Schirm, A. L., & Lazar, N. A. (2019). Moving to a World Beyond “p < 0.05.” *The American Statistician*, 73(sup1), 1–19.
<https://doi.org/10.1080/00031305.2019.1583913>
- Whittingstall, K., Stroink, G., Gates, L., Connolly, J., & Finley, A. (2003). Effects of dipole position, orientation and noise on the accuracy of EEG source localization. *BioMedical Engineering OnLine*, 2(1), 14. <https://doi.org/10.1186/1475-925X-2-14>
- Whittington, M. A., Traub, R. D., & Adams, N. E. (2018). A future for neuronal oscillation research. *Brain and Neuroscience Advances*, 2, 239821281879482.
<https://doi.org/10.1177/2398212818794827>
- Wickham, H. (2021). *Tidyverse: Easily install and load the tidyverse*. Retrieved from <https://CRAN.R-project.org/package=tidyverse>

- Wickham, H., Chang, W., Henry, L., Pedersen, T. L., Takahashi, K., Wilke, C., ... Dunnington, D. (2022). *ggplot2: Create elegant data visualisations using the grammar of graphics*. Retrieved from <https://CRAN.R-project.org/package=ggplot2>
- Widmann, A., Schröger, E., & Maess, B. (2015). Digital filter design for electrophysiological data – a practical approach. *Journal of Neuroscience Methods*, 250, 34–46.
<https://doi.org/10.1016/j.jneumeth.2014.08.002>
- Wirsich, J., Jorge, J., Iannotti, G. R., Shamshiri, E. A., Grouiller, F., Abreu, R., ... Vulliémoz, S. (2021). The relationship between EEG and fMRI connectomes is reproducible across simultaneous EEG-fMRI studies from 1.5T to 7T. *NeuroImage*, 231, 117864.
<https://doi.org/10.1016/j.neuroimage.2021.117864>
- Wu, J., Li, J., Eickhoff, S. B., Scheinost, D., & Genon, S. (2023). The challenges and prospects of brain-based prediction of behaviour. *Nature Human Behaviour*, 7(8), 1255–1264.
<https://doi.org/10.1038/s41562-023-01670-1>
- Xie, M., & Singh, K. (2013). Confidence Distribution, the Frequentist Distribution Estimator of a Parameter: A Review. *International Statistical Review*, 81(1), 3–39.
<https://doi.org/10.1111/insr.12000>
- Xu, T., Opitz, A., Craddock, R. C., Wright, M. J., Zuo, X.-N., & Milham, M. P. (2016). Assessing Variations in Areal Organization for the Intrinsic Brain: From Fingerprints to Reliability. *Cerebral Cortex*, 26(11), 4192–4211. <https://doi.org/10.1093/cercor/bhw241>

Yang, Z., Craddock, R. C., & Milham, M. P. (2014). Impact of hematocrit on measurements of the intrinsic brain. *Frontiers in Neuroscience*, 8, 452.

<https://doi.org/10.3389/fnins.2014.00452>

Yasumoto, A. (2023). *ftExtra: Extensions for flextable*. Retrieved from <https://CRAN.R-project.org/package=ftExtra>

Yeo, B. T. T., Krienen, F. M., Sepulcre, J., Sabuncu, M. R., Lashkari, D., Hollinshead, M., ...

Buckner, R. L. (2011). The organization of the human cerebral cortex estimated by intrinsic functional connectivity. *Journal of Neurophysiology*, 106(3), 1125–1165.

<https://doi.org/10.1152/jn.00338.2011>

Yuste, R. (2015). From the neuron doctrine to neural networks. *Nature Reviews. Neuroscience*, 16(8), 487–497. <https://doi.org/10.1038/nrn3962>

Zhang, S., Heck, P. R., Meyer, M., Chabris, C. F., Goldstein, D. G., & Hofman, J. M. (2022, April 29). *An illusion of predictability in scientific results*.

<https://doi.org/10.31235/osf.io/5tcgs>

Zilles, K., & Amunts, K. (2013). Individual variability is not noise. *Trends in Cognitive Sciences*, 17(4), 153–155. <https://doi.org/10.1016/j.tics.2013.02.003>

Appendix A

Supplementary Results

The supplementary results are separated into four parts. In the first part, we provide the reduced model results of individual-level contrasts estimating the difference in functional connectome similarity within and between participants at various levels of the session and state predictors. In the second part, we provide the reduced model results of our phase coupling analyses when the phase lag index was estimated using the Hilbert transform method. In the third part, we provide the results of our functional connectome similarity analyses derived from the maximal models of functional connectome similarity. In the final part, we provide the results of our functional connectome similarity estimates for amplitude coupling functional connectomes in the delta, theta, beta, and gamma bands.

Additional supplementary results can be found in the Supplementary Material available online at the study's GitHub repository https://github.com/mccarthy-m-g/mccarthy_EEGNetworkVariants_2024 or Open Science Framework (OSF) repository <https://osf.io/xztdk/> (DOI: <https://doi.org/10.5281/zenodo.6578410>). These include: (1) phase, amplitude, and phase (Hilbert transform) coupling functional connectomes with independent fill scales for all recordings, presented as adjacency matrices rather than connectivity profiles (see Phase Coupling Functional Connectomes, Amplitude Coupling Functional Connectomes, and Phase Coupling Functional Connectomes [Hilbert transform]); (2) larger versions of all the similarity matrices presented in this manuscript, as well as alternate versions of these matrices plotted using the Jet colour scale to facilitate visual comparisons between our results and those of Gordon, Laumann, Gilmore, et al. (2017) and Gratton et al. (2018) (see Similarity Matrices); (3)

model summaries for the reduced and maximal group-level mixed beta regression models (see Model Summaries); and (4) diagnostic plots summarizing the distribution of bad EEG channels and bad segments across recordings (see EEG Preprocessing Diagnostics).

Individual-level contrast results

In this section we provide the reduced model results of individual-level contrasts estimating the difference in functional connectome similarity within and between participants at various levels of the session and state predictors. These models were fit to the subset of the similarity matrix belonging to a given participant, but otherwise follow the same parameterizations as the group-level contrasts provided in the main results section. A simple way to conceptualize this is that the group-level contrasts were fit on all observations in the lower triangle of the similarity matrix, whereas the individual-level contrasts were fit on all observations in a given column or row of the similarity matrix belonging to each participant. Thus, we emphasize that the number of observations used in the individual-level contrasts (1,002 observations per model/participant) is considerably smaller than the number of observations used in the group-level contrasts (14,028 observations total), and consequently, the uncertainty of these estimates is considerably larger. Note that although we did conduct individual-level contrasts for amplitude coupling functional connectomes in the delta, theta, beta, and gamma bands, we refrain from displaying them here for the same reasons of interpretability described in the results section of this manuscript.

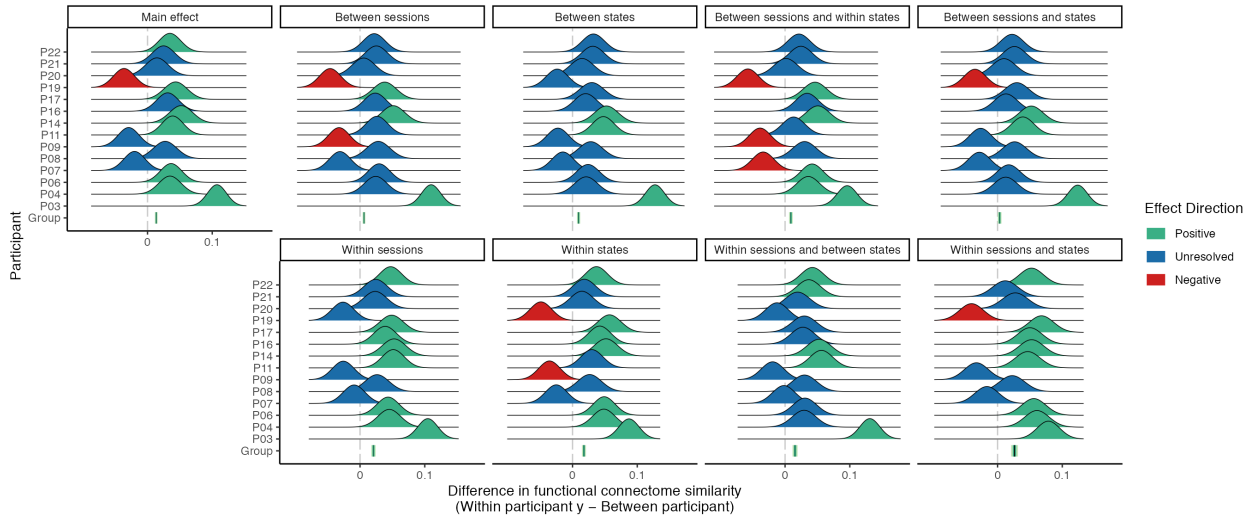


Figure A1. 95% compatibility distributions for individual-level contrasts estimating the difference in functional connectome similarity within and between participants at various levels of the session and state predictors for phase coupling functional connectome similarities in the delta band.

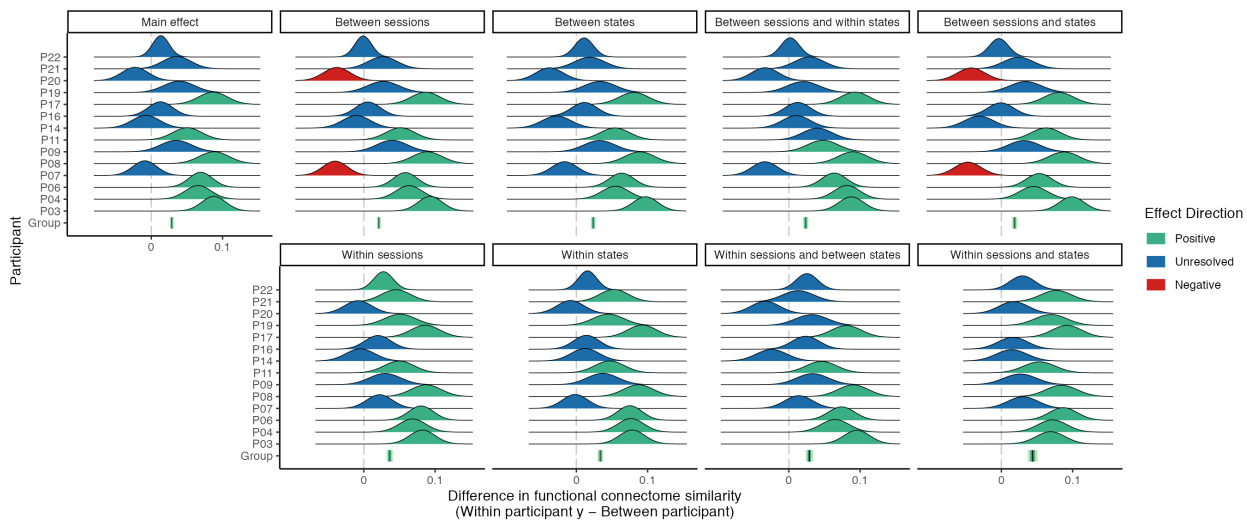


Figure A2. 95% compatibility distributions for individual-level contrasts estimating the difference in functional connectome similarity within and between participants at various levels

of the session and state predictors for phase coupling functional connectome similarities in the theta band.

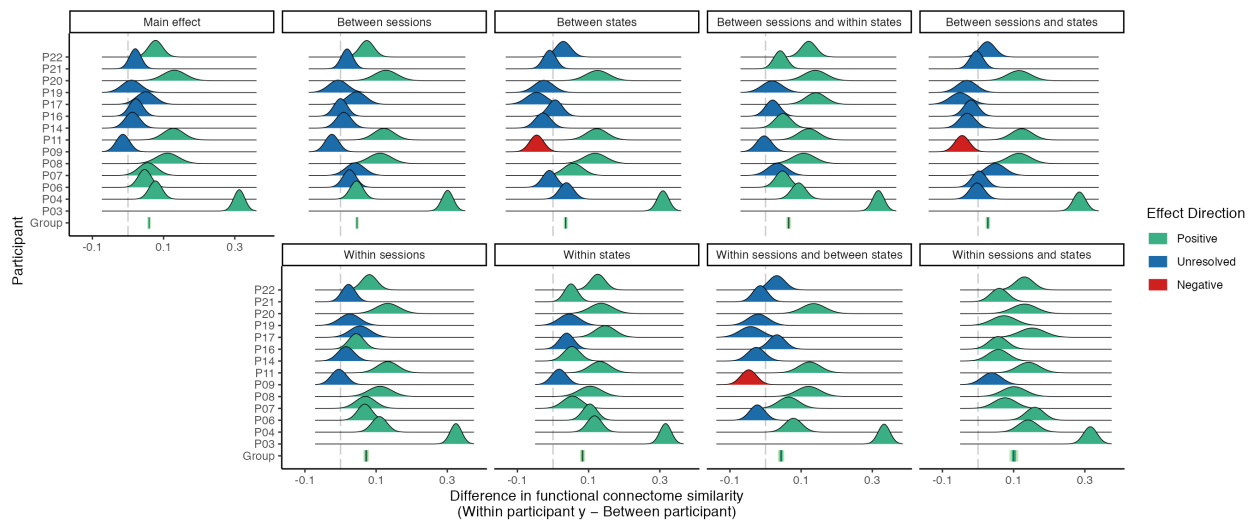


Figure A3. 95% compatibility distributions for individual-level contrasts estimating the difference in functional connectome similarity within and between participants at various levels of the session and state predictors for phase coupling functional connectome similarities in the alpha band.

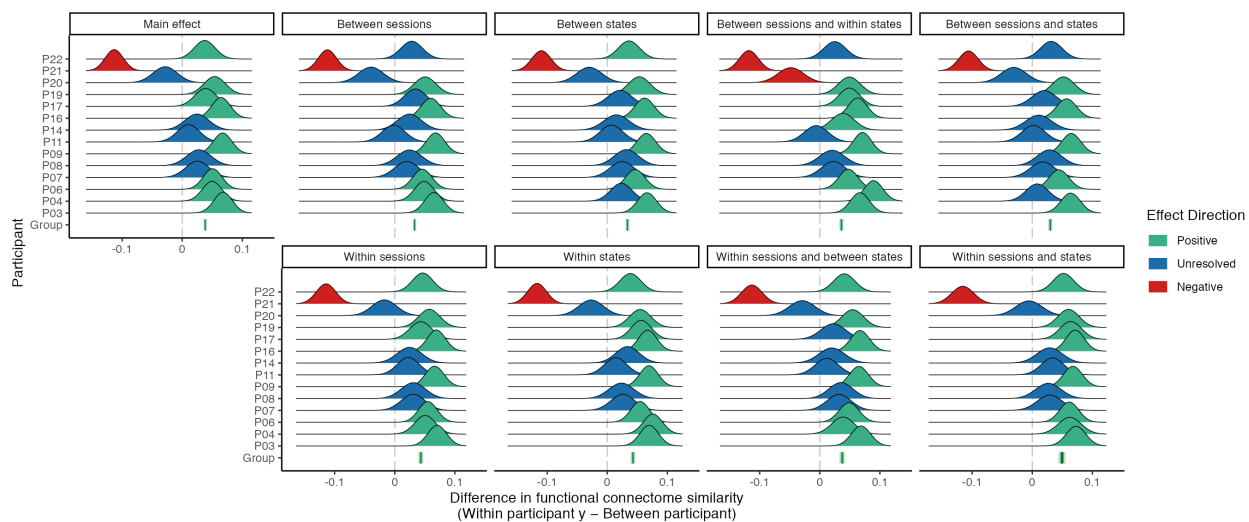


Figure A4. 95% compatibility distributions for individual-level contrasts estimating the difference in functional connectome similarity within and between participants at various levels of the session and state predictors for phase coupling functional connectome similarities in the beta band.

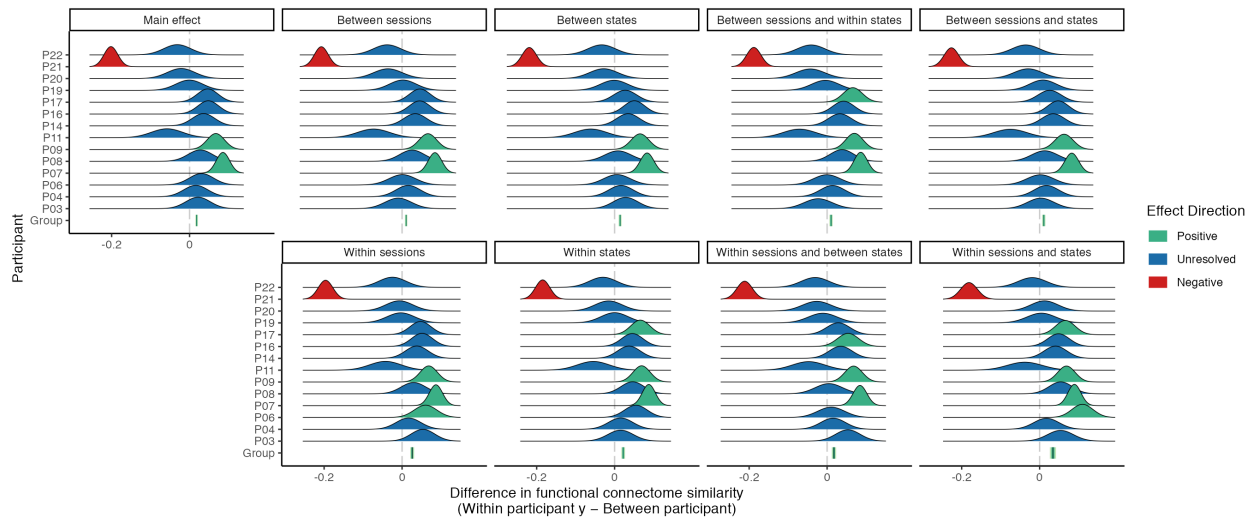


Figure A5. 95% compatibility distributions for individual-level contrasts estimating the difference in functional connectome similarity within and between participants at various levels of the session and state predictors for phase coupling functional connectome similarities in the gamma band.

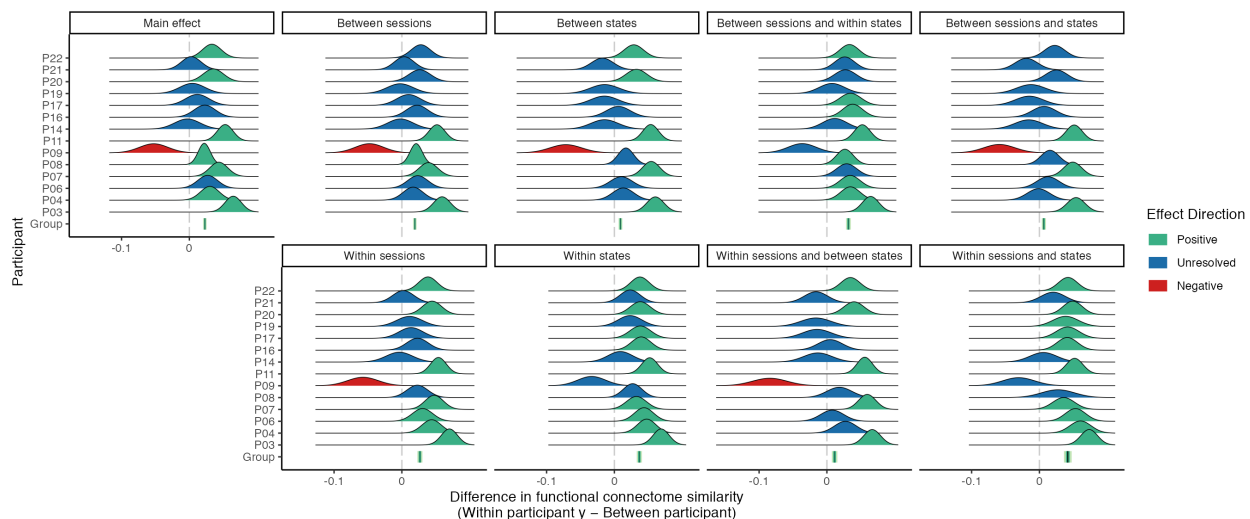


Figure A6. 95% compatibility distributions for individual-level contrasts estimating the difference in functional connectome similarity within and between participants at various levels of the session and state predictors for amplitude coupling functional connectome similarities in the alpha band.

Phase coupling (Hilbert transform) results

In this section we report how functional connectivity and phase-coupling similarities change when the phase lag index is estimated using the Hilbert transform method instead of the multitaper method. Across all five frequency bands we find that (1) functional connectivity is generally lower, but individual patterns of connectivity are similar or the same; (2) functional connectome similarity is generally higher, but patterns of similarity are similar or the same.

We extracted the analytic signal from each channel's time-course using the Hilbert transform and then estimated the phase lag index between them (Stam et al., 2007), given by:

$$\text{PLI}(x, y) = \frac{1}{N} \sum_{i=1}^N \left| \frac{1}{n} \sum_{j=1}^n \text{sign} \left(\text{Im} \left(e^{i(\phi_x - \phi_y)_{ij}} \right) \right) \right|,$$

where N is the number of epochs, n is the number of samples in each epoch, $\text{sign}(\cdot)$ is the signum operator, $\text{Im}(\cdot)$ is the imaginary operator, and $e^{i(\cdot)}$ is Euler's formula, which we apply to difference of the phase angles between ϕ_x and ϕ_y at the individual sample points j in the i th epoch.

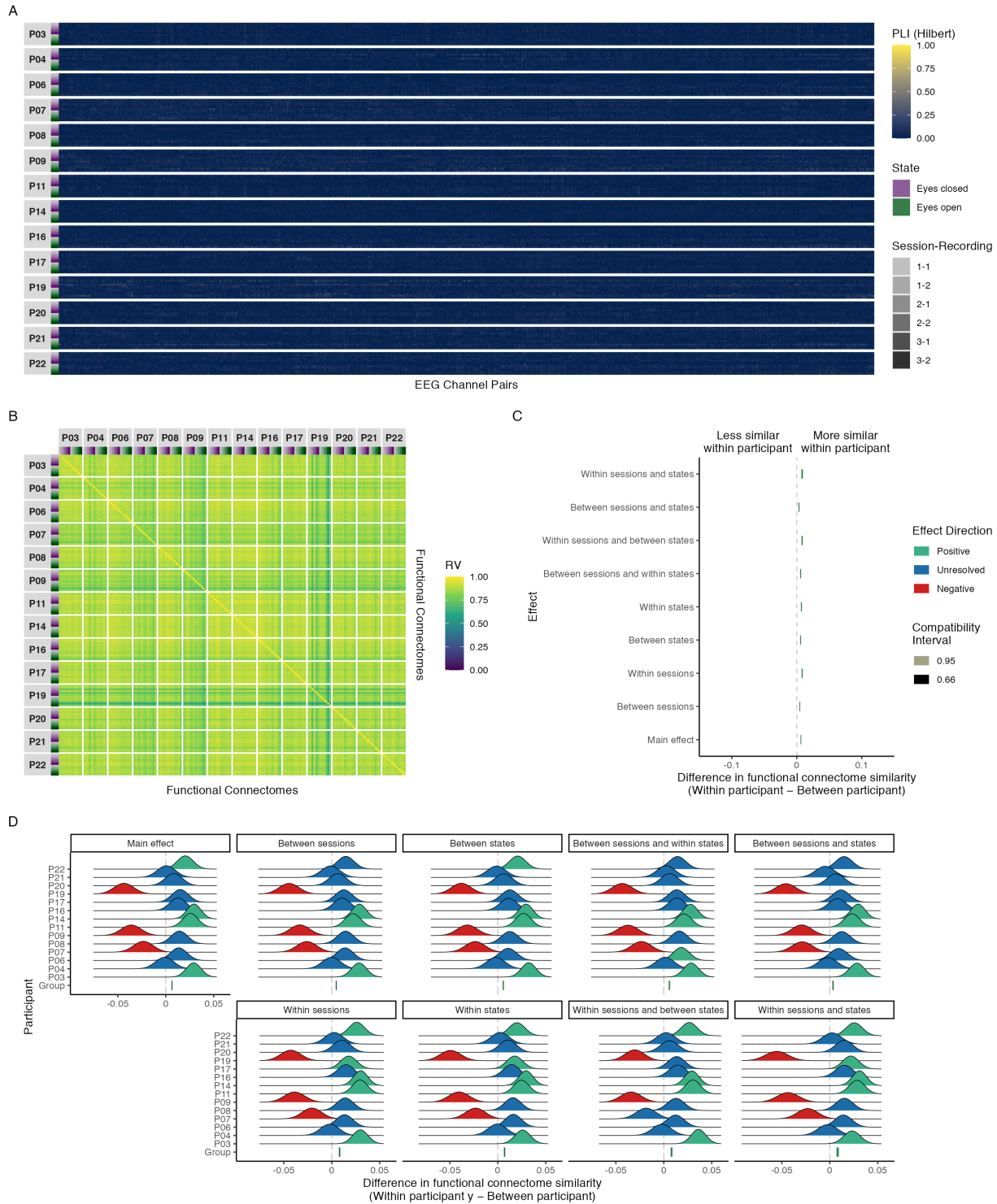


Figure A7. Results of phase coupling (Hilbert transform) analyses in the delta band: (A) connectivity profiles for all functional connectomes, organized by participant and recording; (B)

estimates of functional connectome similarity between all pairs of functional connectomes, organized by participant and recording; group-level (C) and individual-level (D) contrasts estimating the average difference in functional connectome similarity within and between participants across contexts.

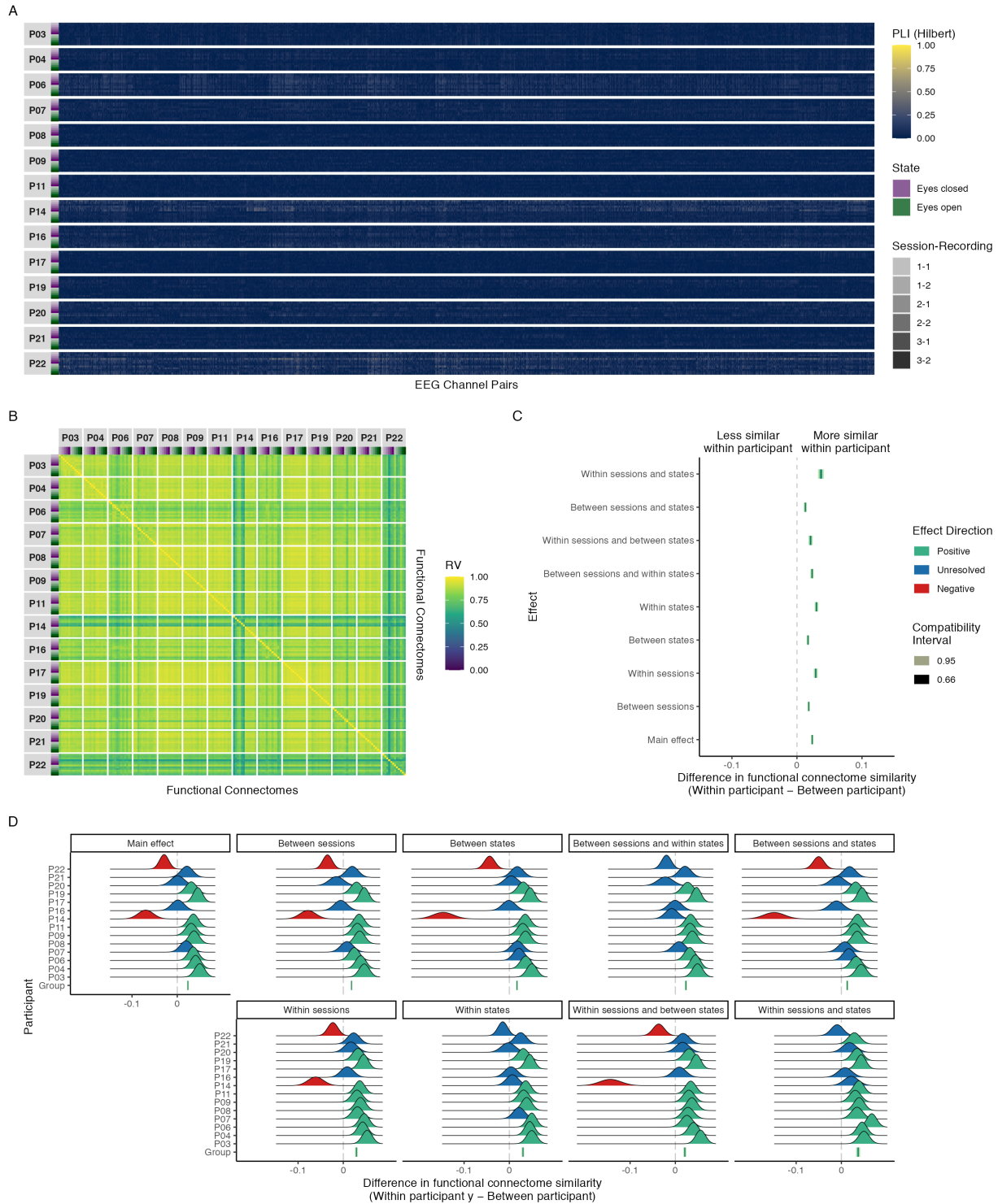


Figure A8. Results of phase coupling (Hilbert transform) analyses in the theta band: (A) connectivity profiles for all functional connectomes, organized by participant and recording; (B)

estimates of functional connectome similarity between all pairs of functional connectomes, organized by participant and recording; group-level (C) and individual-level (D) contrasts estimating the average difference in functional connectome similarity within and between participants across contexts.

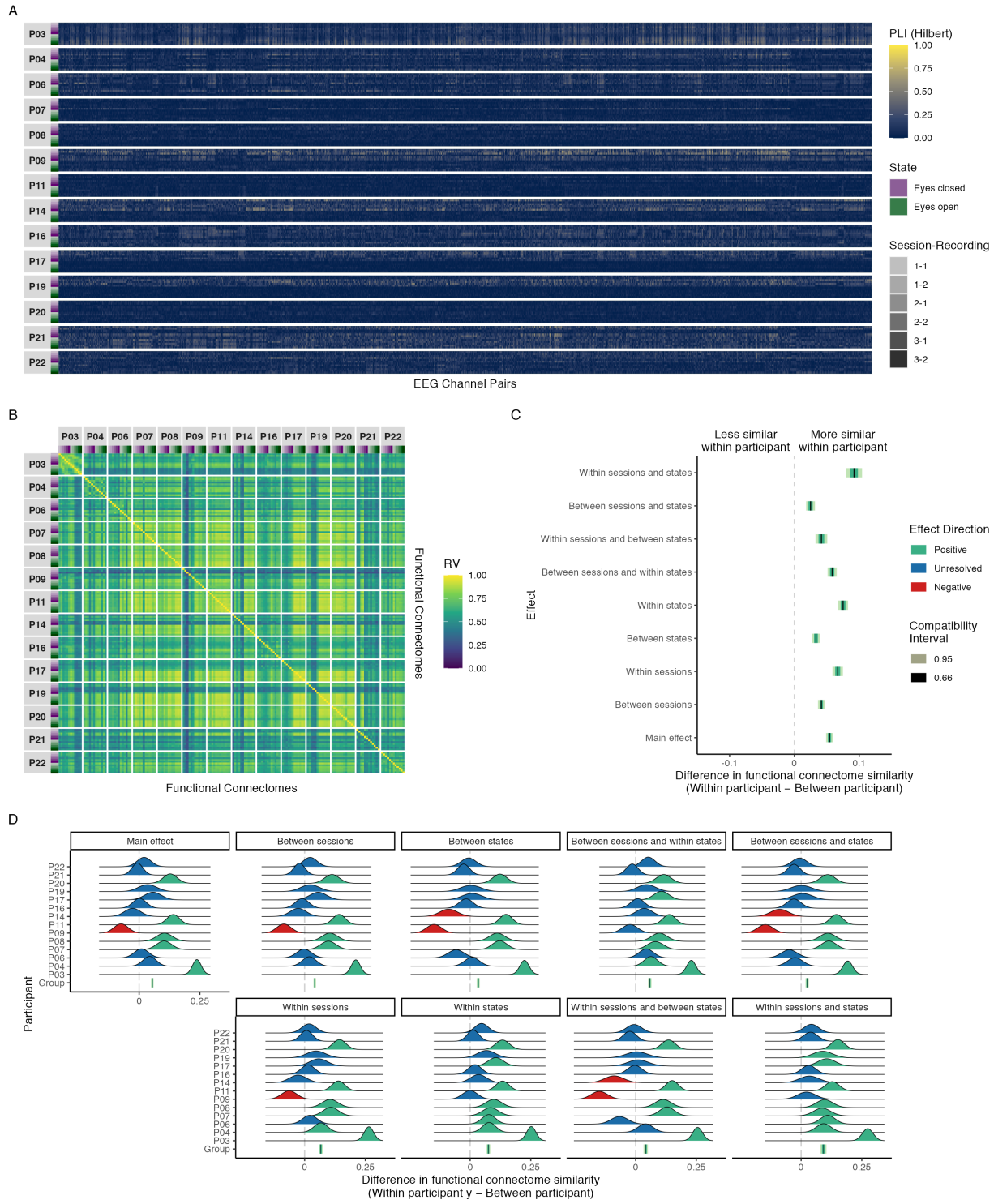


Figure A9. Results of phase coupling (Hilbert transform) analyses in the alpha band: (A) connectivity profiles for all functional connectomes, organized by participant and recording; (B)

estimates of functional connectome similarity between all pairs of functional connectomes, organized by participant and recording; group-level (C) and individual-level (D) contrasts estimating the average difference in functional connectome similarity within and between participants across contexts.

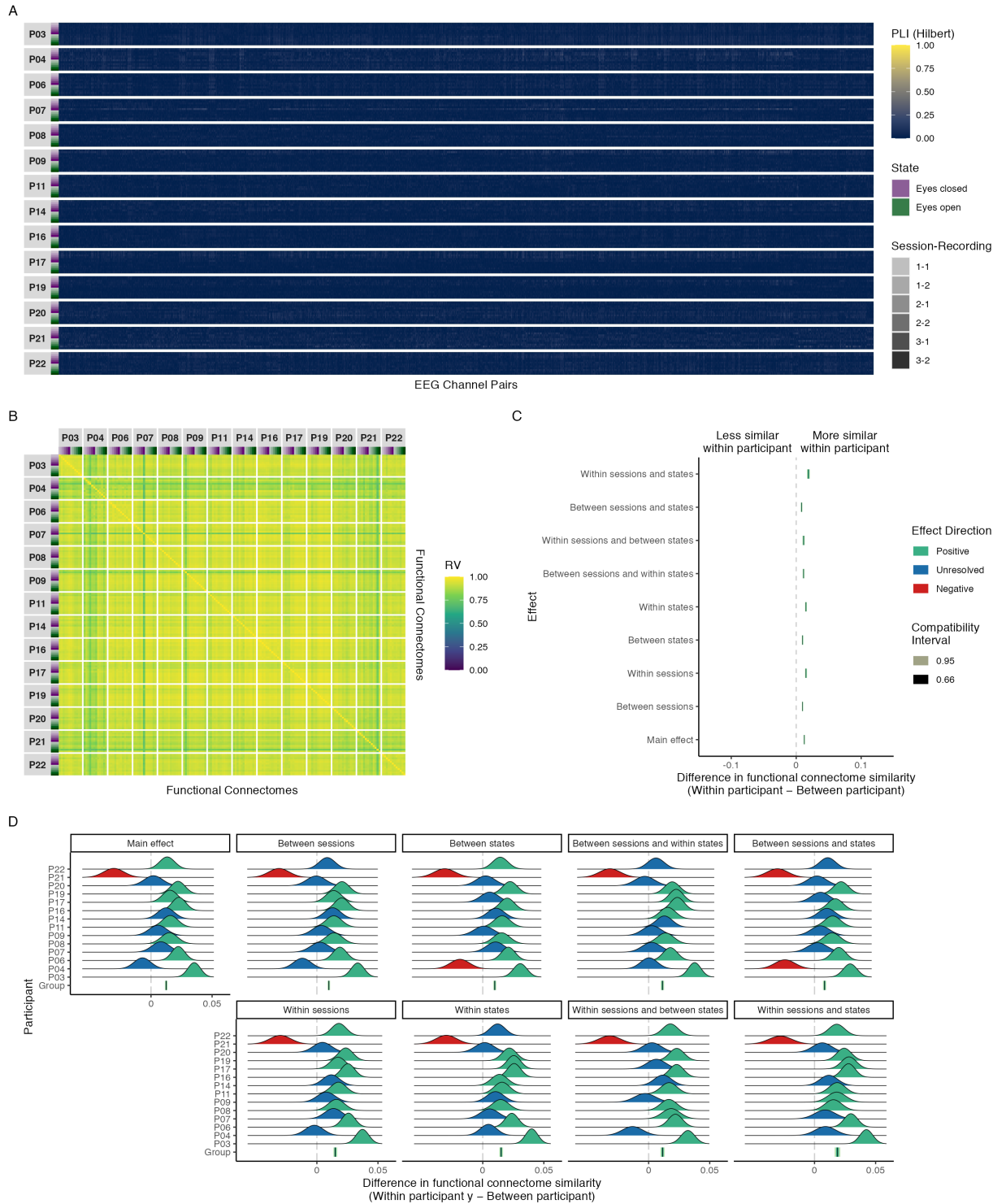


Figure A10. Results of phase coupling (Hilbert transform) analyses in the beta band: (A) connectivity profiles for all functional connectomes, organized by participant and recording; (B)

estimates of functional connectome similarity between all pairs of functional connectomes, organized by participant and recording; group-level (C) and individual-level (D) contrasts estimating the average difference in functional connectome similarity within and between participants across contexts.

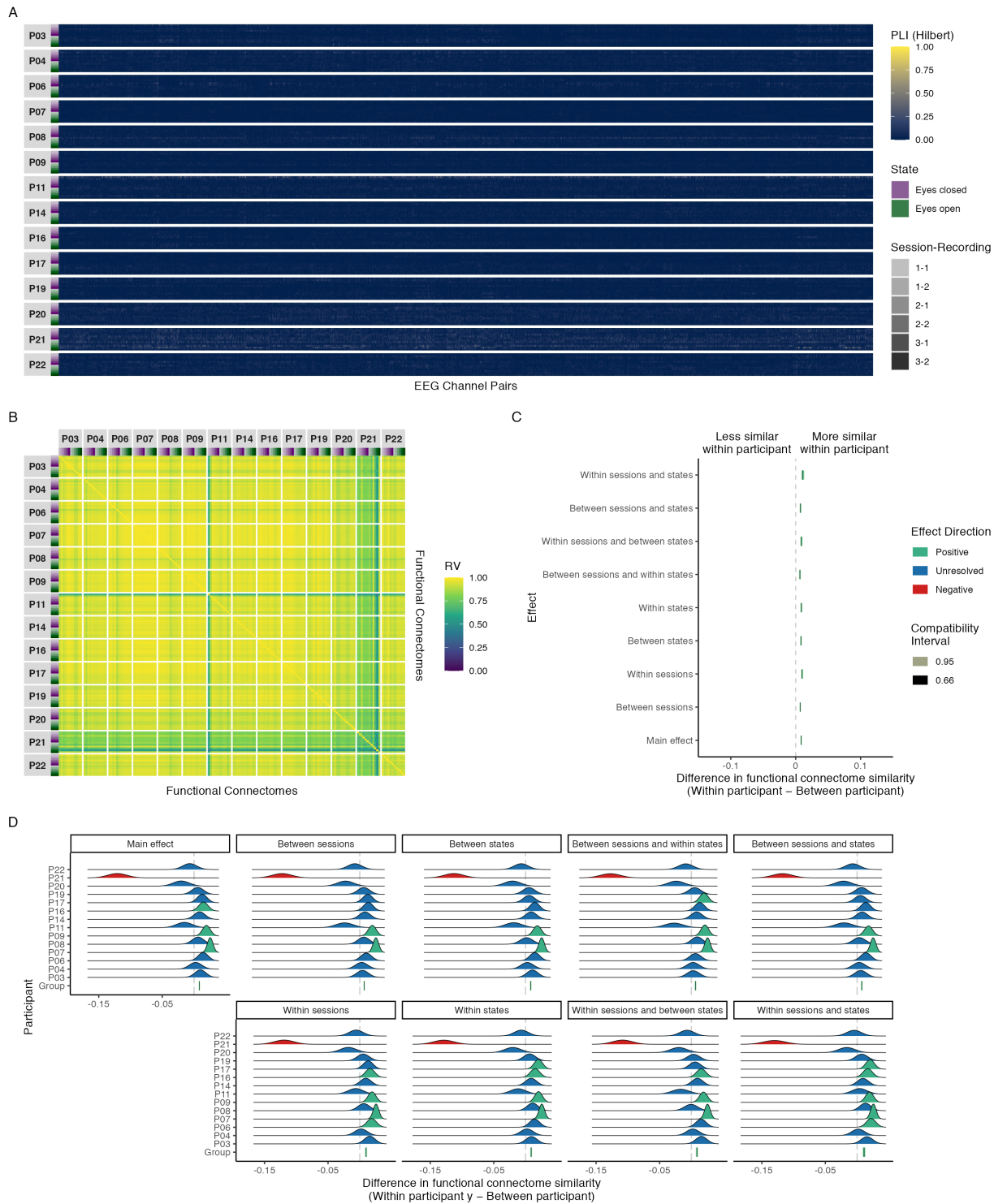


Figure A11. Results of phase coupling (Hilbert transform) analyses in the gamma band: (A) connectivity profiles for all functional connectomes, organized by participant and recording; (B)

estimates of functional connectome similarity between all pairs of functional connectomes, organized by participant and recording; group-level (C) and individual-level (D) contrasts estimating the average difference in functional connectome similarity within and between participants across contexts.

Maximal model results

In this section we provide the results of our functional connectome similarity analyses derived from the maximal models of functional connectome similarity. Note that results are only shown for analyses where the group-level maximal converged and was non-singular (Table A1). Likewise, individual-level contrast results are only shown for converged, non-singular models. Additionally, note that the connectivity profiles and similarity matrices in the following sections are identical to those from the main results section—only the contrast plots depict new results.

Table A1

Results of convergence and singularity checks for each group-level mixed beta regression model of functional connectome similarity, organized by coupling mode and frequency band. Here the maximal and reduced models correspond to, respectively, models with and without a random intercept for the participant pair term.

Coupling Mode	Frequency Band	Reduced Model		Maximal Model	
		Converged	Singular	Converged	Singular
Phase					
Delta		TRUE	FALSE	FALSE	TRUE
Theta		TRUE	FALSE	TRUE	FALSE
Alpha		TRUE	FALSE	TRUE	FALSE
Beta		TRUE	FALSE	TRUE	FALSE
Gamma		TRUE	FALSE	TRUE	FALSE
Amplitude					
Alpha		TRUE	FALSE	TRUE	FALSE
Phase (Hilbert transform)					
Delta		TRUE	FALSE	TRUE	FALSE
Theta		TRUE	FALSE	TRUE	FALSE

Coupling Mode	Frequency Band	Reduced Model		Maximal Model	
		Converged	Singular	Converged	Singular
Alpha		TRUE	FALSE	TRUE	FALSE
Beta		TRUE	FALSE	TRUE	FALSE
Gamma		TRUE	FALSE	TRUE	FALSE

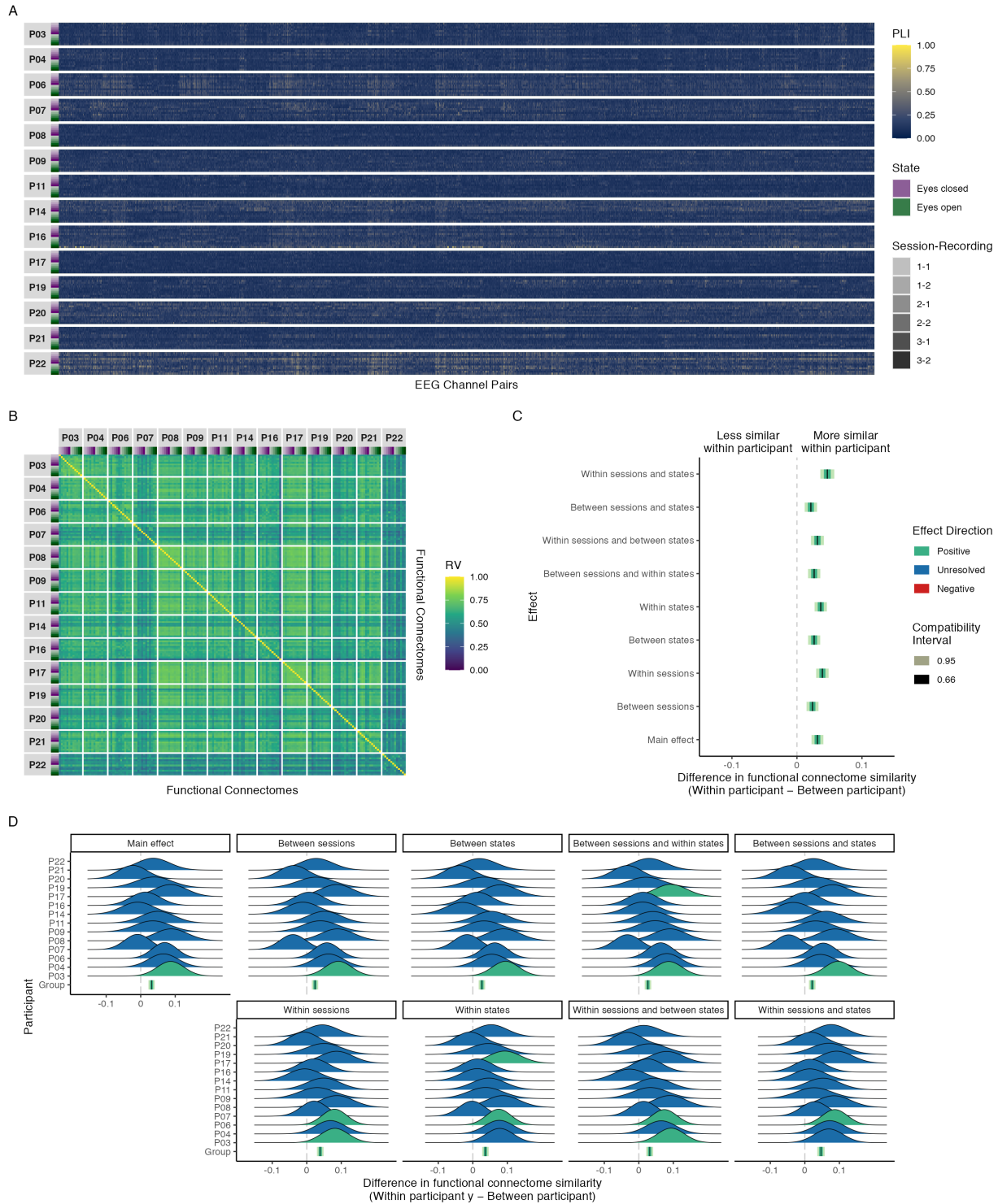


Figure A12. Maximal model results of phase coupling analyses in the theta band: (A) connectivity profiles for all functional connectomes, organized by participant and recording; (B)

estimates of functional connectome similarity between all pairs of functional connectomes, organized by participant and recording; and group-level (C) and individual-level (D) contrasts estimating the average difference in functional connectome similarity within and between participants across contexts.

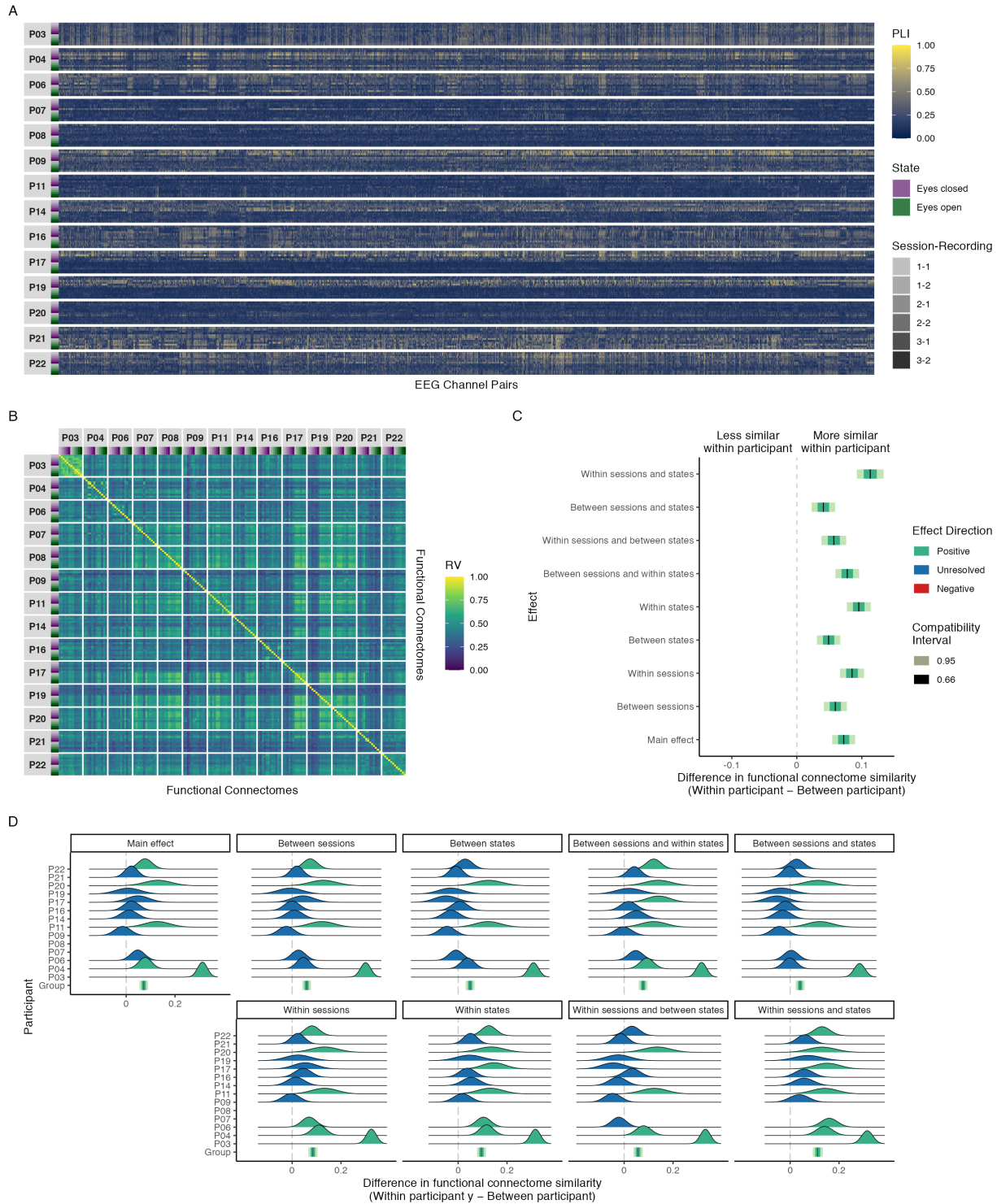


Figure A13. Maximal model results of phase coupling analyses in the alpha band: (A) connectivity profiles for all functional connectomes, organized by participant and recording; (B)

estimates of functional connectome similarity between all pairs of functional connectomes, organized by participant and recording; and group-level (C) and individual-level (D) contrasts estimating the average difference in functional connectome similarity within and between participants across contexts.

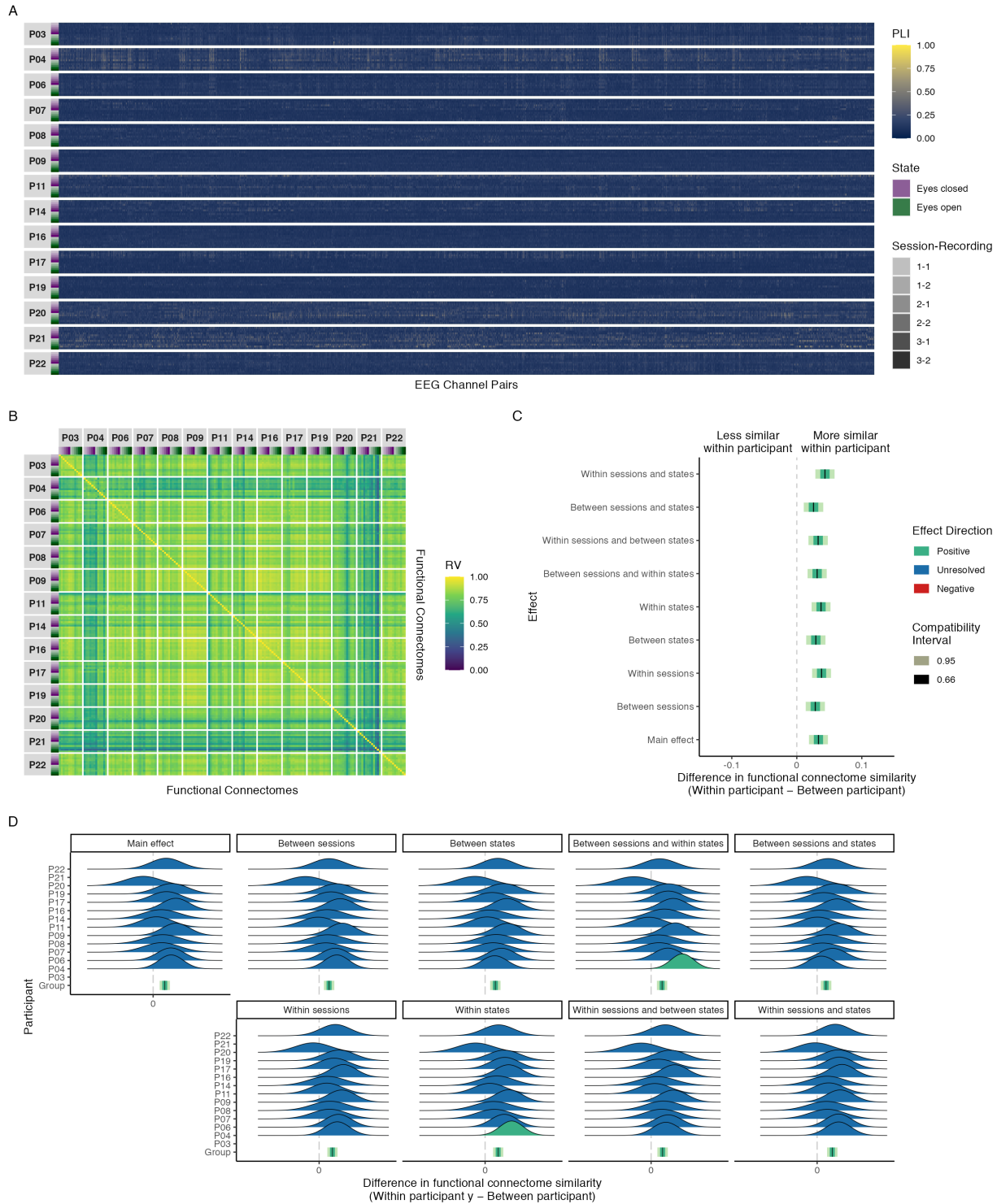


Figure A14. Maximal model results of phase coupling analyses in the beta band: (A) connectivity profiles for all functional connectomes, organized by participant and recording; (B) estimates of

functional connectome similarity between all pairs of functional connectomes, organized by participant and recording; and group-level (C) and individual-level (D) contrasts estimating the average difference in functional connectome similarity within and between participants across contexts.

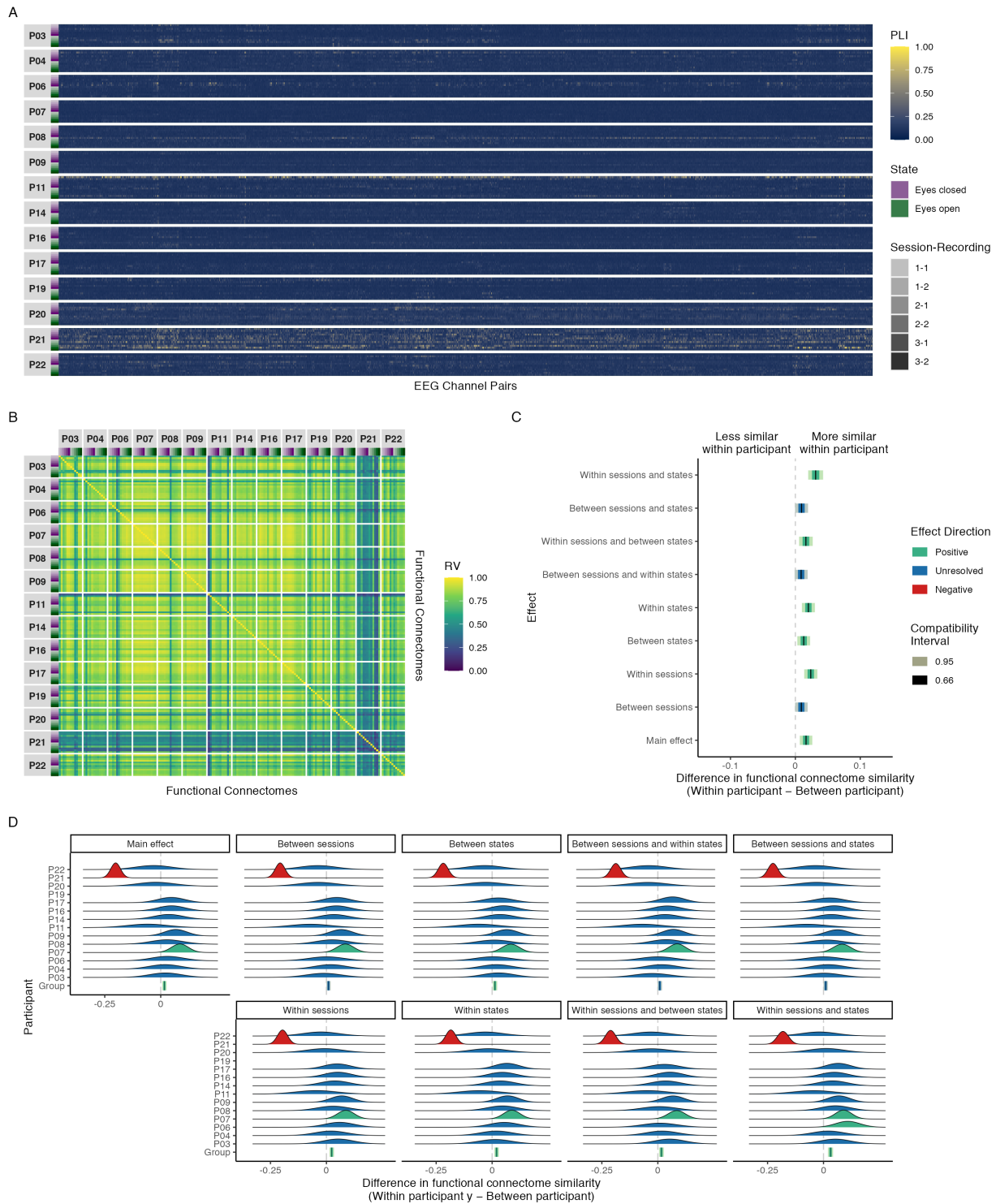


Figure A15. Maximal model results of phase coupling analyses in the gamma band: (A) connectivity profiles for all functional connectomes, organized by participant and recording; (B)

estimates of functional connectome similarity between all pairs of functional connectomes, organized by participant and recording; and group-level (C) and individual-level (D) contrasts estimating the average difference in functional connectome similarity within and between participants across contexts.

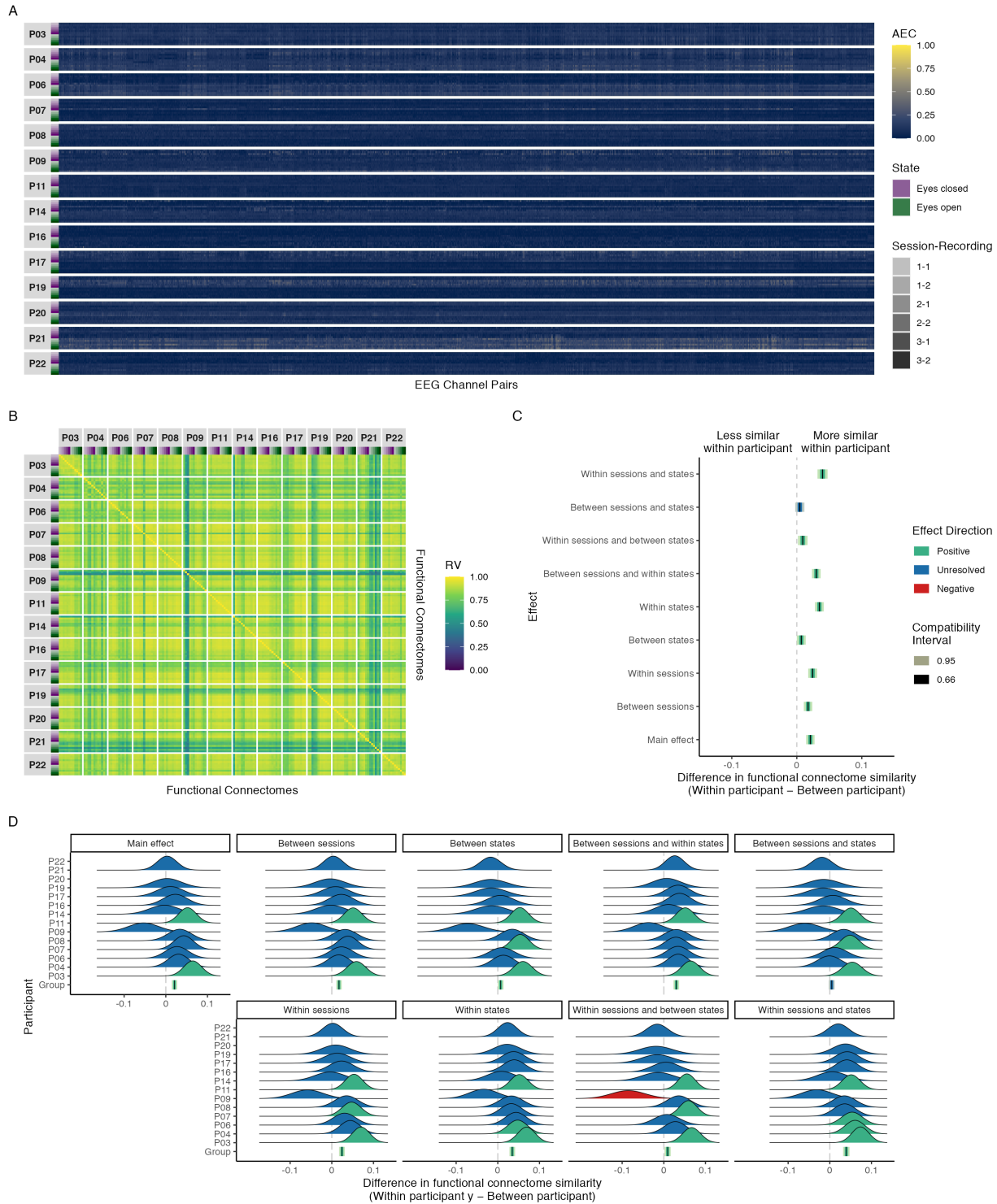


Figure A16. Maximal model results of amplitude coupling analyses in the alpha band: (A) connectivity profiles for all functional connectomes, organized by participant and recording; (B)

estimates of functional connectome similarity between all pairs of functional connectomes, organized by participant and recording; and group-level (C) and individual-level (D) contrasts estimating the average difference in functional connectome similarity within and between participants across contexts.

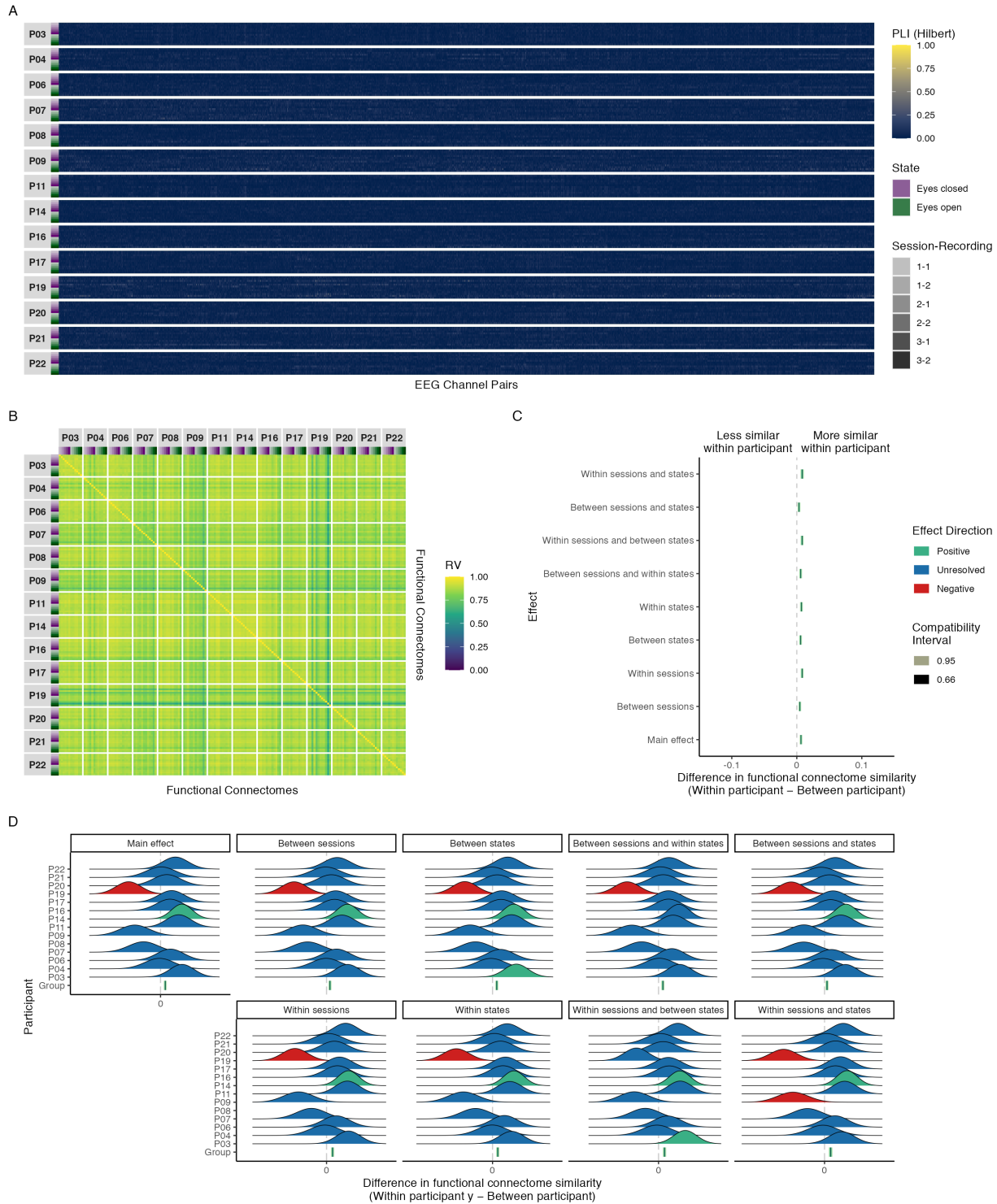


Figure A17. Maximal model results of phase coupling (Hilbert transform) analyses in the delta band: (A) connectivity profiles for all functional connectomes, organized by participant and

recording; (B) estimates of functional connectome similarity between all pairs of functional connectomes, organized by participant and recording; group-level (C) and individual-level (D) contrasts estimating the average difference in functional connectome similarity within and between participants across contexts.

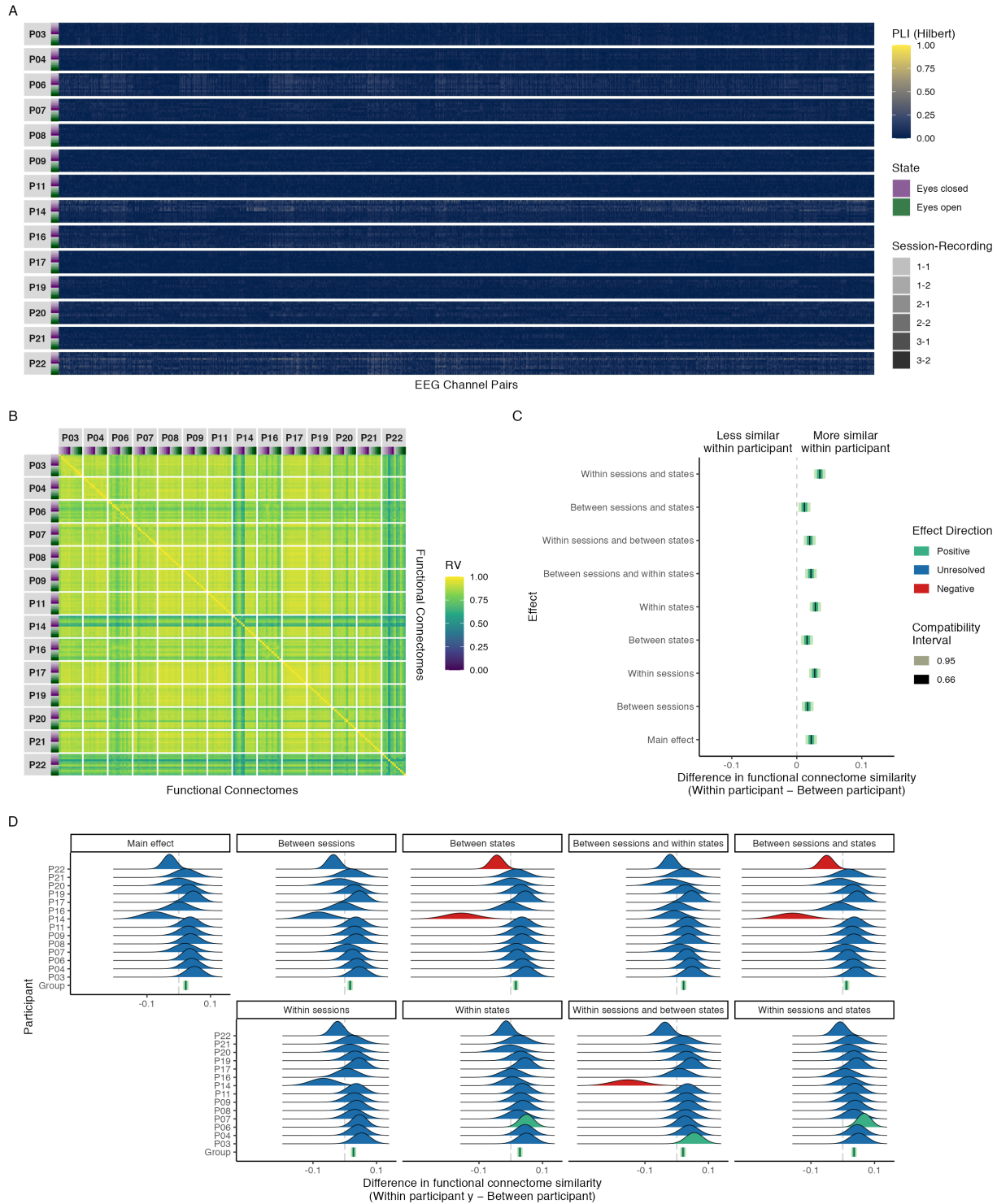


Figure A18. Maximal model results of phase coupling (Hilbert transform) analyses in the theta band: (A) connectivity profiles for all functional connectomes, organized by participant and

recording; (B) estimates of functional connectome similarity between all pairs of functional connectomes, organized by participant and recording; group-level (C) and individual-level (D) contrasts estimating the average difference in functional connectome similarity within and between participants across contexts.

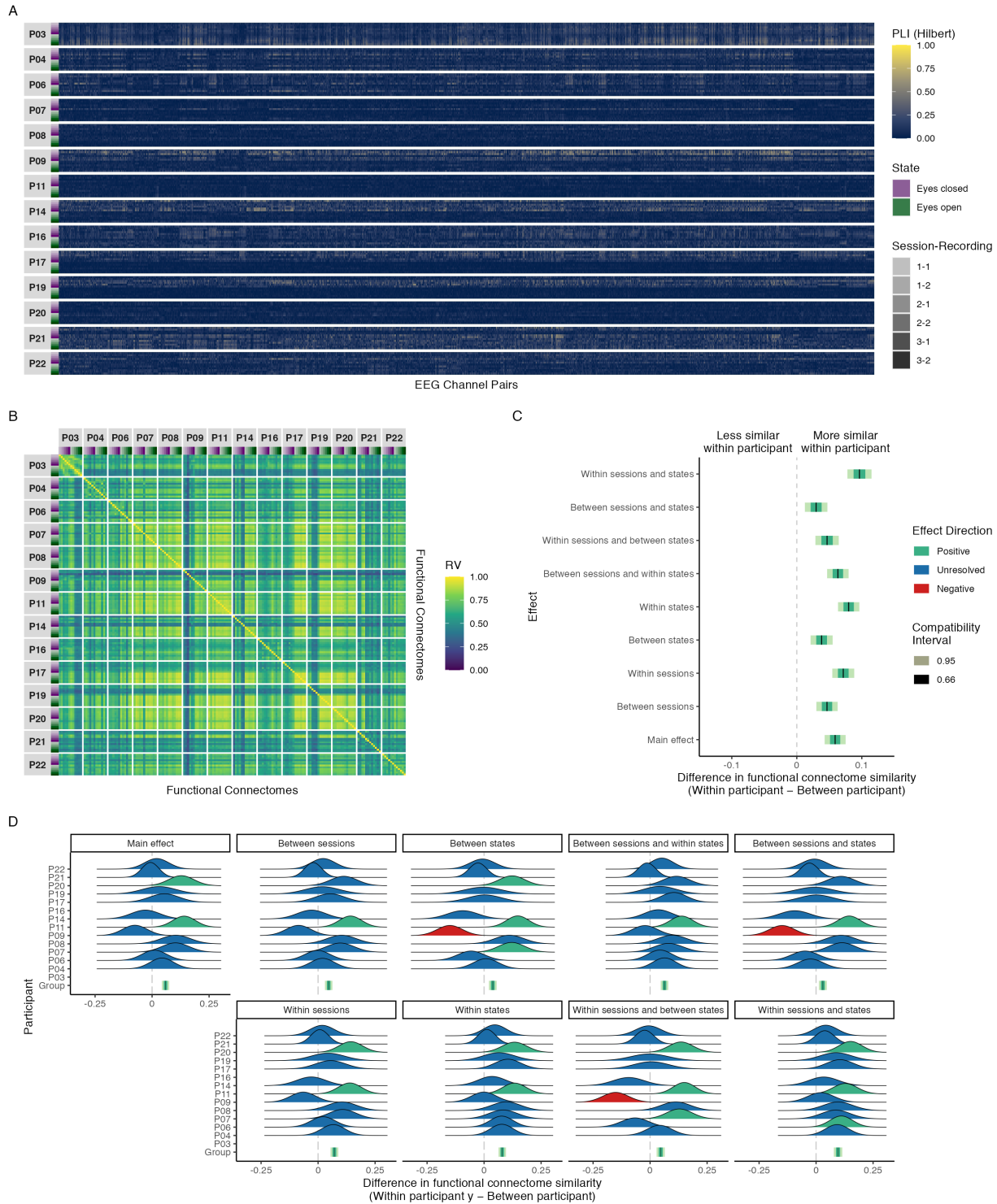


Figure A19. Maximal model results of phase coupling (Hilbert transform) analyses in the alpha band: (A) connectivity profiles for all functional connectomes, organized by participant and

recording; (B) estimates of functional connectome similarity between all pairs of functional connectomes, organized by participant and recording; group-level (C) and individual-level (D) contrasts estimating the average difference in functional connectome similarity within and between participants across contexts.

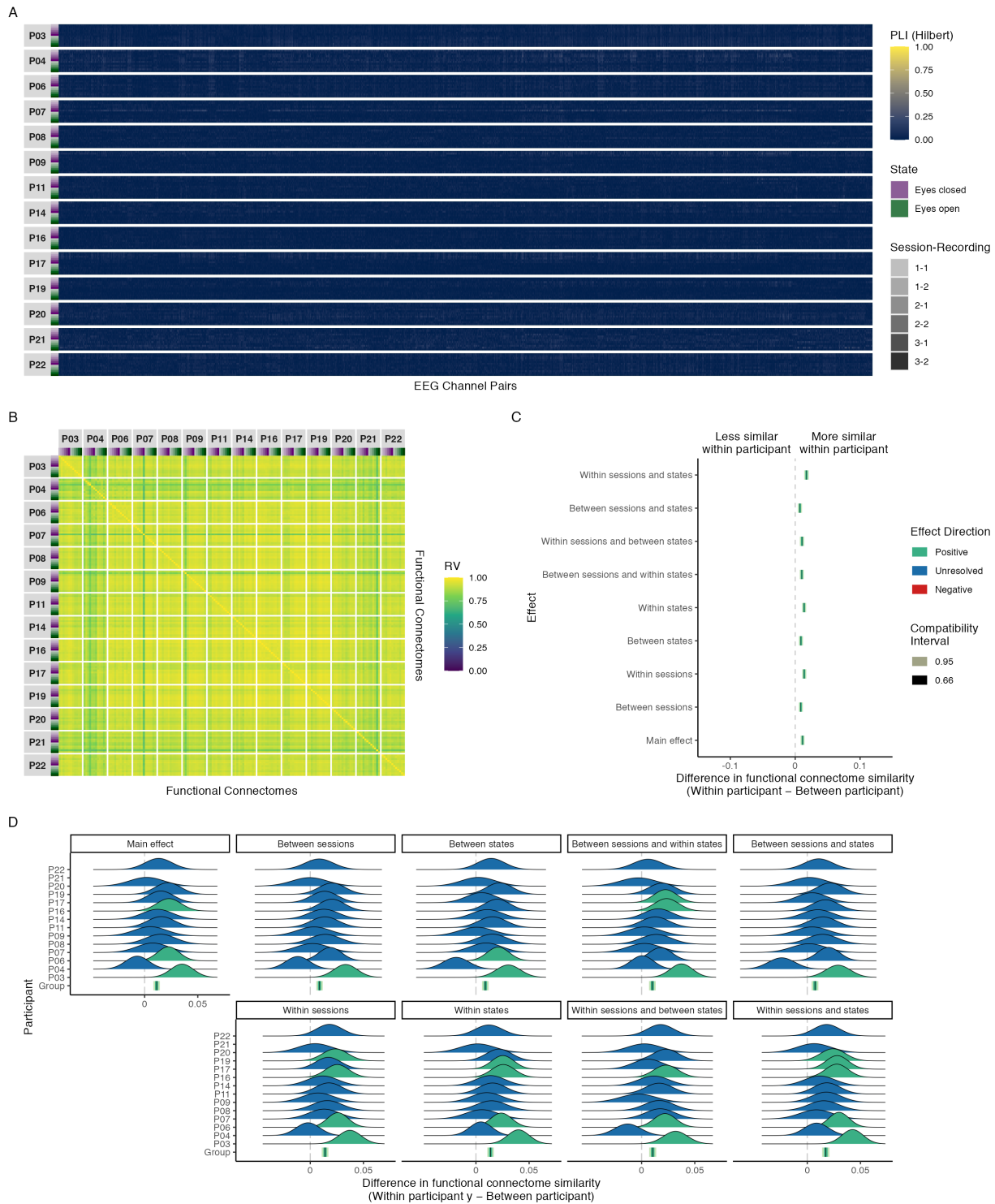


Figure A20. Maximal model results of phase coupling (Hilbert transform) analyses in the beta band: (A) connectivity profiles for all functional connectomes, organized by participant and

recording; (B) estimates of functional connectome similarity between all pairs of functional connectomes, organized by participant and recording; group-level (C) and individual-level (D) contrasts estimating the average difference in functional connectome similarity within and between participants across contexts.

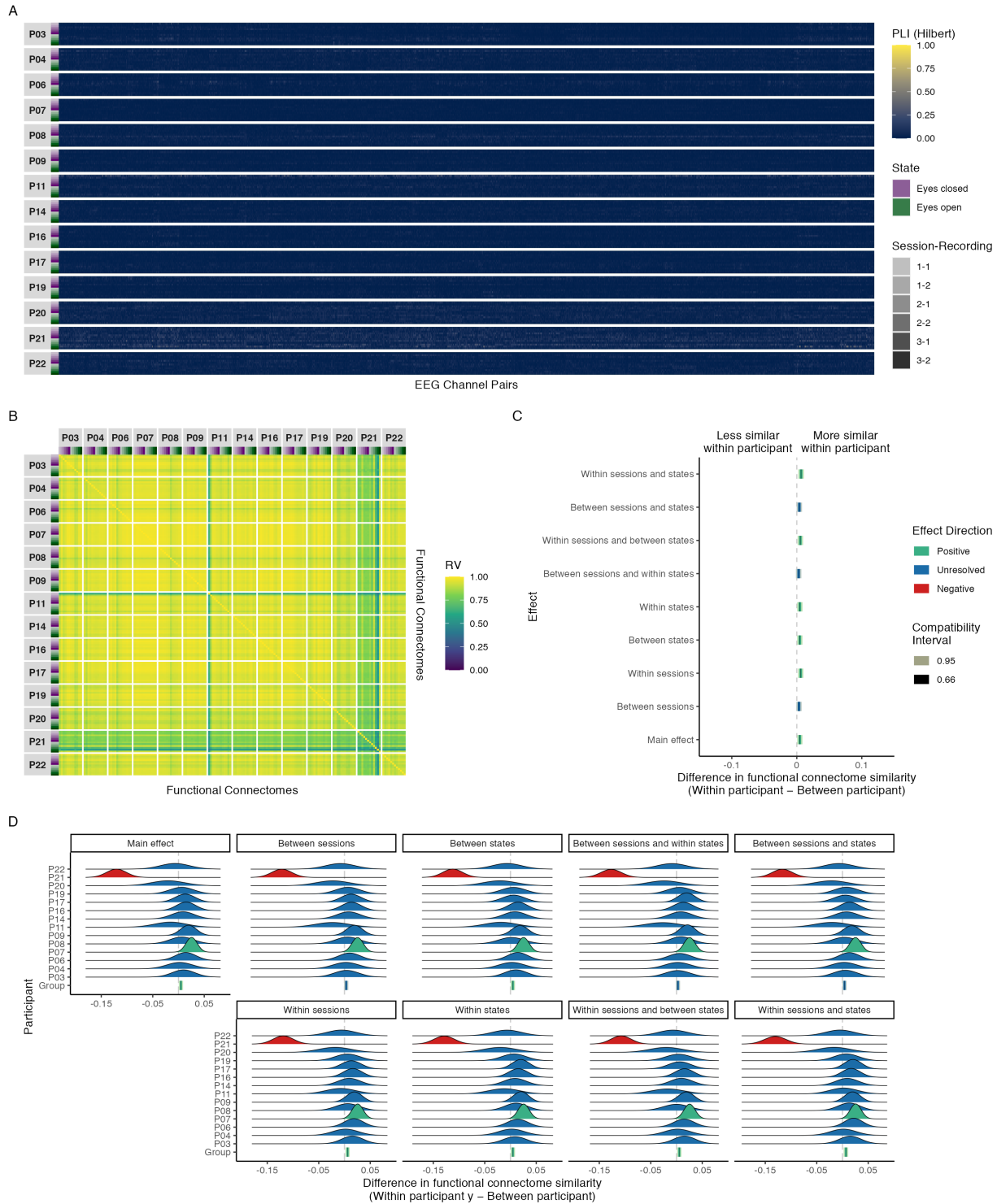


Figure A21. Maximal model results of phase coupling (Hilbert transform) analyses in the gamma band: (A) connectivity profiles for all functional connectomes, organized by participant and

recording; (B) estimates of functional connectome similarity between all pairs of functional connectomes, organized by participant and recording; group-level (C) and individual-level (D) contrasts estimating the average difference in functional connectome similarity within and between participants across contexts.

Amplitude coupling results (delta, theta, beta, gamma)

In this section we provide the results of our functional connectome similarity estimates for amplitude coupling functional connectomes in the delta, theta, beta, and gamma bands. Figure A22 shows the functional connectome similarity estimates between all pairs of amplitude coupling functional connectomes in each frequency band. Note the very high similarity estimates across participants, sessions, and states—particularly in the beta and gamma bands, where similarity is estimated to be near perfect. As we discussed in the results section, while these estimates are a statistically valid reflection of the data due to the relative position of the observations in each connectome being very close together in space, we felt that they were neurophysiologically unrealistic, greatly exaggerating the magnitude of similarity between any pair of functional connectomes and failing to capture the intended nuance across participants, sessions, and states. Thus, we refrain from showing the functional connectome similarity contrast results for these frequency bands here, but note that for each of these frequency bands the effect sizes most compatible with our data, given the background model, were positive but practically nil for all contrasts.

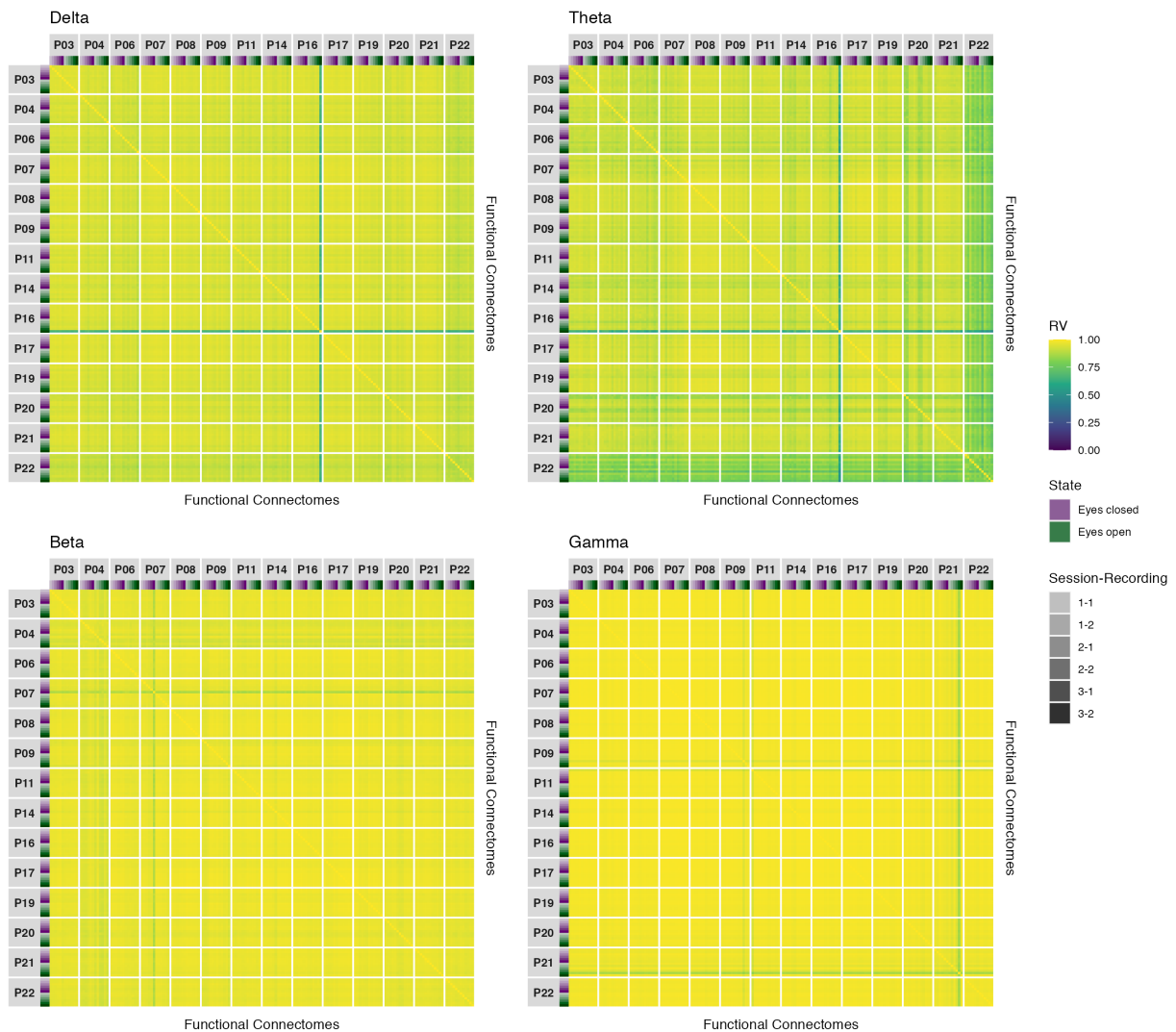


Figure A22. Estimates of functional connectome similarity between all pairs of amplitude coupling functional connectomes in the delta, theta, beta, and gamma bands, organized by participant and recording.

Appendix B

Session Info

Table B1

Session info for R environment.

Setting	Value
version	R version 4.1.2 (2021-11-01)
os	macOS Mojave 10.14.6
system	x86_64, darwin17.0
ui	X11
language	(EN)
collate	en_CA.UTF-8
ctype	en_CA.UTF-8
tz	America/Vancouver
date	2024-01-18
pandoc	2.14.0.3 @ /Applications/RStudio.app/Contents/MacOS/pandoc/ (via rmarkdown)
python	3.9
zotero	6.0.30
better bibtex	6.7.140

Table B2

Session info for R packages.

Package	Version	Source
bookdown	0.25	CRAN (R 4.1.2)
broom	1.0.5	CRAN (R 4.1.2)
broom.mixed	0.2.9.3	CRAN (R 4.1.2)
colorspace	2.0-3	CRAN (R 4.1.2)
datawizard	0.9.1	CRAN (R 4.1.2)
DHARMa	0.4.5	CRAN (R 4.1.2)
distributional	0.3.0	CRAN (R 4.1.2)
dplyr	1.1.2	CRAN (R 4.1.2)
emmeans	1.7.3	CRAN (R 4.1.2)
FactoMineR	2.4	CRAN (R 4.1.0)
flextable	0.9.4	CRAN (R 4.1.2)
forcats	1.0.0	CRAN (R 4.1.2)
fs	1.6.2	CRAN (R 4.1.2)
ftExtra	0.6.1	CRAN (R 4.1.2)
ggdist	3.1.1.9001	Github (@25a813d366ecf3ae4eff7e616f97de42f776a7a8)
ggh4x	0.2.1	CRAN (R 4.1.0)
ggnewscale	0.4.7	CRAN (R 4.1.2)
ggplot2	3.3.6	CRAN (R 4.1.2)
ggpubr	0.4.0	CRAN (R 4.1.0)
glmmTMB	1.1.2	local (/Users/user/LTtC3fU2/glmmTMB_1.1.2.tar.gz)
gtsummary	1.7.2	CRAN (R 4.1.2)
here	1.0.1	CRAN (R 4.1.0)
insight	0.19.7	CRAN (R 4.1.2)
knitr	1.40	CRAN (R 4.1.2)
Matrix	1.3-3	CRAN (R 4.1.0)
officedown	0.3.1	CRAN (R 4.1.2)

Package	Version	Source
officer	0.6.3	CRAN (R 4.1.2)
palettes	0.1.1	CRAN (R 4.1.2)
papaja	0.1.1	CRAN (R 4.1.2)
patchwork	1.1.1	CRAN (R 4.1.0)
performance	0.10.8	CRAN (R 4.1.2)
purrr	1.0.1	CRAN (R 4.1.2)
qqplotr	0.0.5	CRAN (R 4.1.0)
ragg	1.2.2	CRAN (R 4.1.2)
rbbt	0.0.0.9000	Github (@ec1ebe1e9b7e60bc4523e6cb2ca47f73a9cbfba3)
readr	2.1.2	CRAN (R 4.1.2)
renv	0.15.4	CRAN (R 4.1.2)
reticulate	1.25	CRAN (R 4.1.2)
rlang	1.1.1	CRAN (R 4.1.2)
rmarkdown	2.13	CRAN (R 4.1.2)
scales	1.2.1	CRAN (R 4.1.2)
see	0.7.0	CRAN (R 4.1.2)
sessioninfo	1.2.2	CRAN (R 4.1.0)
shiny	1.7.1	CRAN (R 4.1.0)
stringr	1.4.0	CRAN (R 4.1.0)
tarchetypes	0.6.0	CRAN (R 4.1.2)
targets	0.12.0	CRAN (R 4.1.2)
tibble	3.2.1	CRAN (R 4.1.2)
tidyverse	1.2.0	CRAN (R 4.1.2)
tidyselect	1.2.0	CRAN (R 4.1.2)
tidyverse	1.3.1	CRAN (R 4.1.0)
xfun	0.39	CRAN (R 4.1.2)